In Silico Understanding of the Hydrogen Bond Network in Organic Solvent Mixtures

Dissertation

zur

Erlangung des Doktorgrades (Dr. rer. nat.)

der

Mathematisch-Naturwissenschaftlichen Fakultät

der

Rheinischen Friedrich-Wilhelms-Universität Bonn

vorgelegt von

Gwydyon Marchelli

aus

Turin, Italien

Bonn, 2022

Angefertigt mit Genehmigung der Mathematisch-Naturwissenschaftlichen Fakultät

der

Rheinischen Friedrich-Wilhelms-Universität Bonn

Erster Gutachterin: Prof. Dr. Barbara Kirchner

Zweiter Gutachter: Prof. Dr. Thomas Bredow

Tag der Promotion: 08.03.2022

Erscheinungsjahr: 2022

"To succeed, planning alone is insufficient.
One must improvise as well."
Isaac Asimov, *The Foundation*

Publications

1. **G. Marchelli**, J. Ingenmey, B. Kirchner, "Activity coefficients of binary methanol alcohol mixtures from cluster weighting", *ChemistryOpen*, **2020**, *9 (7)*, 774–785, *doi:10.1002/open.202000171*.

2. **G. Marchelli**, J. Ingenmey, A. Chaumont, O.Holloczki, B. Kirchner, "Hydrogen bonding and vaporization thermodynamics in hexafluoroisopropanol-acetone and -methanol mixtures. A joined cluster analysis and molecular dynamic study.", *ChemPhysChem*, **2021**, *23*, 50-62, *doi:10.1002/cphc.202100620*.

Further publications (not part of this thesis):

3. M. von Domaros, E. Perlt, J. Ingenmey, **G. Marchelli**, B. Kirchner, "Peacemaker 2: Making Clusters Talk About Binary Mixtures and Neat Liquids", *SoftwareX*, **2018**, *7*, 356–359, *doi:10.1016/j.softx.2018.11.002*.

4. J. Ingenmey, J. Blasius, **G. Marchelli**, A. Riegel, B. Kirchner, "A Cluster Approach for Activity Coefficients: General Theory and Implementation", *J. Chem. Eng. Data*, **2019**, *64 (1)*, 255–261, *doi:10.1021/acs.jced.8b00779*.

Abstract

In the framework of green chemistry, it is fundamental to further investigate the intermolecular interactions that define the dynamics and structure of liquids and their mixtures. Among those, the hydrogen bond in particular has a remarkable influence on the structure and properties of condensed matter. A better insight into the principles and processes that govern the hydrogen bond network will allow the design and tuning of novel sustainable solvents in the foreseeable future.

The binary quantum cluster equilibrium method (bQCE) allows to model the liquid and gas phase of both, neat systems and binary mixtures by using an ensemble of molecular clusters generated and optimized via quantum chemical methods. In this thesis, a protocol based on the bQCE theory is applied to investigate the intermolecular interactions in the condensed phase of various organic solvent mixtures.

In the first part of the thesis, the mixtures of methanol with several small alcohols are studied via cluster analysis. In particular, the investigation is focused on the effect of chain length and branching over the thermodynamic properties of these mixtures. Vaporization enthalpies, activity coefficients, and combined distribution functions of the hydrogen bonds are evaluated with a combination of semi-empirical calculations and the bQCE approach. It is shown how the branching and the chain length influence the geometric features of the hydrogen bond network and how this affects the activity coefficients of the different species. Overall, a large deviation from ideality is observed when increasing the size of the alcohol; on the other hand, an increase in the branching of the alcohol leads to a more ideal mixture.

In the second part of the thesis, the hydrogen bond networks of the binary mixtures of hexafluoroisopropanol with methanol and acetone are investigated using a combination of

both classical molecular dynamics and bQCE. The densities of the mixtures at different temperatures are obtained from simulations and subsequently used as reference for the optimization of bQCE parameters. This removes the requirement for experimental reference data and allows the application of the bQCE method to complex systems with little to no available reference data. The bQCE theory is extended to include the temperature dependent adjustment of parameters. The structure of the hydrogen bond network is analyzed for both mixtures; their vaporization enthalpies and entropies are calculated and discussed. In both systems mixed clusters are favored even at low concentrations of hexafluoroisopropanol, and tetrameric and pentameric ring structures are strongly populated also in the neat systems.

In summary, the present thesis investigates the structure and dynamics of binary organic solvent mixtures with a special focus on their hydrogen bond networks. A variety of classical and quantum chemical methods are used with a general aim for computational efficiency. This allows the application of the presented approaches to complex systems. Therefore, the results discussed in this thesis represent a starting point in the investigation of multi-component solvent systems that will be needed to develop sustainable compounds in accordance to the principles of green chemistry.

Contents

List of Figures

List of Tables

1. Introduction

The development of novel sustainable solvents is a top priority in scientific research.[5] This is due to the increasing demand for industrial processes that respect the conditions of green chemistry.[6] Many studies, both experimental and computational, focus on this field. In the recent decades, organic solvents have been progressively substituted by novel kinds of compounds, e.g. ionic liquids and deep eutectic solvents (DESs), which allow—to some extent—to fulfill the sustainability requirement.[7–9] In particular, ionic liquids and DESs consist of mixtures of ionic compounds that can be complicated to synthesize.[8] Moreover, the fact that they often exhibit hydrophilic properties hinders their application in some fields, such as the liquid-liquid extraction of metals.[10] In the case of DESs, typically two components interact via strong hydrogen bonds.[8,9,11] A new kind of DESs,[12] was recently developed, that is formed by neutral rather than ionic compounds, thereby avoiding the hydrophilicity of other DESs, and features a structure closer to the mixtures of organic solvents. As the hydrogen bond network seems to have a significant influence on the properties of the resulting DES system, it is imperative to better understand its structure in binary liquid state mixtures. This first step could then allow to model and tune a wide range of both traditional organic and novel sustainable solvents.

It is important to recall that the modeling of the liquid phase presents some challenges. In fact, in the liquid state hydrogen bonds are continuously broken and formed anew, so most of the analysis requires a statistical treatment. In this thesis the prevalent approach applied is the binary quantum cluster method, which will be explained in more detail in this and in the next chapter.

1.1. The Hydrogen Bond Network in Fluids

The study of hydrogen bonds is an extremely common motif in literature as it determines the structure and dynamics of a large variety of liquids.[13–16] Nevertheless, the definition of what constitutes a hydrogen bond remains vague even 100 years after its discovery by Latimer and Rodebush.[17] In 1920, their first work on hydrogen bonds described the hydrogen bond as an intermolecular interaction in which "a free pair of electrons on one water molecule might be able to exert sufficient force on a hydrogen held by a pair of electrons on another water molecule to bind the two molecules together";[17] in the same work, still discussing about liquid water, the authors speculate that the liquid structure "may be made up of large aggregates of molecules, continually breaking and reforming".[17] From this first description, the hydrogen bond seemed electrostatic in nature; however, it is now recognized as a more complicated interaction, which can present different grades of bond strength and directionality.[16] It shows similarities to both van der Waals interactions and covalent bonds.[15,18] In 2011, the International Union of Pure and Applied Chemistry (IUPAC) gave an updated definition of the hydrogen bond as "an attractive interaction between a hydrogen atom from a molecule or a molecular fragment X–H in which X is more electronegative than H, and an atom or a group of atoms in the same or a different molecule, in which there is evidence of bond formation."[19] This definition is still broad and can lead to multiple possible interpretations; however, what the scientific community generally agrees on is its strong influence over the structure of liquids.[14,15] Therefore, it is fundamental to investigate this intermolecular interaction. In particular, the features that make it a key ingredient to fully describe the properties of liquids are its directionality and the possibility to easily break and reform anew.[20–22] Computational tools, in particular molecular dynamics, have been employed to obtain insights on hydrogen bonds, in particular in water, and describe its effect on dynamics and structure.[23–27] Other hydrogen bond-based liquids have been investigated both experimentally – e.g. via NMR spectroscopy[28,29] or X-ray scattering[30–36] – and theoretically, via classical and ab-initio molecular dynamics.[37–40] In this thesis, the hydrogen bond network will be investigated with a novel method, called the quantum cluster equilibrium (QCE) theory.

1.2. The Quantum Cluster Equilibrium Theory

The simulation and modeling of the liquid phase presents various challenges. While classical molecular dynamics is able to describe large systems, the results are often limited by the low level of theory offered by the force fields applied. On the other end, higher levels of theory, such as ab-initio molecular dynamics, are unfeasible to describe large systems due to their computational cost. Hence, a method based on a different approach has been developed in the last decades to investigate the liquid state. This method aims to describe the liquid phase as an ensemble of molecular clusters. Even though the gas phase and the liquid phase are distinct aggregate states with different properties, there is a continuous transition between them, proven by the existence of the gas-liquid critical point.[41] Molecular clusters can be seen as the intermediate state between the vapor phase populated by monomers or small clusters of a few molecules, and the fully aggregated liquid state. Starting from this assumption, the QCE method was developed by Frank Weinhold, who published its theory in 1998[42] but had already demonstrated its effectiveness in describing hydrogen bond-based liquids in the years before.[43,44] Within the QCE theory, the molecular clusters are weighted by their relative population in the canonical ensemble of the classical statistical thermodynamics. The theory was further developed and expanded extensively by the Kirchner group in 2005[27] and the years thereafter.[2,3,45] In 2011 it was rewritten to comprehend and describe binary mixtures instead of only neat systems.[45] This new extended theory takes the name of binary QCE (bQCE) and it has been used extensively in the present thesis.

The group has implemented the bQCE method in the publicly available PEACEMAKER code, released in 2005. The bQCE theory has been added in the second release of the software in 2018, as PEACEMAKER2, which can be freely downloaded from the webpage of the research group under the GNU general public license.

This method has been applied in various studies to different solvents and mixtures, such as water,[27,46–56] alcohols,[57–63] amides,[43,44,64,65] hydrogen halides,[66–69] ammonia,[70,71] and weak acids.[72–74] The bQCE method has been used to calculate the ionic product of water,[75] to cluster-weight vibrational circular dichroism (VCD) spectra,[76,77] and to calculate the mixing thermodynamics of binary mixtures.[1,4,45,65,78,79] These types of analyses

are also presented in Chapter 3 of this thesis.[1]

The bQCE method relies on geometrically optimized clusters whose frequencies have been previously calculated. The advantage of this approach is that it reduces the size of the problem from hundreds or thousands of molecules, to clusters of less than twenty molecules which can be modeled at a higher level of theory. The problem, however, is shifted on how those clusters need to be defined. Many approaches have been used in the last decades: they have been based on experimentally observed molecular configurations,[80] derived from computational parameters,[4,81] or designed in accordance to the chemical intuition of the author.[49,82] In this thesis, a more objective approach has been used. The clusters are built from a genetic algorithm at force field level and then further optimized at an higher level of theory. This approach avoids any kind of subjective bias on the clusters and allows the user to dispose of a great number of clusters; as a downside, the highest levels of theory are not accessible due to computational cost. Nevertheless, recent works[3,4] have shown the reliability of this approach. Further details on the method are presented in Chapter 2.

1.3. Scope of the Thesis

Up to recent times, the bQCE theory has been used to reproduce experimental data, or well known properties of neat liquids. Only in the last few years this method has been used as a predictive tool for the properties of mixtures of small molecules. This thesis aims to use the bQCE theory to investigate the thermodynamic properties of mixtures composed by small organic molecules, varying their geometries and minimizing the request of experimental data from literature. A second goal of it, is to extensively investigate the behavior and effect of the hydrogen bond network in mixtures of small organic solvents. As previously discussed, it is fundamental to investigate the intermolecular interactions in the liquid state in order to design novel mixtures of solvents or tune their properties. Using all the tools at disposal (bQCE theory, classical MD, quantum mechanics calculations), Chapter 3 of this thesis focuses on the hydrogen bond networks of small alcohols mixtures, while Chapter 4 takes an additional step, and investigates the mixtures of hexafluoroiso-

propanol (HFIP) with a hydrogen bond acceptor (acetone) and a hydrogen bond donor and acceptor (MeOH). These studies on small systems are important to fully understand the possibilities of novel methods and the nature of the intermolecular interactions in the liquid phase.

2. Methodology

In this chapter, the main methods used in this thesis will be briefly described. First, the fundamentals of Density Fuctional Theory (DFT) – necessary to the full understanding of the dissertation – will be delineated. This is a necessary step for the geometry optimization and frequency calculations of small molecular clusters, key element of the Quantum Cluster Equilibrium Theory (QCE), explained in detail in par. 2.2. In the end, keys elements of classical molecular dynamics (MD) will be described.

2.1. Static Quantum Chemical Calculations

The main target of static quantum chemistry is to determine the correct geometries, the total energy, and properties of molecular systems. Electronic structure methods are the most reliable, accurate, and used in this field. In this thesis the Density Functional Theory (DFT), formulated by Pierre Hohenberg and Walter Konh in 1964,[83] is employed in Chapter 4, and it will be briefly explained in this section. A short description of semi-empirical methods, used in Chapter 3, is also included.

2.1.1. Principles of Density Functional Theory

The present description takes inspiration from *The handbook of computational quantum chemistry* by David B. Cook.[84] According to DFT, in the case of a non-degenerate ground state, its energy and related molecular properties are uniquely determined by the electron density $\rho_0(x, y, z)$. The time-independent, non-relativistic Schrödinger equation reads

$$\hat{H}\Psi = E\Psi, \tag{2.1}$$

where E is the eigenvalue of the non-relativistic and non-magnetic Hamiltonian operator ($\hat{H}$), applied to the wave function Ψ. ($\hat{H}$ can be written as the sum of two terms

$$\hat{H} = \hat{T} + \hat{V}, \tag{2.2}$$

where $\hat{T}$ and $\hat{V}$ are the kinetic and potential energy operators, respectively. Since in this thesis heavy atoms are not calculated, relativistic effect are not considered, therefore the Born-Oppenheimer approximation,[85] which considers the motion of the electrons to be separated from the motion of the nuclei, can be applied. This approximation considers the nuclei to be stationary with respect to the motions of the electrons, so that it is possible to evaluate only the electronic wave function Ψ_e in a stationary configuration of nuclei. The electronic Hamiltonian can be described as:

$$\hat{H}_{elec} = -\frac{1}{2}\sum_{i=1}^{n}\nabla^2 - \sum_{i=1}^{n}\upsilon(r_i) + \sum_{i,j<i=1}^{n}\frac{1}{r_{ij}}, \tag{2.3}$$

in atomic units, where $r_{ia} = |r_i - R_A|$, $r_{ij} = |r_i - r_j|$, and $\upsilon(r_i) = \sum_A^M \frac{Z_A}{r_{ia}}$. The first term is the kinetic energy operator T_e, the second the nucleus-electron interaction V_{Ne}, and the third one the electron-electron interaction V_{ee}.

The Schrödinger equation has infinite solutions. To find the lowest energy solution, corresponding to the ground state, some kind of assumptions are required. The most common is the variation principle: considering the mean value of the energy related to the many-electron wave function $\tilde{\Psi} = \sum_{j=1}^{\infty} B_j \Psi_j$ described as

$$\tilde{E} = \frac{\langle\tilde{\Psi}|\hat{H}|\tilde{\Psi}\rangle}{\langle\tilde{\Psi}|\tilde{\Psi}\rangle}; \tag{2.4}$$

it is possible to apply on it the variational principle, that states

$$\tilde{E} = \frac{\langle\tilde{\Psi}|\hat{H}|\tilde{\Psi}\rangle}{\langle\tilde{\Psi}|\tilde{\Psi}\rangle} \geq E_1, \tag{2.5}$$

which means the energy of the ground state E_1 is always lower than the energy of any trial wave function $\tilde{\Psi}$ that can be imagined.

Different strategies can be considered to calculate the energy of the electronic structure; all of them are based on finding suitable approximations of the Schrödinger equation with an appropriate description of the wave function and the Hamiltonian. The most common methods are the Wave Function Theory (WFT) and the DFT. The first family of methods uses the Hartree-Fock (HF) approach,[86,87] which is based on a self-consistent field procedure where the electron-electron interaction is approximated by the motion of an electron in the mean-field created by the other electrons. The wave function is described by a single Slater determinant of the one-electron wave functions; the electron correlation is not taken into account. The second approach, DFT, is instead based on the electron density, reducing the problem from the $3N$ coordinates of an N-electron system of the WFT to a function of three coordinates. Every wave function generates a density matrix, but the opposite is not always true. This can lead to non-physical solutions, so some considerations and restrictions must be applied. DFT is based on the two theorems formulated by Hohenberg and Kohn. In the first one, it is proven that the ground-state wave function and energy are determined by the ground-state electron density. The second theorem states that the variational principle can be applied to the energy defined by a specific electron density. Kohn and Sham have then developed a method to make use of these theorems, defining the strategy to obtain the ground state electron density.[88] In their approach, they considered a fictitious reference system consisting of n non-interacting electrons, all experiencing the same external potential energy function, constructed to reproduce the ground-state electron density. The eigenvalue problem related to each non-interacting electron reads

$$\hat{h}_i^{KS}\theta_i^{KS} = \epsilon_i^{KS}\theta_i^{KS}, \tag{2.6}$$

where ϵ_i^{KS} is the orbital energy, $\hat{h}_i^{KS}$ is the one electron Hamiltonian and θ_i^{KS} is the spatial part of each spin-orbital.

The energy—which is a functional of the electron density—$E[\rho]$ can be divided into its different contributions:

$$E[\rho] = T[\rho] + E_{ee}[\rho] + E_{ne}[\rho] \tag{2.7}$$

where $E_{ne}[\rho]$ represents the nucleus-electron interactions, $T[\rho]$ is the kinetic component and $E_{ee}[\rho]$ the electron-electron interactions. This last term can be separated in a Coulomb $J[\rho]$ and an exchange part $K[\rho]$. Since the system is generated only by the non-interacting electrons, $T[\rho]$ is not known outside for the one-electron contribution. A new term $\Delta T = T[\rho] - T_s[\rho]$ can be defined where $T_s[\rho]$ is the kinetic energy of the non-interacting electrons' system. ΔT is then incorporated with the exchange contribution $K[\rho]$ into the exchange-correlation function $E_{xc}[\rho]$. Now the energy expression reads

$$E[\rho] = T_s[\rho] + J[\rho] + E_{ne}[\rho] + E_{xc}[\rho] \tag{2.8}$$

where all the terms are known except for the exchange correlation contribution; this formulation is an exact expression, and the problem is moved on the definition of $E_{xc}[\rho]$. Various different functional have been defined, and they are categorized into the so-called Jacob's ladder which is represented by the following steps:[89]

- the Local Density Approximation (LDA). The density depends only on the spatial coordinates x, y, z.
- The Generalized Gradient Approximation (GGA). The density is not defined only from the spatial coordinates but also on their gradients ∇x, ∇y, ∇z. The BP86 functional, used extensively in this thesis, belongs to this category.
- Meta GGA. These functionals include an explicit dependence on the kinetic energy.
- Hybrid functionals. They incorporate an exact HF exchange rate on the occupied KS orbitals; e.g. the B3LYP functional used in this thesis includes 20% exact HF exchange.
- In the fifth step, fully not local treatment with a partial exact correlation term is included.

The inclusion of terms and parameters can lead to a better definition of $E_{xc}[\rho]$. However, higher steps can have an important computational cost that does not directly correlate to a better result.

2.1.2. Semi-Empirical Methods

Semi-empirical quantum methods (SQMs) can be considered as a bridge between classical (e.g. force fields) and ab-initio approaches.[90] They typically use minimal, valence-only basis sets; they are based on self-consistent fields derived from HF or DFT, with drastic integrals approximations. Since they can be up to two orders of magnitude faster than ab-initio methods, the loss in robustness and accuracy is balanced; if the SQM is correctly parameterized, the calculated properties and geometrical structure are reliable.[91] Even if SQMs are typically applied to large molecular systems, the low computational time required makes them also suitable for the calculation of a great number of smaller-sized clusters. Therefore, they can be applied in combination with cluster weighting methods, such as the Quantum Cluster Equilibrium approach (QCE). In this thesis the extended tight binding method GFN2-xTB 6.0.1[91,92] has been used, because of its following features:

- its basis set consists of a minimal, valence-only basis set of atom centered, contracted Gaussian functions, where a single 1s function is assigned to the hydrogen atom;
- its Hamiltonian – which resembles the one in the DFTB3 method[93] – includes electrostatic interactions and exchange-correlation effects up to second order in the multipole expansion;
- it includes D4 dispersion correction,[94,95] that accounts for the London dispersion energy.

Since this SQM focuses on the calculation of ground state properties – such as vibrational frequencies and geometrical structure – it is well-suited for the purposes of this thesis.

2.2. Principles of Quantum Cluster Equilibrium Theory

QCE has been first introduced by Weinhold *et al.*[42] in 1998. According to this approach, it is possible to define molecular clusters as intermediate between the monomeric description of the vapor face and the fully aggregated condensed phase. A thermodynamic equilibrium exists between liquid and vapor phase, and in principle clusters that can describe a dense vapor phase must be able to do the same also in the condensed one by changing of temperature and pressure. It is in principle possible to imagine a complete set of molecular clusters – which can be investigated by quantum methods – that can give a quantitative thermodynamics description of the liquid state. This complete cluster set is not realistic to achieve, but it is possible to generate a set of dominant clusters that can provide an accurate description of the liquid phase. In 2011, Barbara Kirchner has expanded this theory past the study of neat solvents, to treat also binary mixtures under the name of binary QCE (bQCE).[27,45] This novel approach has been the basis of the work presented in this thesis.

2.2.1. Principles of Statistical Thermodynamics

The energy state for every quantum-mechanical system is quantized. This holds true for molecules, atoms, clusters of molecules, and their energy can be found solving the Schrödinger equation. In a system consisting of different particles, it is important to know which fraction falls in each specific state. For a system with N particles, at the temperature T, and with volume V, the probability p_j to find the system at a specific energy E_j is proportional to the Boltzmann factor

$$p_j \propto \mathrm{e}^{-\frac{E_j}{k_\mathrm{B}T}}, \tag{2.9}$$

where k_b is the Boltzmann constant and T is expressed in K. The bQCE theory operates in the canonical ensemble, where N, T, V are fixed. The sum of all probabilities p_j must

be equal to 1:

$$Q(N,V,T) = \sum_j \mathrm{e}^{-\frac{E_j(N,V,T)}{k_\mathrm{B}T}}, \tag{2.10}$$

so $1/Q(N,V,T)$ is the normalization factor and $Q(N,V,T)$ is called partition function. The partition function allows for the calculation of the thermodynamic state function of the system – e.g. the mean energy can be derived as:

$$\begin{aligned}\langle E\rangle &= \sum_j E_j(N,V,T)p_j(N,V,T)\\ &= \sum_j E_j(N,V,T)\frac{\mathrm{e}^{-\frac{E_j(N,V,T)}{k_\mathrm{B}T}}}{Q(N,V,T)}.\end{aligned} \tag{2.11}$$

It is possible to differentiate $\ln Q(N,V,T)$ with respect the temperature to get:

$$\begin{aligned}\left(\frac{\partial \ln Q(N,V,T)}{\partial T}\right) &= \frac{1}{Q(N,V,T)}\left(\frac{\partial Q(N,V)}{\partial T}\right)\\ &= \frac{1}{k_\mathrm{B}T^2}\sum_j E_j(N,V)\cdot\frac{\mathrm{e}^{-\frac{E_j(N,V)}{k_\mathrm{B}T}}}{Q(N,V)}.\end{aligned} \tag{2.12}$$

By replacing the sum in ref 2.12 in eq. 2.11, the $\langle E\rangle$ becomes

$$\langle E\rangle = k_\mathrm{B}T^2\left(\frac{\partial \ln Q(N,V,T)}{\partial T}\right). \tag{2.13}$$

For a system of indistinguishable particles the partition function can be written as

$$Q(N,V,T) = \frac{1}{N!}\,q(N,V)^N, \tag{2.14}$$

where $q(N,V)$ is the single particle partition function. It must be noted that this equation is valid only for a number of particles smaller than the number of possible states with value $k_\mathrm{B}T^2$. Fortunately, this is usually the case for fluids at room temperature. The energy ε of a single particle can be written as the sum of its translational, rotational, vibrational and electronic components:

$$\varepsilon = \varepsilon^{\mathrm{trans}} + \varepsilon^{\mathrm{rot}} + \varepsilon^{\mathrm{vib}} + \varepsilon^{\mathrm{elec}}. \tag{2.15}$$

The partition function of the single particle can therefore be rewritten as

$$q = q^{\text{trans}}\, q^{\text{rot}}\, q^{\text{vib}}\, q^{\text{elec}}, \tag{2.16}$$

where q^{trans}, q^{rot}, q^{vib}, q^{elec} are the translational, rotational, vibrational, and eletrical partition function respectively. For the purpose of the bQCE theory, q^{trans} can be described by the particle in a box

$$q^{\text{trans}} = \frac{V}{\Lambda^3}, \tag{2.17}$$

where $\Lambda = \sqrt{\frac{h^2}{2\pi m k_{\text{B}} T}}$, h is the Planck constant, and m the mass of the particle.

q^{rot} can be described by the rigid rotor:

$$q^{\text{rot}} = \frac{\pi^{1/2}}{\sigma}\sqrt{\frac{T^3}{\Theta_A^{\text{rot}}\Theta_B^{\text{rot}}\Theta_C^{\text{rot}}}}, \tag{2.18}$$

where $\Theta_j^{\text{rot}} = \frac{h^2}{8\pi^2 I_j k_{\text{B}}}$, σ is the rotational symmetry number, and I_j the moment of inertia.

q^{vib} can be described by the harmonic oscillator

$$q^{\text{vib}} = \prod_{i=1}^{3N-x} \frac{\mathrm{e}^{-\Theta_i^{\text{vib}}/2T}}{1-\mathrm{e}^{-\Theta_i^{\text{vib}}/T}}, \tag{2.19}$$

where $\Theta_i^{\text{vib}} = \frac{h\nu_i}{k_{\text{B}}}$, $3N - x$ is the number of vibrational degrees of freedom, and ν_i the vibrational frequency of the ith normal mode.

q^{elec} is calculated assuming that all the particles are, under certain conditions, in the ground state, with energy $\varepsilon_1^{\text{elec}}$:

$$q^{\text{elec}} = g_1 \mathrm{e}^{-\frac{\varepsilon_1^{\text{elec}}}{k_{\text{B}}T}}, \tag{2.20}$$

where g_1 is the degeneracy of the ground state.

2.2.2. Binary Quantum Cluster Equilibrium Theory

The bQCE theory has been explored and extended in different works;[2,3,45] The assumption is to describe the liquid state as a dense gas phase composed of different clusters of interacting molecules. The main concepts and key equations of this theory will be

presented and explained. The molecular clusters that compose the system, according to the bQCE theory, are built starting from the monomers of one or two components. The first scenario corresponds to a neat system, the second one to a binary system. This cluster gas is assumed to be in thermodynamic equilibrium between the aggregated and disaggregated forms, according to the following reactions:

$$i(\mathcal{P})\mathrm{C}_1 + j(\mathcal{P})\mathrm{C}_2 \rightleftharpoons \mathrm{C}_{\mathcal{P}}, \tag{2.21}$$

where $i(\mathcal{P})$ and $j(\mathcal{P})$ represent the number of monomers of the components C_1 and C_2 in the cluster $\mathcal{P}$. This generic allows to consider different conformers and motifs for the cluster $\mathcal{P}$, e.g. chains or rings that coordinate the different monomers that compose the structure of the cluster.

Given a volume V, a temperature T, and a total particle number defined by $N^{\mathrm{tot}} = N_1^{\mathrm{tot}} + N_2^{\mathrm{tot}}$, the bQCE method aims to find a particle distribution $\{N_i\}$ that minimizes the free energy of the system:

$$F = -k_{\mathrm{B}} T \ln Q, \tag{2.22}$$

where Q is the total partition function of the distinguishable molecular clusters system, and it is given by

$$Q = \prod_i^M \frac{1}{N_i!}\, q_i^{N_i}. \tag{2.23}$$

Here, N_i is the population of the i-cluster with partition function q_i, and M being the total number of clusters included in the selected finite cluster set. The cluster partition function follows Eq. 2.16, and the translational, rotational and vibrational components are calculated according to Eqs. 2.17–2.19. The electronic partition function is calculated from the adiabatic binding energy

$$\Delta_{\mathrm{bind}}\varepsilon_i^{\mathrm{elec}} = \varepsilon_i^{\mathrm{elec}} - n_i^1 \varepsilon_1^{\mathrm{elec}} - n_i^2 \varepsilon_2^{\mathrm{elec}}, \tag{2.24}$$

where $\varepsilon_i^{\mathrm{elec}}$ is the electronic energy of the cluster's ground state $\mathcal{P}_i$, n_i^1 and n_i^2 are the number of monomers of the components 1 and 2 of the cluster, respectively, $\varepsilon_1^{\mathrm{elec}}$ and $\varepsilon_2^{\mathrm{elec}}$ are the corresponding ground states energies. This term is not enough to describe

the electronic partition function, as it does not take into account the inter-cluster interaction energy. For this reason, an additional term in the form of a mean-field energy is introduced, namely a_{mf}, weighted by the volume and cluster size; it has the dimension of an energy over volume and describes the average inter-cluster interaction. The final expression of q_i^{elec} reads

$$q_i^{\mathrm{elec}} = \exp\left\{-\frac{\Delta_{\mathrm{bind}}\varepsilon_i^{\mathrm{elec}} - (n_i^1 + n_i^2)\frac{a_{\mathrm{mf}}}{V}}{k_{\mathrm{B}}T}\right\}. \tag{2.25}$$

Since the particles in the molecular clusters are not punctiform, a fraction of the volume is not accessible by translation, and a correction term is required to describe the full volume of the molecule. This volume takes the name of exclusion volume (V_{ex}) and reads:

$$\begin{aligned} V_{\mathrm{ex}} &= b_{\mathrm{xv}} \sum_i^L N_i v_i = b_{\mathrm{xv}} \sum_i^L N_i (n_i^1 v_1 + n_i^2 v_2) \\ &= b_{\mathrm{xv}} (v_1 N_1^{\mathrm{tot}} + v_2 N_2^{\mathrm{tot}}), \end{aligned} \tag{2.26}$$

where v_1 and v_2 are the cluster volumes of the components 1 and 2, respectively, and b_{xv} is a dimensionless empirical parameter needed to correctly scale the particle volumes. This scaling is required due the high sensitivity of cluster volume schemes to the choice of atomic radii.[96] In Eq. 2.26 the translation partition function can be extended as

$$q_i^{\mathrm{trans}} = \frac{V - b_{\mathrm{xv}}(v_1 N_1^{\mathrm{tot}} + v_2 N_2^{\mathrm{tot}})}{\Lambda^3}. \tag{2.27}$$

Now all the pieces needed to fully describe the cluster gas are given. At this point, the partition function must be calculated in order to get meaningful thermodynamic data. To achieve this goal, all the independent quantities that characterize the canonical ensemble, as well as the empirical parameters, must be known. a_{mf} and b_{xv} are optimized to minimize the deviation of the bQCE results from experimental references, typically density and boiling points. In order to determine the independent quantities $(\{N_i\}, V, T)$, the canonical ensemble condition that requires the conservation of the particle numbers,

will be considered:

$$N_1^{\mathrm{tot}} + N_2^{\mathrm{tot}} = \sum_i^L (n_i^1 + n_i^2) N_i,$$
$$0 = \sum_i^L \frac{(n_i^1 + n_i^2) N_i}{N_1^{\mathrm{tot}} + N_2^{\mathrm{tot}}} - 1 = \sum_i^L \tilde{N}_i - 1, \tag{2.28}$$

where $\tilde{N}_i$ is the normalized cluster population of the component i. It is important to notice that the exclusion volume does not introduce any population dependency to the cluster equilibrium function. The second condition of the canonical ensemble is now applied, which states that the system must be in thermodynamic equilibrium, and any infinitesimal change in the population of any cluster i cannot effect the free energy:

$$0 = \sum_i^L n_i^a \, \frac{\partial F}{\partial N_1} \, d\lambda \; + \; \sum_i^L n_i^b \, \frac{\partial F}{\partial N_2} \, d\lambda \; - \; \sum_i^L \frac{\partial F}{\partial N_i} \, d\lambda; \tag{2.29}$$

in this equation $d\lambda$ has the meaning of the reaction's progression. This condition must be fulfilled for every $d\lambda$ and for each cluster independently. Therefore, it is possible to simplify Eq. 2.29 as

$$\frac{\partial F}{\partial N_i} = n_i^1 \, \frac{\partial F}{\partial N_1} + n_i^2 \, \frac{\partial F}{\partial N_2}. \tag{2.30}$$

Recalling Eq. 2.22 and considering

$$\ln Q = \ln \left(\prod_i^L \frac{1}{N_i!} q_i^{N_i} \right) = \sum_i^L \left(N_i \ln q_i - \ln N_i! \right), \tag{2.31}$$

it is possible to rearrange Eq. 2.30 to

$$\frac{\partial}{\partial N_i} \sum_i^L (N_i \ln q_i - \ln N_i!) = n_i^1 \left(\frac{\partial}{\partial N_1} \sum_i^L (N_i \ln q_i - \ln N_i!) \right)$$
$$+ n_i^2 \left(\frac{\partial}{\partial N_2} \sum_i^L (N_i \ln q_i - \ln N_i!) \right). \tag{2.32}$$

Applying the Stirling approximation*, it is possible to solve these differential equations

*$\ln(n!) \approx n \cdot \ln(n) - n$

to directly express the relationship between the total cluster population and the monomer populations as:

$$\ln \frac{q_i}{N_i} = n_i^a \ln \frac{q_1}{N_1} + n_i^b \ln \frac{q_2}{N_2},$$
$$N_i = q_i \left(\frac{N_1}{q_1}\right)^{n_i^1} \left(\frac{N_2}{q_2}\right)^{n_i^2}. \tag{2.33}$$

The problem is now reduced from finding the whole set of cluster populations to determine only the ones of the neat components. By including Eq. 2.33 into Eq. 2.28 we get the so-called population polynomials,

$$0 = \sum_i^L \frac{n_i^a + n_i^b}{N_1^{\text{tot}} + N_2^{\text{tot}}} \cdot q_i \left(\frac{N_1}{q_1}\right)^{n_i^a} \left(\frac{N_2}{q_2}\right)^{n_i^b} - 1, \tag{2.34}$$

which is one of the key equations of the bQCE theory. For neat systems it can be solved easily to find the monomer population N_1, since $N_2^{\text{tot}} = 0$ and $n_i^2 = 0$. This is not the case for a binary system, where another condition must be defined in order to obtain the two populations N_1^{tot} and N_2^{tot}. This additional equation used in the bQCE theory is the conservation of mass:

$$M_1 N_1^{\text{tot}} + M_2 N_2^{\text{tot}} = \sum_i^L (n_i^1 M_1 + n_i^2 M_2) N_i,$$
$$0 = \sum_i^L \frac{n_i^1 M_1 + n_i^2 M_2}{M_1 N_1^{\text{tot}} + M_2 N_2^{\text{tot}}} N_i - 1, \tag{2.35}$$

where M_1 and M_2 are the molecular masses for the components 1 and 2, respectively. As for the population, a so-called mass polynomial in the form of

$$0 = \sum_i^L \frac{n_i^a M_1 + n_i^b M_2}{M_1 N_1^{\text{tot}} + M_2 N_2^{\text{tot}}} \cdot q_i \left(\frac{N_1}{q_1}\right)^{n_i^a} \left(\frac{N_2}{q_2}\right)^{n_i^b} - 1 \tag{2.36}$$

can be defined. This non-linear system of equations is solved employing the Newton-Raphson algorithm.[97] If the volume is given, these equations are sufficient to calculate the partition function of the system at any temperature. However, the volume is obtained from the cluster populations as an intrinsic property. Considering the calculation of the

pressure p from the partition function:

$$\begin{aligned} p &= -\frac{\partial F}{\partial V}, \\ 0 &= -p + k_\mathrm{B}T \, \frac{\partial \ln Q}{\partial V}, \end{aligned} \tag{2.37}$$

only the electronic and translational partition function are volume dependent, so the other partition functions disappear when a partial differentiation of Eq. 2.37 with respect to the volume is carried out. As a result, the so-called volume polynomial reads

$$\begin{aligned} 0 = &- pV^3 + \left(\sum_i^L k_\mathrm{B}T N_i + p\, b_\mathrm{xv}(v_1 N_1^\mathrm{tot} + v_2 N_2^\mathrm{tot}) \right) V^2 \\ &- \left(\sum_i^L N_i (n_i^1 + n_i^2) a_\mathrm{mf} \right) V \\ &+ \sum_i^L N_i (n_i^1 + n_i^2) a_\mathrm{mf} \cdot b_\mathrm{xv}(v_1 N_1^\mathrm{tot} + v_2 N_2^\mathrm{tot}). \end{aligned} \tag{2.38}$$

Since the cluster population must be known to solve Eq. 2.38 with respect to the volume, and it must be known to solve the population polynomial in Eq. 2.34, the equations are solved iteratively. The first step consist in solving the population polynomial with a starting guess for the volume. As convergence criterion, the absolute difference in the Gibbs energy $|\Delta G|$ is used. In the case of multiple solutions (V,$\{N_i\}$) the one that minimizes the Gibbs energy is selected:

$$G = -k_\mathrm{B}T \ln Q + V k_\mathrm{B}T \, \frac{\partial \ln Q'}{\partial V}\,. \tag{2.39}$$

More thermodynamic functions, such as the inner energy U, the enthalpy H, and the entropy S can be derived as:

$$U = k_\mathrm{B}T^2 \, \frac{\partial \ln Q}{\partial T}, \tag{2.40}$$

$$H = U + pV = k_\mathrm{B}T^2 \, \frac{\partial \ln Q}{\partial T} + V k_\mathrm{B}T \, \frac{\partial \ln Q}{\partial V}, \tag{2.41}$$

$$S = \frac{U - F}{T} = k_\mathrm{B}T \, \frac{\partial \ln Q}{\partial T} + k_\mathrm{B} \ln Q. \tag{2.42}$$

2.2.3. Peacemaker2

The bQCE theory is implemented in the open-source code PEACEMAKER 2, publicly available under the GNU general Public License.[3] The code is written in Fortran 2008, and it does not make use of external libraries with the exception of Townsend's varying string module,[98] under GNU Lesser General Public License. The cluster set is written in an input file, where for each cluster the geometry, adiabatic binding energy, and vibrational frequencies are listed. In a second input file, the temperature range and pressure are defined by the user. Other instructions, and the experimental reference data to optimize the bQCE calculation can be included in this file, if necessary. The user can either specify the empirical parameters a_{mf} and b_{xv} in the input file or define a grid to obtain them through stepwise sampling. In the latter case, the sampling is based on the experimental reference data of densities, volumes, and boiling points. An additional strategy is introduced in Chapter 4 of this thesis, consisting in the definition of a linear dependence of b_{xv} on the temperature:

$$b_{\mathrm{xv}}(T) = T \cdot \beta_{\mathrm{xv}} + b^0_{\mathrm{xv}}. \tag{2.43}$$

Here, β_{xv} is the exclusion volume expansion coefficient and b^0_{xv} is the ideal value of the parameter at 0 K. Since the grid sampling algorithm cannot be used with the inclusion of this additional parameter, the Differential Evolution algorithm[99] implemented in the SciPy library[100] for PYTHON 3.4 is interfaced with the PEACEMAKER code. The PEACEMAKER 2 code follows the following steps (in the main iteration the parameters are kept constant):

1. the initial volume $V^0 = V$ is estimated from the ideal gas law.

2. All the cluster partition functions q_i are calculated at the phase volume V and temperature T for all clusters P_i.

3. The cluster distributions $\{N_i\}$ are determined solving the polynomial population described in Eq. 2.34.

4. From $\{N_i\}$, a new phase volume V is obtained from the volume polynomial of Eq. 2.38.

5. The relative change in the Gibbs energy is used as convergence criterion. If $\Delta G > \varepsilon_G$, the code returns to Step 2.

6. If multiple solutions $[\{N_i\}, V]$ exist, the one that minimizes the Gibbs energy is chosen.

This procedure is repeated for every temperature in the specified temperature range. At every new T, the volume obtained in the previous cycle is used as a starting guess. To prevent meta-stable solutions, the PEACEMAKER 2 main iteration is repeated two times at any given temperature; the first one accounts for the so-called gas phase interaction, while the second accounts for the liquid phase interaction.[65] In the first one the ideal gas volume V^{id} is used as initial volume guess and the mean-field parameter a_{mf} is set to 0, to cancel all inter-cluster interactions. The liquid phase iteration uses instead $V^0 = V^{\mathrm{id}}/100$ as initial volume guess and keeps the a_{mf} parameter constant. The solution with the lowest Gibbs energy is chosen if both iterations converge; this allows PEACEMAKER 2 to model a realistic phase transition. If experimental reference data are provided, PEACEMAKER 2 will compare the QCE results to the available reference. As experimental input PEACEMAKER 2 can accept an isobar of the molar volume V, a density ρ at a specific temperature, a boiling point temperature T_{b}, or any combination of them. PEACEMAKER 2 calculates the error as difference between the QCE results and the experimental data. During the parameter sampling, PEACEMAKER 2 (or the Python external script, in the modification described in Chapter 4) will use this error as criterion to determine the best values for the empirical parameters. The error equation reads

$$\mathrm{error} = w_\rho \left(\frac{\rho - \rho^{\mathrm{exp}}}{\rho^{\mathrm{exp}}} \right)^2 + w_V \frac{1}{N} \sum_{i=1}^{N} \left(\frac{V_i - V_i^{\mathrm{exp}}}{V_i^{\mathrm{exp}}} \right)^2 + w_T \left(\frac{T_{\mathrm{b}} - T_{\mathrm{b}}^{\mathrm{exp}}}{T_{\mathrm{b}}^{\mathrm{exp}}} \right)^2, \tag{2.44}$$

where w_ρ, w_V, and w_T are weighting parameters for the individual errors of density, isobar, and boiling point, respectively, and N is the number of volumes V_i included in the isobar; these weighting parameters are set to 1 by default, but can be changed by the user.

2.3. Principles of Classical Molecular Dynamics

Molecular dynamics (MD) is a computational method to describe the physical motion of particles, usually atoms or molecules. In the classical MD, the Newton's equation of motion is solved to describe the equilibrium, structure, and various properties of a many-body system. The main advantage of this method lies in the velocity of the calculation and the relatively small computational cost even when a large number of particles are included. At the same time, this method is strongly dependent on parameters fitted on empirical data. For this reason only well-known and established models are reliable to make good predictions about the system investigated. The classical equation of motion reads:

$$\mathbf{f_i} = m_i \mathbf{a}, \tag{2.45}$$

where $\mathbf{f_i}$ is the force acting on the particle i with mass m_i and acceleration $\mathbf{a}$. At the same time the force is related to the potential energy of the system (U) by the following relation:

$$\mathbf{f_i} = -\frac{\partial U}{\partial r_i} \tag{2.46}$$

with r_i being the position of the particle i. What has been described so far is related to a simple system of one particle. In a system with N particles, the potential energy is a function of r^{3N}, which denotes the $3N$ coordinates necessary to define the system. In the classical molecular dynamics, $U(r^{3N})$ is described by a force-field defined by empirical parameters. Usually, a force field has the form of a functional that includes terms for covalent bonds and non-bonded interactions. Hence, there are two main components of the potential energy of the system: one describes the intramolecular (bonded, U_b), and the other one the intermolecular (non-bonded, U_nb) contributions. The bonded part can itself be written as a sum of smaller terms as:

$$U_b = U_{bonds} + U_{angles} + U_{dihedral} + U_{improper}, \tag{2.47}$$

where U_{bonds} describes the stretches of the bond, U_{angles} the angle flexing, $U_{dihedral}$ the torsional rotations, and $U_{improper}$ the improper interactions.

The unbonded potential energy of the force fields considered in this thesis take into account only the two-body interactions – i.e. the pair potential –, since three body and higher terms are expensive to calculate. The pair potential used in this thesis takes the form of a Lennard-Jones potential, and it reads

$$v^{LJ} = 4\epsilon \left[\left(\frac{\sigma}{r} \right)^{12} - \left(\frac{\sigma}{r} \right)^{6} \right], \tag{2.48}$$

where ϵ is the well depth, σ the diameter and r the pair-wise distance. The electrostatic interaction is calculated using the Coulomb potential

$$v^{Coulomb}(r) = \frac{q_1 q_2}{4\pi\epsilon_0 r}, \tag{2.49}$$

where q_1 and q_2 are the charges of the two interacting particles, and ϵ_0 is the permittivity in the void.

In the classical molecular dynamics, the atoms are treated by means of classical mechanics and the electronic energy is described only by a parametric function depending solely on the atomic position. The parameters are usually fitted to experimental references or to data obtained at higher level of theory. Each atoms is assigned an atom type that depends mainly on the atomic number, the atom mass and the type of chemical bond they are involved in. All the force fields used in this thesis are "all-atoms", which means that all atoms in the system are parameterized, and not grouped together. The explicit functional form can differ greatly between force fields. In this thesis the OPLS-AA force field[101] has been used in Chapter 4. The OPLS-AA force field functional reads

$$\begin{aligned} E_{\mathbf{tot}}^{\text{OPLS-AA}} = & \sum_{\mathbf{bonds}} K_r (r - r_0)^2 + \sum_{\mathbf{angles}} K_\theta (\theta - \theta_0)^2 \\ & + \sum_{\mathbf{dihedrals}} \sum_{n=1}^{4} \frac{\mathcal{V}_{\phi,n}}{2} [1 + (-1)^n \cos(n\phi)] \\ & + \sum_{i<j} \left\{ 4\epsilon_{ij} \left[\left(\frac{\sigma_{ij}}{r_{ij}} \right)^{12} - \left(\frac{\sigma_{ij}}{r_{ij}} \right)^{6} \right] + \frac{q_i q_j}{\varepsilon r_{ij}} \right\}. \end{aligned} \tag{2.50}$$

In both chapters 3 and 4, the AMBER[102] force field has been interfaced with the

OGOLEM genetic algorithm,[103,104] which relies on the force-field-based description of the molecular interactions. The AMBER force functional is generally represented by:

$$E_{\mathbf{tot}}^{\mathrm{AMBER}} = \sum_{\mathbf{bonds}} K_r(r - r_0)^2 + \sum_{\mathbf{angles}} K_\theta(\theta - \theta_0)^2 + \sum_{\mathbf{dihedrals}} \mathcal{V}_\phi[1 + d\cos(n\phi)] + \sum_{i<j} \left\{ 4\epsilon_{ij} \left[\left(\frac{\sigma_{ij}}{r_{ij}} \right)^{12} - \left(\frac{\sigma_{ij}}{r_{ij}} \right)^{6} \right] + \frac{q_i q_j}{\varepsilon r_{ij}} \right\}. \tag{2.51}$$

In both force field expressions, K is the force constant, r_0 and θ_0 are the reference values, $\mathcal{V}$ is the Fourier coefficient, d and n are prefactors. To obtain the parameters describing the interaction of the atoms i and j (σ_{ij} and ϵ_{ij}), different mixing rules can be applied—e.g. the Lorentz–Berthelot mixing rules—[105,106]employed in this thesis. Both the force fields describe the stretching and bending of bonds employing the harmonic expressions, while the non-bonded interactions are described using Lennard-Jones and Coulomb electrostatic potentials. The torsional energy of the dihedrals is instead treated differently by the two fuctionals. In the OPLS-AA framework, it is possibile to consider up to $n = 4$ different energy profiles, while in the AMBER functional only one contribution is allowed. It can be noticed, for simple torsion energy profiles (no combination), both frameworks will provide the same dihedral energy term.

In this thesis, the AMBER force field has been used to generate a first guess of molecular cluster set for bQCE application, has described in both chapters 3 and 4. Classical molecular dynamics calculations, using the OPLS-AA force field, have been carried out in Chapter 4. The calculated densities at different temperatures has been then employed as reference data for following bQCE calculations.

3. Activity Coefficients of Binary Methanol Alcohol Mixtures

Reprinted (adapted) with permission from
G. Marchelli, J. Ingenmey and B. Kirchner ChemistryOpen, **2020**, *9*,,7, 774-785

DOI: 10.1002/open.202000171

Contributions to the manuscript

- Performing the QM calculations and making the analysis of all the systems.
- Discussing of the results.
- Writing the manuscript.

Summary

In the following chapter, the bQCE theory is used to investigate the thermodynamic properties and hydrogen bond network of small alcohols mixtures. In particular, the authors focus on the binary mixtures of methanol with other alcohols with the aliphatic carbon chain ranging in length from two to four atoms, taking branching into account. The scope of this investigation is to understand how the chain length and the branching of these compounds can affect their properties. This is particularly relevant as these effects play an important role in different fields, especially in the extraction of solvents or metals in the liquid phase.[107] Due to the large number and size of the clusters considered for the bQCE calculations, the semi-empirical method GFN2-xTB[91,92] has been used for the geometry optimization and frequencies calculations. This method has been used in the past and has been proven to lead to reliable results even if it is at a low level of theory, with the advantage of the small computational cost, which allows to optimize a great number of clusters. In this study, dimer clusters are calculated also at DFT level of theory, and the hydrogen bond length, angles, and interaction energies are compared between the different methods and functionals. The interaction energies – normalized on the number of monomers – are presented for neat systems of increasing cluster size, and their trend is compared both by chain weight and branching. The cooperativity of pure methanol and *n*-butanol is presented with respect to the increasing cluster size. After these analyses based on quantum chemical calculations, the clusters optimized at semi-empirical level of theory are used as input for the bQCE calculations. For this step, the Peacemaker 2.8 code was used. The cluster populations and the thermodynamic properties are calculated and presented; in particular, the Gibbs energy of mixing at a temperature of 298.15 K and pressure of 1 atm is shown for all the binary systems. The activity coefficients of methanol in each solvent—and vice-versa—are calculated from the excess Gibbs energy of mixing. The activity coefficients give an indication of the deviation from ideality of the mixtures. Finally, combined distribution functions of the distances against the angles of the hydrogen bonds are calculated for both neat and mixed clusters, using the same cluster set used for the bQCE calculations, and weighting each cluster by the equilibrium population employed. In conclusion, increasing the chain length of the alcohol, a larger

deviation from ideality is noticeable; the presence of branching, on the other hand, leads to a mixture closer to ideality.

Activity coefficients of binary methanol alcohol mixtures from cluster weighting

Gwydyon Marchelli* Johannes Ingenmey*

Prof. Dr. Barbara Kirchner*

Received: 07 June 2020, Revised: 16 June 2020, Published: 23 July 2020

3.1. Abstract

The hydrogen bond network of different small alcohols is investigated via cluster analysis. Methanol/alcohol mixtures are studied with increasing chain length and branching of the molecule. Those changes can play an important role in different fields, including solvent and metal extraction. The extended tight binding method GFN2-xTB allows the evaluation and geometry optimization of thousands of clusters built via a genetic algorithm. Interaction energies and geometries are evaluated and discussed for the neat systems. Thermodynamic properties, such as vaporization enthalpies and activity coefficients, are

* Mulliken Center for Theoretical Chemistry, Rheinische Friedrich-Wilhelms-Universität Bonn, Beringstr. 4+6, D-53115 Bonn, Germany

calculated with the binary quantum cluster equilibrium (bQCE) approach using our in-house code PEACEMAKER 2.8. Combined distribution functions of the distances against the angles of the hydrogen bonds are evaluated for neat and mixed clusters and weighted by the equilibrium populations achieved from bQCE calculations.

3.2. Introduction

Aliphatic alcohols are readily accessible low cost solvents, which are easy to extract and recover. Due to those properties their applications are considered and investigated in different fields such as alternative fuel production, solvometallurgy, hydrometallurgy, and solvent extraction. A potential extraction solvent must meet many criteria for a successful implementation, such as extraction performance, chemical stability, solvent regeneration, safety, and low environmental risk.[107–111] Since they well match those criteria, for a long time, alcohols have been used to extract different metal ions. For example, Co(II) and Tl(I) chelat complexes are easily extracted by aliphatic alcohols in aqueous solvents.[110] Indium forms a chelat with pyridylazonaphthol that can be extracted by butyl and pentyl alcohols.[111] Gold(I) can be extracted from cyanide solutions such as $Au(CN)_2$ by various alcohols.[111] Vanadium and Niobium can be extracted from n-octanol.[112] Aliphatic alcohols are also known for their applications in the field of liquid/liquid solvent extractions.[107,109] There is evidence in literature, that the branching of an alcohol as well as the location of the hydroxyl group within the molecule does affect the extraction's capacity.[107,113,114] If the branching of an alcohol is increased while the molecular weight stays constant, it was found that the separation factor increases as well.[107]

Offeman *et al.*[107] proved that the position of the hydroxyl group, as well as the branching and chain length are important parameters that affect the ethanol extraction performance. From these considerations, it can be seen that the size and branching of alcohols affect their properties as hydrogen bond donors/acceptors. It is fundamental to understand how the hydrogen donor effect is related with the molecular configuration of alcohols.

Infrared and Raman spectroscopy were used to investigate the hydrogen network in alcohols and how it is affected by the alcohol's branching. Both experimental and quantum

mechanical techniques were employed.[115–117]

Fourier transform microwave spectroscopy has been used in the past to investigate clusters of simple alcohols. In particular, many works investigated chiral dimers of methanol, ethanol, propanol, and butanol.[118–122] These works found that the possible conformations of alcohol dimers involve significant dispersion interactions.

Classical molecular dynamics simulations[123] and Monte Carlo simulations[124] have been performed in the past, in order to investigate the hydrogen bond networks formed in different linear and branched alcohols. The results have shown systematic differences in their hydrogen-bonded structures, depending both on hydroxyl group position and the molecular weight.

The hydrogen bond network of alcohols was investigated in the past with quantum mechanical approaches. Many works on this topic are present in literature, for instance, the conformation of 1-butanol in the liquid phase was already studied in 1994 by Ohno *et al.*,[125] wherein they demonstrated the importance of taking into account different conformations. The donor/acceptor configuration was investigated by Finneran *et al.*[126] for the ethanol/methanol dimer. Rowley *et al.*[127] analyzed the potential surface of many small alcohols, and Vargas *et al.*[128] showed how the global minimum of the ethanol dimer is stabilized by the hydrogen bond.

An alternative approach to face the challenge is based on the binary quantum cluster equilibrium (bQCE) theory.[4,45,65] bQCE is an extension of Weinhold's quantum cluster method for pure liquids[27,42,129–131] and has been successfully applied to predict the miscibility of binary mixtures, the ionic product of water, activity coefficients, and mole fraction dependent dissociation for weak acids.[4,74,75,132,133]

By applying models of statistical thermodynamics to quantum chemically calculated clusters, the thermodynamic description of neat liquids and their mixtures at non-zero temperature and pressure is possible in the condensed and gaseous phase. Self-consistent-field calculations lead to equilibrium populations of these clusters and thus an ensemble of different structural states is generated similar to molecular dynamics simulations.[45,65,129] A first step in order to study hydrogen bond donor/acceptor systems was done by Brüssel *et al.* investigating the dimethyl sulfoxide/water system.[45] Later, Matisz *et al.* were

the first to study the binary methanol/water system.[78] They found that cubic and spiro clusters are the dominant motifs in the mixed phase. Studies on methanol found that the liquid phase is formed mainly by cyclic ring structures.[60–62] Liquid ethanol was found to be comprised mainly of the monomer, cyclic tetramer, and cyclic pentamer.[134]

From the quantum cluster approach we are able to evaluate the activity coefficients of binary mixtures.[4] Those values are needed to determine phase equilibria,[135,136] and they are directly related to different phenomena, such as vapor pressure lowering and freezing point depression.[135,136] Activity coefficients are a convenient indicator for the deviation from ideal behavior[137] and their theoretical determination is desirable, since in many cases they are not easily accessible experimentally. In particular, activity coefficients can be an important tool in the investigation and design of novel solvent mixtures. One example are deep eutectic solvents (DES),[138] which since the beginning of last decade generated great interest[139] and find a wide range of applications, such as metal extraction processes.[10]

In this article, we apply the quantum cluster approach to binary mixtures of methanol with different alcohols. In particular, we investigate the effect of molecule size and branching on the deviation from ideal behavior for small size alcohols (one to four carbon atoms). Our methodology can be found in the appendix, including details on the theoretical derivation of the binary quantum cluster equilibrium approach and the properties obtained from it, the computational details, and the generation of cluster sets.

3.3. Results and Discussion

Here, a large range of alcohols and their binary mixtures with methanol are investigated. The alcohols are chosen considering two factors: the number of carbon atoms (ranging from two to four) and the branching. Hence, both propanol isomers, *n*-propanol and *iso*-propanol, are considered as well as three isomers of butanol, namely *n*-, *iso*-, and *tert*-butanol. Figure 3.1 shows a selection of clusters used in this work. Displayed are methanol clusters at different cluster sizes, dimers of all neat alcohols, and a set of mixed methanol/*iso*-propanol clusters with different compositions. In total, 5760 cluster structures where quantum chemically optimized, and subsequently 1144 of them where selected

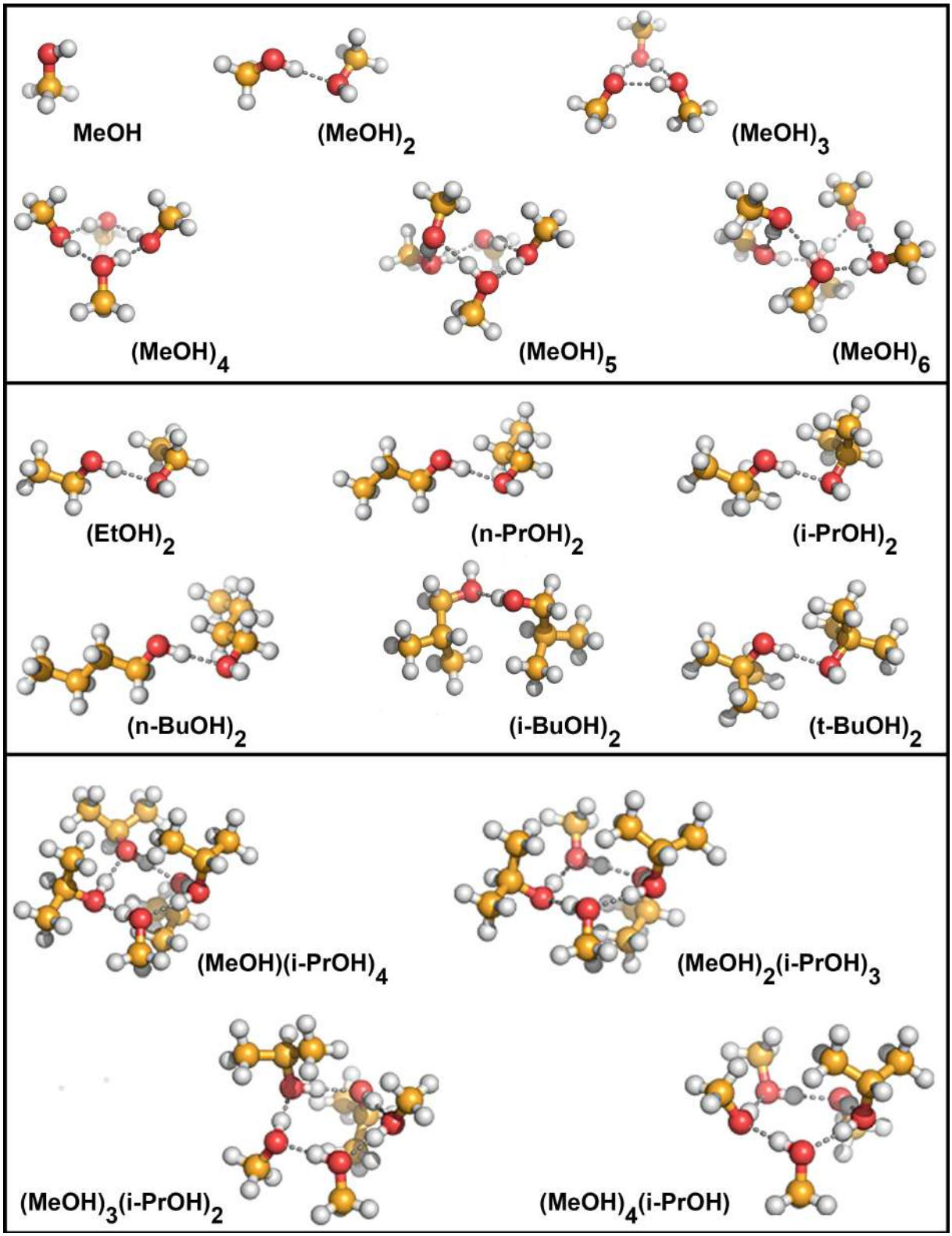

Figure 3.1. Ball-and-stick models of some selected clusters. Top: methanol clusters at the size of 1–6 molecules. Center: Dimer geometries of the different alcohols. Bottom: Mixed methanol/*iso*-propanol pentamers at different compositions. Please note that this selection shows only a small excerpt of all 1144 clusters.

by geometric and vibrational criteria (see the appendix for further explanations of the selection methodology). The binary mixture methanol/ethanol was already studied with the quantum cluster approach in an earlier work.[4]

Our results are mainly obtained via the extended tight binding method GFN2-xTB[91] (henceforth called xTB, see the appendix for details), which includes the D4 dispersion correction[94,95] accounting for the London dispersion energy and is an improved revision of the GFN-xTB method,[92] which we successfully employed for the calculation of activities and vaporization enthalpies in the past.[4] xTB is a highly efficient method optimized for the calculation of geometries, vibrational frequencies, and noncovalent interactions, allowing the evaluation of thousands of cluster conformations which would not be feasible on DFT level. Additionally, xTB was found to perform well at computing the interaction energies of hydrogen-bonded water clusters, outperforming even some GGA and hybrid DFT functionals such as BLYP and PBE0.[91] Hence, we find this method is optimally suited for our approach.

3.3.1. Hydrogen Bond Analysis

Cluster Analysis

Here, we will consider the interaction energy per monomer $\Delta_{\text{int}}\bar{E} = \Delta_{\text{int}}E/n$, where $\Delta_{\text{int}}E$ is the total adiabatic interaction energy in a cluster of the size of n molecules. Figure 3.2 shows the averaged interaction energies $\Delta_{\text{int}}\bar{E}$ plotted against the cluster size n for the neat alcohols, as obtained from xTB. This average is taken from up to ten clusters per cluster size. The exact numbers of clusters per cluster size are included in the supporting information.

In the case of the linear systems, depicted in the left panel, an increase in the cluster size leads to stronger (i.e. lower) interaction energies per monomer. In the middle panel *n*-propanol and *iso*-propanol are compared, but no particular differences are present. The right panel shows the different isomers of butanol investigated in this article. Whereas less stable in the case of the dimer, increasing the cluster size, the unbranched alcohol has slightly lower interaction energies compared to its more branched isomers. Table 3.1 shows the interaction energies of the global minimum methanol and *n*-butanol clusters

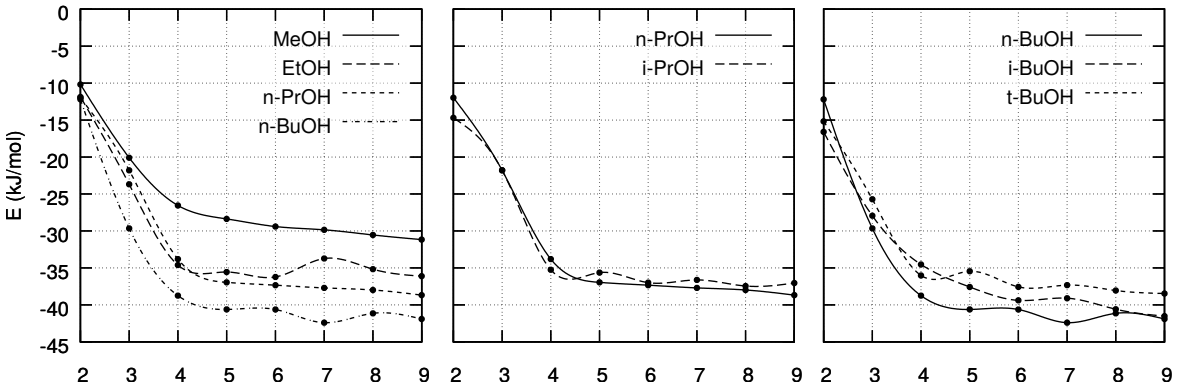

Figure 3.2. Interaction energy $\Delta_{\text{int}}\bar{E}$ per monomer for the neat alcohols, averaged over multiple geometries at each cluster size. The left panel shows the effect of increasing chain length, the center and right panels display the effect of branching. Lines are meant to guide the eye.

in more detail, along with the dispersion energy $\Delta_{\text{disp}}\bar{E}$ and remaining energy $\Delta_{\text{rem}}\bar{E}$ where $\Delta_{\text{int}}\bar{E} = \Delta_{\text{disp}}\bar{E} + \Delta_{\text{rem}}\bar{E}$. The set of global minimum structures of methanol is displayed in Fig. 3.1. Again, we can observe that $\Delta_{\text{int}}\bar{E}$ increases with the cluster size. With each additional molecule there's a gain in interaction strength that can be attributed to cooperativity effects, calculated as coop. $= \Delta_{\text{int}}\bar{E}_n/\Delta_{\text{int}}\bar{E}_{n-1}$ where $\Delta_{\text{int}}\bar{E}_n$ is the average interaction energy per monomer in a cluster of size n. This cooperative gain decreases rapidly and seems to be mostly saturated at a cluster size of four molecules. In comparison, whereas $\Delta_{\text{rem}}E$ is of similar size in methanol and n-butanol, dispersion forces are considerably stronger in the latter. While smaller in magnitude, $\Delta_{\text{disp}}E$ levels out less rapidly than $\Delta_{\text{rem}}E$ and benefits from cooperative effects even in larger clusters.

Table 3.2 lists the interaction energies of the global minimum structures of $(\text{ROH})_2$ dimers, in order to compare the performance of xTB against GGA methods. The complete list of interaction energies $\Delta_{\text{int}}E$ of all the 1144 clusters are given in the supporting information. The interaction energies obtained via the xTB method are compared to those obtained from single point calculations on the same geometries employing DFT methods, namely the GGA functional BP86 and the hybrid functional B3LYP. Overall, xTB interaction energies are weaker for unbranched alcohols and stronger for branched ones with respect to the DFT methods energies. Nevertheless, the trends are similar.

Table 3.1. Average interaction energies $\Delta_{\text{int}}\bar{E}$, remaining energies $\Delta_{\text{rem}}\bar{E}$, and dispersion energies $\Delta_{\text{disp}}\bar{E}$ per molecule in kJ/mol for the global minimum of methanol and n-butanol clusters of size n, as obtained on the xTB level of theory, as well as the relative cooperative gain in %.

	Methanol				n-Butanol			
n	$\Delta_{\text{int}}\bar{E}$	$\Delta_{\text{disp}}\bar{E}$	$\Delta_{\text{rem}}\bar{E}$	coop.	$\Delta_{\text{int}}\bar{E}$	$\Delta_{\text{disp}}\bar{E}$	$\Delta_{\text{rem}}\bar{E}$	coop.
2	-10.2	-1.7	-8.8		-12.2	-5.4	-6.8	
3	-20.0	-3.4	-16.9	97.5	-30.6	-8.6	-22.0	150.7
4	-26.8	-4.2	-22.6	33.4	-38.8	-12.8	-26.0	26.7
5	-28.5	-5.5	-23.0	6.1	-40.6	-13.9	-26.8	4.8
6	-29.5	-5.9	-23.6	3.7	-41.0	-15.8	-25.2	1.0
7	-30.2	-6.2	-23.9	2.3	-42.8	-15.4	-27.4	4.3
8	-31.4	-6.4	-25.0	4.0	-41.8	-16.4	-25.4	-2.4
9	-31.3	-7.0	-24.3	-0.3	-42.3	-18.2	-24.1	1.3

Regardless of the method, the lowest and highest interaction energies are found for i-BuOH and MeOH, respectively.

The differences in interaction energies become less pronounced for the mixed dimers formed by methanol and an additional alcohol, listed in Table 3.2. Increasing the branching of the molecule, the differences between the methods become smaller. The intermolecular hydrogen-oxygen distances and the complementary O-H$\cdots$O angle within the dimers are listed in Table 3.3, for both xTB and BP86 optimized geometries. Overall, the distances are in good agreement, whereas the angles are slightly different. In the following, we will focus on our xTB results, exclusively, based on the 1144 calculated clusters optimized on that level. We observe that xTB can reproduce energetic and geometric features with sufficient accuracy and find that the ability to quantitatively evaluate a wide range of potential cluster geometries justifies the use of this method. Results obtained via the GGA method BP86 are available in the supporting information.

Increasing either chain length or branching of the molecule, the interaction energy is decreasing, both for the mixed methanol/alcohols dimers and the pure systems. No similar trend is observed for the hydrogen bond distance and angle. Nevertheless, the methanol dimer shows both a larger distance and wider angle as compared to the other dimers. The

Table 3.2. Interaction energies $\Delta_{\text{int}}E$ (kJ/mol) of alcohol dimer geometries optimized at xTB level, as obtained from single point calculations at different levels of theory. The energies correspond to the global minimum geometries of the pure ROH-ROH and mixed MeOH-ROH dimers.

	$\Delta_{\text{int}}E$(ROH-ROH)			$\Delta_{\text{int}}E$(MeOH-ROH)		
ROH	xTB	BP86	B3LYP	xTB	BP86	B3LYP
MeOH	-20.4	-22.7	-23.8	–	–	–
EtOH	-23.8	-26.1	-27.4	-23.9	-25.8	-27.1
n-PrOH	-24.0	-26.6	-27.7	-23.9	-26.1	-27.4
i-PrOH	-29.4	-27.3	-28.4	-27.5	-27.4	-28.4
n-BuOH	-24.4	-27.0	-28.1	-24.2	-26.5	-27.7
i-BuOH	-33.8	-28.1	-28.8	-24.7	-26.0	-27.3
t-BuOH	-30.4	-27.5	-28.7	-27.8	-27.8	-28.8

iso-propanol containing dimers show a wider hydrogen bond angle compared to the other alcohols except methanol. The *tert*-butanol containing dimers show the widest angle of the investigated butanol isomers. The hydrogen bond distance of 188.8 pm in the neat ethanol dimer is lower than the literature value of 191.0 pm found by Vargas *et al.*[128] This difference can be imputed to the different level of theory. Nevertheless, both results are in acceptable agreement. The distance of 189.6 pm in the neat methanol dimer is in good agreement with the MP2 value of 187.2 pm reported by Provencal *et al.*[140]

Population-weighted Analysis

In earlier works, we presented sophisticated methods for detecting and quantifying hydrogen bonds.[141,142] From a geometrical perspective, hydrogen bonds are often characterized by their length and angle.[140,143] Different bond lengths and angles can bring to light distinct behaviors of the investigated species forming the hydrogen bonds. For this reason, we show combined distribution functions (CDF) of the different alcohols, constructed from the intermolecular hydrogen-oxygen distances and the angular distribution of the complementary O-H$\cdots$O angle. Since our cluster sets not only include global minimum structures but also those more distant from the enthalpically optimal binding situation, by combining the collected data of all investigated clusters, in total 1144, and weighting

Table 3.3. Hydrogen bond distances r (pm) and the complementary O-H$\cdots$O angles α (°) of geometry optimized dimer structures at xTB and BP86 level of theory. The distances and angles correspond to the global minimum geometries of the pure ROH-ROH and mixed MeOH-ROH dimers.

	Pure dimers ROH-ROH				Mixed dimers MeOH-ROH			
	r(xTB)	r(BP86)	α(xTB)	α(BP86)	r(xTB)	r(BP86)	α(xTB)	α(BP86)
MeOH	189.6	190.1	9.3	7.6	–	–	–	–
EtOH	188.7	189.2	2.4	10.7	188.4	189.2	2.3	10.2
n-PrOH	188.3	188.8	2.4	10.4	182.2	189.1	1.8	10.0
i-PrOH	188.0	190.1	6.1	13.2	186.2	188.8	7.8	12.3
n-BuOH	188.7	189.0	3.0	10.7	188.4	189.2	1.5	9.7
i-BuOH	190.0	189.6	1.9	6.7	188.0	189.1	0.3	10.3
t-BuOH	187.9	190.1	4.5	14.2	185.5	188.0	6.5	12.4

them by their bQCE populations (see appendix for method), we obtain CDFs similar in appearance to those of a MD simulation. Through the weighting by population, these CDFs are accessible for any temperature and pressure investigated in the bQCE calculation. Here, we investigate methanol, ethanol, *n*-butanol, and *tert*-butanol in order to include both linear and branched alcohols. For all of them, the complete cluster set is analyzed with our in-house trajectory analysis code TRAVIS;[144] then, the data of each cluster is collected and weighted by the cluster population at 298.15 K, as obtained by bQCE calculations.

In Fig. 3.3 the CDFs of the neat systems are reported. The color scale is relative and referenced to the maximum value of all systems. The average of the hydrogen bond distance is in the range of 170–180 pm, which is in good agreement with the literature values of methanol of both ∼180 pm[143] (obtained by a combined experimental and molecular dynamics investigation). Several ab-initio molecular dynamics studies employing the BLYP functional find the first peak of the radial distribution function of the O–H$\cdots$O distance around 190 pm,[145,146] in good agreement with our results of 189.6 pm for methanol dimer (Table 3.3). Our CDFs show a range lower than this value, but are still in good agreement.

Comparing the different alcohols in Figure 3.3, it can be seen that the CDFs become more localized with increasing size of the alcohol, from methanol to *n*-butanol and *tert*-

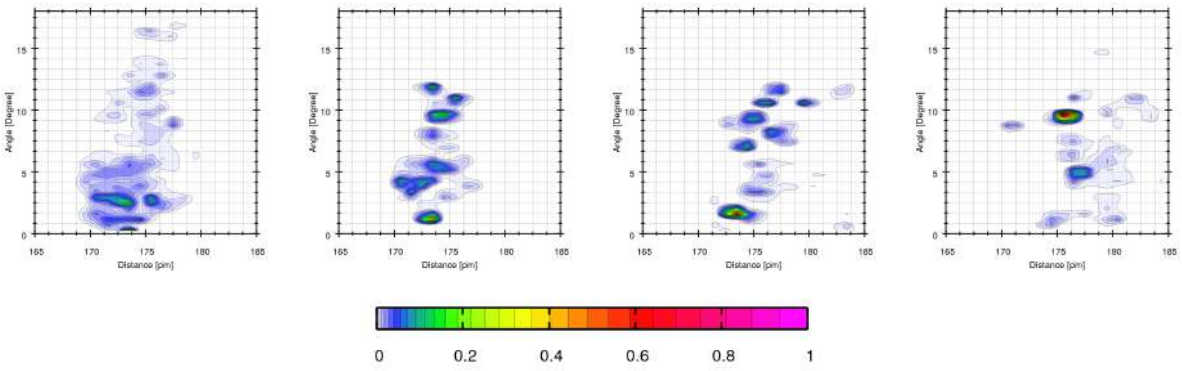

Figure 3.3. Combined distribution functions of the intermolecular hydrogen-oxygen distance against the complementary of the O-H$\cdots$O angle in (left to right) methanol, ethanol, *n*-butanol, and (bottom) *tert*-butanol.

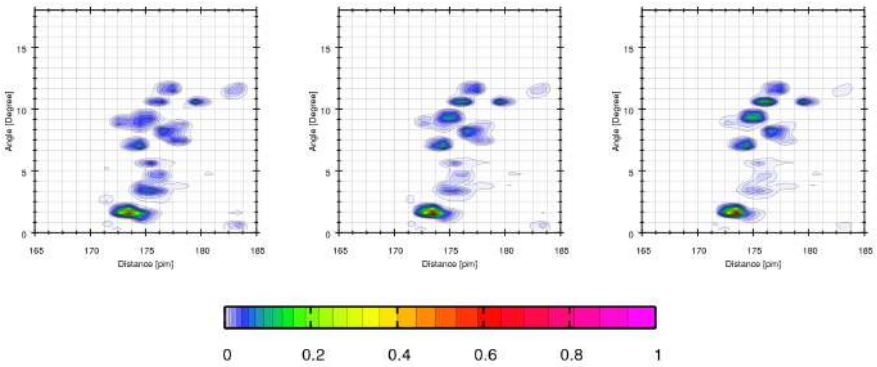

Figure 3.4. Combined distribution functions of the intermolecular hydrogen-oxygen distance against the complementary of the O-H$\cdots$O angle of *n*-butanol, at the temperature (from left to right) 248.15 K, 298.15 K, 348.15 K.

butanol, with an increasingly distinct maximum observable in the distribution. Comparing the other alcohols to *tert*-butanol, a shift of this maximum from 1–2° to a wider angle of 9–10° can be observed, which can be attributed to the different steric restrictions in the branched alcohol.

Figure 3.4 shows the CDFs of *n*-butanol at a temperature of 248.15 K, 298.15 K, and 348.15 K, comprising a large span within the liquid range of *n*-butanol. While the overall structure of the distributions remains the same, as expected, with increasing temperature, the hydrogen bonds become less localized in the lower range of angles and an increased distribution over the range of 8–12° is observed. Thus, with rising temperature, the average hydrogen bond angle increases.

a) methanol/ethanol

b) methanol/*n*-butanol

c) methanol/*tert*-butanol

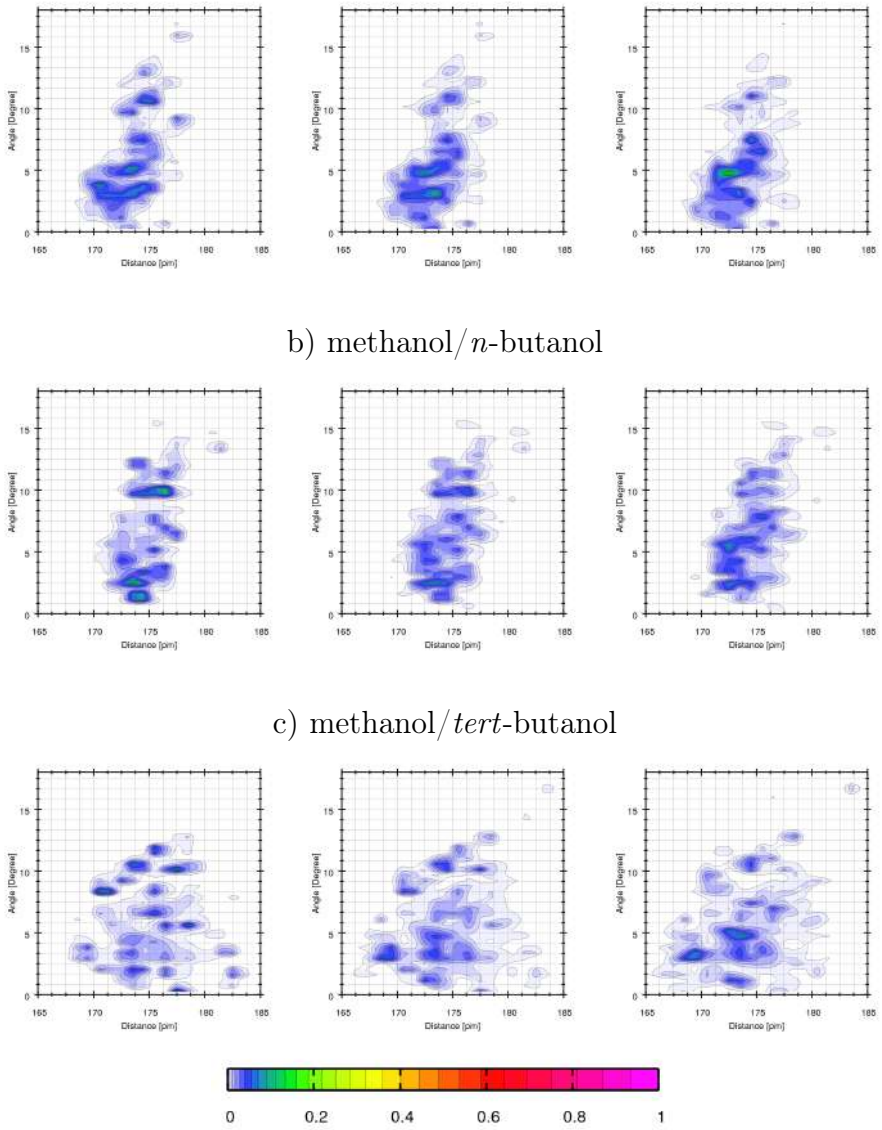

Figure 3.5. Combined distribution functions of the intermolecular hydrogen-oxygen distance against the complementary of the O-H$\cdots$O angle for the mixtures of methanol with ethanol (a), *n*-butanol (b), and *tert*-butanol (c) at mole fractions of methanol of (from left to right) 0.2, 0.5, and 0.8.

Figure 3.5 shows the CDFs of methanol/ethanol (a), methanol/*n*-butanol (b), and methanol/*tert*-butanol (c) for increasing mole fractions of methanol of 0.2, 0.5, and 0.8. In general, for small mole fractions of methanol the systems show a more localized maximum of the hydrogen bond distribution. For the methanol/*tert*-butanol system, it is visible that the preferred angle is shifting from larger to smaller values with an increasing mole fraction of methanol. Even more, compared to the other binary systems, this mixture is

less localized due to the branching of *tert*-butanol.

3.3.2. Thermodynamic Properties of Neat Systems

In earlier works, we established our approach of calculating $\Delta_{\mathrm{vap}}H$ from QCE, by performing so-called QCE^0 calculations wherein a_{mf} is set to 0, as reference for the gas phase.[4,81] For QCE^0 calculations, the cluster sets are reduced to clusters up to the size of three molecules. $\Delta_{\mathrm{vap}}H$ can then be obtained for any temperature simply as difference of the total enthalpies in the liquid and gaseous phase respectively. In Table 3.4 our calculated enthalpies of vaporization at 298.15 K are listed next to their experimental reference value for every neat system investigated in this work. A good agreement with experimental data can be seen for most systems. For ethanol, an improved result with respect to the previous work[4] (44.09 kJ mol^{-1}) is obtained, due to the increased size and number of clusters. Our approach appears more accurate for the non-branched systems methanol, ethanol, *n*-propanol and *n*-butanol. The system that deviates most from experiment is also the most branched, namely *tert*-butanol. In general a larger deviation from experimental results can be seen with an increased branching of the molecule.

Table 3.4. Calculated and experimental enthalpies of vaporization $\Delta_{\mathrm{vap}}H$ and $\Delta_{\mathrm{vap}}H^{\mathrm{exp}}$ in kJ mol^{-1} for the neat systems at standard conditions. Experimental enthalpies of vaporization are taken from the NIST Chemistry WebBook.[147]

	$\Delta_{\mathrm{vap}}H$	$\Delta_{\mathrm{vap}}H^{\mathrm{exp}}$
methanol	39.33	37.60
ethanol	43.36	42.30
n-propanol	47.17	47.00
iso-propanol	47.49	45.00
n-butanol	51.37	52.00
iso-butanol	49.81	51.00
tert-butanol	46.71	39.70

3.3.3. Thermodynamic Properties of Binary Mixtures

As shown in earlier works, via the quantum cluster approach we are able to reproduce quantitatively the experimental Gibbs energies of mixing $\Delta_{\text{mix}}G$, using the density and phase transition temperature as only experimental input data.[4,65,79] The Gibbs energy of mixing at 328.15 K is depicted in Figure 3.6 for the binary mixtures of methanol with ethanol, *n*-propanol, *iso*-propanol , *n*-butanol, *iso*-propanol, *tert*-butanol. Of all the investigated systems, methanol/ethanol is the one that most resembles an ideal mixture. In contrast, methanol/*n*-butanol is the system deviating the strongest from ideality. In general, an increase in the deviation from ideality can be seen with an increasing size of the molecule, from ethanol to butanol. In order to investigate the deviation from the ideal mixture in more depth, activity coefficients are calculated. Activity coefficients are directly connected to the excess Gibbs energy of mixing $\Delta_{\text{mix}}G^{\text{e}}$ as shown in Equation 3.9. In Table 3.5, activity coefficients of all mixtures are shown over the complete mixing range. As described before and in our previous work,[4] the mixture methanol/ethanol is the most ideal system; the activity coefficients f_{MeOH} and f_{EtOH} of both methanol in ethanol and the opposite respectively are near to one for every mole fraction. An increase in the activity coefficient at infinite dilution can be observed with increasing size of the alcohol;

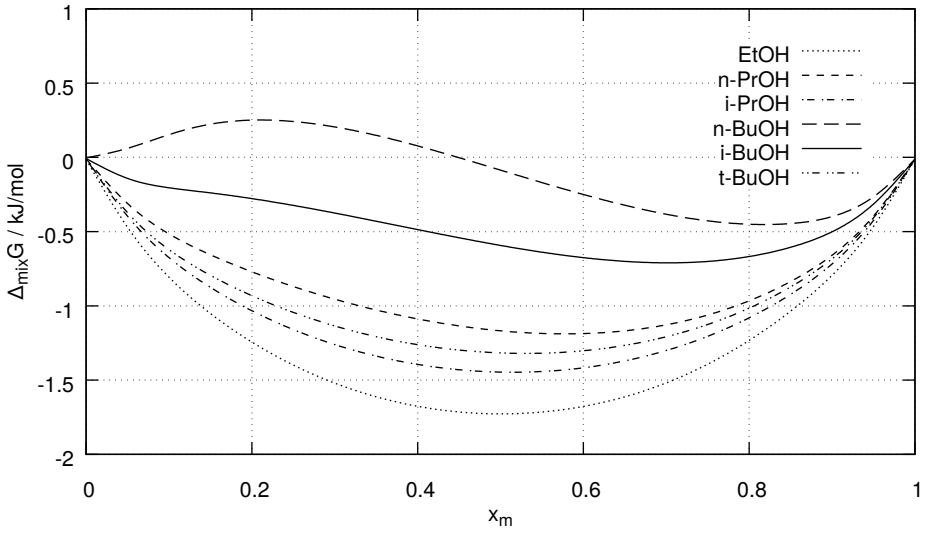

Figure 3.6. Calculated Gibbs energies of mixing $\Delta_{\text{mix}}G$ for binary mixtures of methanol with an alcohol ROH at 298.15 K. x_m indicates the mole fraction of methanol.

Table 3.5. Activity coefficients f_{ROH} of both components in mixtures of methanol (MeOH) with an alcohol ROH, where x_{m} is the molar fraction of methanol.

	ethanol		*n*-propanol		*iso*-propanol		*n*-butanol		*iso*-butanol		*tert*-butanol	
x_{m}	f_{MeOH}	f_{EtOH}	f_{MeOH}	f_{nPrOH}	f_{MeOH}	f_{iPrOH}	f_{MeOH}	f_{nBuOH}	f_{MeOH}	f_{iBuOH}	f_{MeOH}	f_{tBuOH}
0.00	1.03	1.00	4.39	1.00	2.03	1.00	148.21	1.00	21.09	1.00	2.49	1.00
0.10	0.99	1.00	2.58	1.03	1.51	1.01	20.01	1.10	6.99	1.06	1.87	1.01
0.20	0.99	1.00	1.83	1.09	1.31	1.04	5.82	1.36	3.40	1.20	1.53	1.05
0.30	0.99	1.00	1.45	1.18	1.21	1.07	2.77	1.74	2.12	1.40	1.33	1.10
0.40	0.99	1.00	1.24	1.28	1.14	1.10	1.78	2.20	1.56	1.64	1.21	1.16
0.50	1.00	1.00	1.13	1.39	1.09	1.14	1.37	2.72	1.29	1.92	1.13	1.23
0.60	1.00	0.99	1.06	1.49	1.05	1.19	1.18	3.27	1.15	2.21	1.07	1.30
0.70	1.01	0.98	1.03	1.57	1.03	1.24	1.08	3.85	1.07	2.51	1.04	1.38
0.80	1.01	0.97	1.02	1.64	1.02	1.30	1.03	4.44	1.03	2.81	1.02	1.47
0.90	1.01	1.00	1.01	1.73	1.01	1.37	1.00	4.99	1.01	3.19	1.01	1.58
1.00	1.00	1.16	1.00	1.98	1.00	1.55	1.00	5.43	1.00	3.82	1.00	1.76

methanol at infinite dilution in *n*-propanol and *n*-butanol shows activity coefficients of 4.39 and 148.21 respectively as compared to 1.03 in ethanol. Increasing the branching of the molecule, the activity coefficients are decreasing to values closer to one; this is in good agreement with the Gibbs energies of mixing in Figure 3.6, where the most branched system, methanol/*tert*-butanol, is the closest to ideality second to only methanol/ethanol. The activity coefficients of methanol in *iso*-propanol compared to methanol in *n*-propanol confirm this behavior. For a better visualization, the activity coefficients are shown in Figure 3.7 and Figure 3.8 with respect to the methanol mole fraction. From these graphs it can be seen that for low mole fractions of methanol its activity coefficient in alcohols is increasing with the size of the solvent and decreasing with its branching. The same behavior can be found for the activities of alcohols diluted in methanol. We can conclude that in mixtures of methanol with an alcohol, increasing the size of the alcohol leads to a larger deviation from ideality. On the other hand, an increase in the branching of the alcohol leads to a more ideal mixture. The same behavior can be found in the experimentally calculated excess Gibbs energy of mixing from Polak *et al.*[148] for isomeric

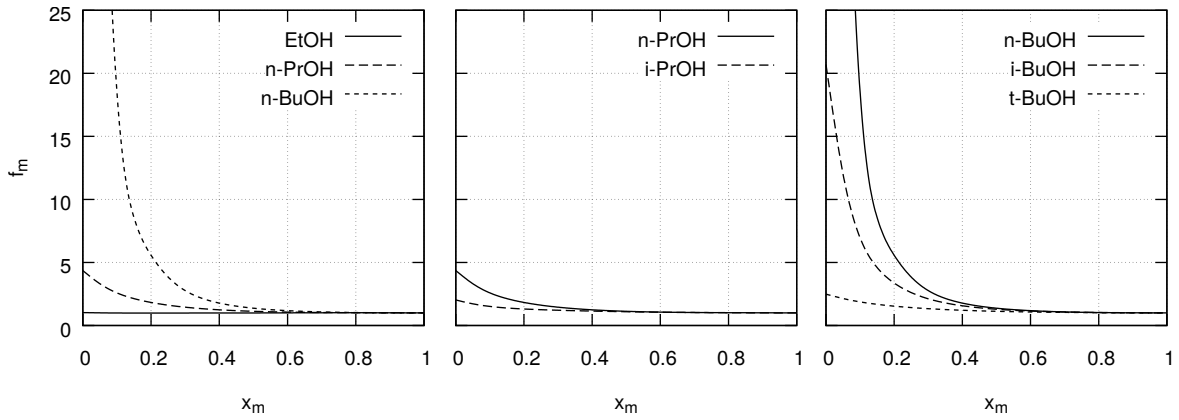

Figure 3.7. Activity coefficients of methanol in binary mixtures with an alcohol ROH at 298.15 K. x_m indicates the mole fraction of methanol.

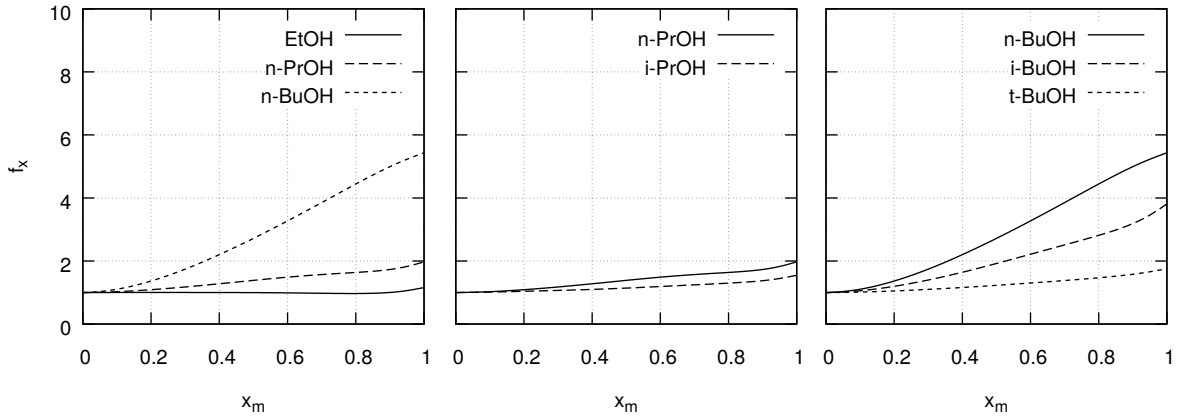

Figure 3.8. Activity coefficients of alcohols ROH in a binary mixture with methanol. x_m indicates the mole fraction of methanol.

butanol, where *n*-butanol shows the largest deviation from ideality, and *tert*-butanol the lowest.

3.4. Conclusions

In order to understand the liquid behavior we optimized 5760 cluster geometries of which 1144 were further analyzed. The average interaction energies per monomer have been evaluated for all neat dimers and stronger interactions with increasing chain length and branching of the molecule are found. Combined distribution functions of distances and angular distributions of hydrogen bonds are calculated for several neat and mixed sys-

tems, demonstrating how the different size and branching of the alcohol lead to different geometrical conditions of the hydrogen bonds. In this article we applied the quantum cluster approach to calculate the activity coefficient of different methanol/alcohol mixtures. This approach relies on the binary quantum cluster equilibrium theory.[3,4,45,65] With respect to our previous work,[4] we increased the maximal size of the clusters from six to nine molecules, ensuring a better accuracy in the quantum cluster approach simulations. Furthermore, we studied a much wider range of MeOH-alcohol mixtures. The vaporization enthalpies of all pure substances were calculated at room temperature; while overall a good agreement with experimental data can be observed, the deviation increases with the alcohol's branching, with *tert*-butanol showing the largest deviation. Using Redlich–Kister polynomials and calculating their derivatives allows access to the activity coefficients, further establishing the bQCE approach as a novel and conceptually outstanding method of computing such quantities. In this article we demonstrated that in mixtures of methanol with an alcohol, increasing the size of the alcohol leads to a larger deviation from ideality. On the other hand, an increase in the branching of the alcohol leads to a more ideal mixture. This case study will help to move our approach to complex solvent media, adding to the tools used in application driven solvent design.

Appendix

The bQCE Method

The bQCE method has been established and its underlying theory detailed in depth in many earlier works.[4,27,45,65] Here, we will present only a short overview of the key equations of bQCE.

First, we consider a system of non-interacting clusters in thermodynamic equilibrium, built up from one (neat substances) or two (binary systems) monomers. The equilibrium reaction between clusters of a binary system can be written as

$$i(\wp)\mathrm{C}_1 + j(\wp)\mathrm{C}_2 \rightleftharpoons \mathrm{C}_\wp, \tag{3.1}$$

where $i(\wp)$ and $j(\wp)$ are the number of monomers of each component C_1 and C_2 that form the cluster $\wp$. The system's total partition function Q^{tot} at volume V and temperature T is given by

$$Q^{\mathrm{tot}}(\{N_\wp\}, V, T) = \prod_{\wp=1}^{N} \frac{1}{N_\wp!} \left[q_\wp^{\mathrm{tot}}(V,T)\right]^{N_\wp}, \tag{3.2}$$

where $q_\wp^{\mathrm{tot}}$ is the partition function corresponding to the single cluster $\wp$ and $\{N_\wp\}$ is the full set of total cluster populations $N_\wp$. From calculating Q^{tot} all the thermodynamic properties of the system are accessible. Each cluster partition function $q_\wp^{\mathrm{tot}}$ can be evaluated as product of partition functions corresponding to the cluster's different degrees of freedom:

$$q_\wp^{\mathrm{tot}}(V,T) = q_\wp^{\mathrm{trans}}(V,T) q_\wp^{\mathrm{rot}}(T) q_\wp^{\mathrm{vib}}(T) q_\wp^{\mathrm{elec}}(T), \tag{3.3}$$

where $q_\wp^{\mathrm{trans}}$, $q_\wp^{\mathrm{rot}}$, and $q_\wp^{\mathrm{vib}}$ are the translational, rotational, and vibrational partition function. They can be calculated from standard equations for the particle in a box, rigid rotator, and harmonic oscillator respectively.[27,149] The electronic partition function $q_\wp^{\mathrm{elec}}$ is calculated from the adiabatic binding energy $\Delta_{\mathrm{bind}} E_\wp^{\mathrm{elec}}$ of the cluster.[150]

In order to describe $q_\wp^{\mathrm{trans}}$, the phase volume V must account for an exclusion volume V_{ex} which attributes a volume $v_\wp$ to the non-punctiform clusters. The exclusion volume is calculated as

$$V_{\mathrm{ex}} = b_{\mathrm{xv}} \sum_{\wp=1}^{N} N_\wp v_\wp, \tag{3.4}$$

wherein $v_\wp$ is the cluster volume. Since cluster volumes are sensitive to the choice of atomic radii, a scaling parameter b_{xv} must be introduced. Additionally, $q_\wp^{\mathrm{elec}}$ is extended by a correction term to account for the interactions between clusters in form of a volume and cluster size dependent mean-field energy. The electronic partition function then reads

$$q_\wp^{\mathrm{elec}}(V,T) = \exp\left\{ -\frac{\Delta_{\mathrm{int}} E_\wp^{\mathrm{elec}} - [i(\wp) + j(\wp)] \frac{a_{\mathrm{mf}}}{V}}{k_{\mathrm{B}} T} \right\}, \tag{3.5}$$

where k_{B} is the Boltzmann constant and the mean-field parameter a_{mf} ($\mathrm{Jm^3/mol^2}$) is a second empirical parameter, that is scaling the strength of inter cluster interactions. In an optimized bQCE calculation, the parameters are chosen such that the deviation of the bQCE results from a given experimental input, such as densities and phase transition

temperatures, becomes minimal.

To calculate Q^{tot}, all independent variables $(\{N_\wp\}, V, T)$ need to be known. The temperature must be set by the user and the volume is restricted with respect to an externally applied pressure

$$p = k_{\mathrm{B}} T \left(\frac{\partial \ln Q^{\mathrm{tot}}}{\partial V} \right)_{T,\{N_\wp\}} . \tag{3.6}$$

If several combinations of V and $\{N_\wp\}$ exist that fulfill this condition, then the solution with the lowest Gibbs energy

$$G \ = -k_{\mathrm{B}} T \ln Q^{\mathrm{tot}} + V k_{\mathrm{B}} T \left(\frac{\partial \ln Q^{\mathrm{tot}}}{\partial V} \right)_{T,\{N_\wp\}} \tag{3.7}$$

is chosen. Using this approach, good performance has been demonstrated for mixed systems in several studies.[4,65,81]

Activity Coefficients from bQCE

An accurate and detailed description of the calculation of activity coefficients via the quantum cluster approach can be found in a previous work.[4]

For a binary mixture, the excess Gibbs energy of mixing $\Delta_{\mathrm{mix}} G^{\mathrm{e}}$ can then be calculated as

$$\Delta_{\mathrm{mix}} G^{\mathrm{e}} = \Delta_{\mathrm{mix}} G - \Delta_{\mathrm{mix}} G^{\mathrm{id}}, \tag{3.8}$$

where $\Delta_{\mathrm{mix}} G$ and $\Delta_{\mathrm{mix}} G^{\mathrm{id}}$ are the Gibbs energy and the ideal Gibbs energy of mixing respectively. Activity coefficients f_i are directly related to the excess Gibbs energy of mixing (labeled as G^{e}) by

$$f_i = \exp\left(\frac{1}{RT} \frac{\partial G^{\mathrm{e}}}{\partial N_i} \right), \tag{3.9}$$

where R is the ideal gas constant, T is the temperature, and N_i is the particle number of component i. Since no analytical expression for G^{e} is available, we calculate its derivative numerically through a Redlich–Kister (RK) style polynomial fit which smooths out all local inconsistencies.[151] We denote the Gibbs energy $G^{\mathrm{e}}_{\mathrm{RK}}(x_i)$ with

$$G^{\mathrm{e}}_{\mathrm{RK}}(x_i) = x_i(1 - x_i) \sum_n g_n (1 - 2x_i)^n, \tag{3.10}$$

wherein g_n are the Redlich–Kister parameters.[151] In this work we used up to five parameters ($0 \leq n < 5$). With $x_i = \frac{N_i}{N_i+N_j}$ we can write $G^{\mathrm{e}}_{\mathrm{RK}}$ as function of N_i and N_j:

$$G^{\mathrm{e}}_{\mathrm{RK}} = N_i(1 - \frac{N_i}{N_i + N_j}) \sum_n g_n \left(1 - 2\frac{N_i}{N_i + N_j}\right)^n . \tag{3.11}$$

Equation 3.11 gives an analytical expression for G^{e} that can be differentiated with respect to the number of particles N_i:

$$\frac{\partial G^{\mathrm{e}}_{\mathrm{RK}}}{\partial N_i} = x_j^2 \sum_n g_n \left(1 - 2x_i\right)^n - 2 \cdot x_i \cdot x_j^2 \sum_n n \cdot g_n \left(1 - 2x_i\right)^{n-1} .$$

Analogously, we can evaluate

$$\frac{\partial G^{\mathrm{e}}_{\mathrm{RK}}}{\partial N_j} = x_i^2 \sum_n g_n \left(2x_j - 1\right)^n + 2 \cdot x_j \cdot x_i^2 \sum_n n \cdot g_n \left(2x_j - 1\right)^{n-1} .$$

wherein $x_i = \frac{N_i}{N_i+N_j}$ and $x_j = \frac{N_j}{N_i+N_j}$. Inserting these expressions into Equation 3.9 allows the evaluation of the activity coefficients.

Computational Details and Cluster Search

The selection of the cluster set is a crucial step of the quantum cluster equilibrium approach.[45,129] In this work, we increased the cluster size (up to nine molecules) compared to our previous work,[4] in order to increase the accuracy of the calculations. In Figure 3.9 the cluster generation procedure is explained. In the first step, the global minimum structure of each cluster composition is searched for by running a genetic structure optimization algorithm at the classical force field level of theory. For this purpose the OGOLEM framework,[103,104] interfaced with the AMBER 2016 molecular dynamics package[152] and the general amber force filed (GAFF),[102] is used. During the optimization, the number of individuals in each generation as well as the total number of individuals are set accordingly with the cluster size. For each cluster a number between 2000 and 6000 structures are evaluated, with each generation consisting of 100 to 300 individual structures. For each respective cluster composition, fifteen clusters are chosen from the final generation in order to sample a set of energetically and geometrically diverse individuals, which

represent the global and local minima of that structure. These clusters are geometrical optimized at semi-empirical level of theory, using the extended tight binding method GFN2-xTB 6.0.1,[91,92] which includes the D4 dispersion correction[94,95] accounting for the London dispersion energy. Frequency calculations are performed with the same method. All the clusters with a first normal mode below a threshold (in this case, 10 cm^{-1}) are removed from the cluster pool in order to avoid imaginary or low frequencies that could affect the simulations. Likewise, structural duplicates of already existing clusters are removed from the cluster set. The conformational similarity of two clusters is quantified by their geometrical distance d:[153]

$$d(\wp, \wp') = \left[\left(\frac{I_A - I'_A}{I_A} \right)^2 + \left(\frac{I_B - I'_B}{I_B} \right)^2 + \left(\frac{I_C - I'_C}{I_C} \right)^2 \right]^{\frac{1}{2}}, \tag{3.12}$$

wherein I and I' are principal moments of inertia of the clusters $\wp$ and $\wp'$ respectively. Clusters $\wp'$ with a geometrical distance of $d\wp, \wp' < 0.01$ were removed from the cluster set. For the geometrical investigation of hydrogen bonds, the cluster sets were analyzed with our in-house trajectory analysis code TRAVIS.[144] Note, that the all cluster geometries can be obtained from the authors upon request.

Additionally, a select set of systems were optimized on the DFT level of theory. Here, we used the ORCA 4.0.0[154] quantum chemical code employing the GGA functional BP86 with the 6-31G* basis set, D3 dispersion correction, and geometrical counter-poise correction.[155] Due to the increased computational cost, we reduced the cluster set size to a maximum of six molecules. We observed no improvement in the results, hence, we excluded the analysis of those clusters in this article. However, interaction energies and thermodynamic results of those systems are presented in the supporting information. Additionally, single point simulations where also performed employing the hybrid functional B3LYP, using the same 6-31G* basis set.

bQCE calculations were performed with the PEACEMAKER 2.8 program package[3] which has successfully been used to describe binary mixtures previously.[4,65,78,79] All calculations were performed at a fixed pressure of 1.01325 bar and temperature ranging from 273 to 500 K. Cluster volumes were calculated employing van der Waals volumes. The pa-

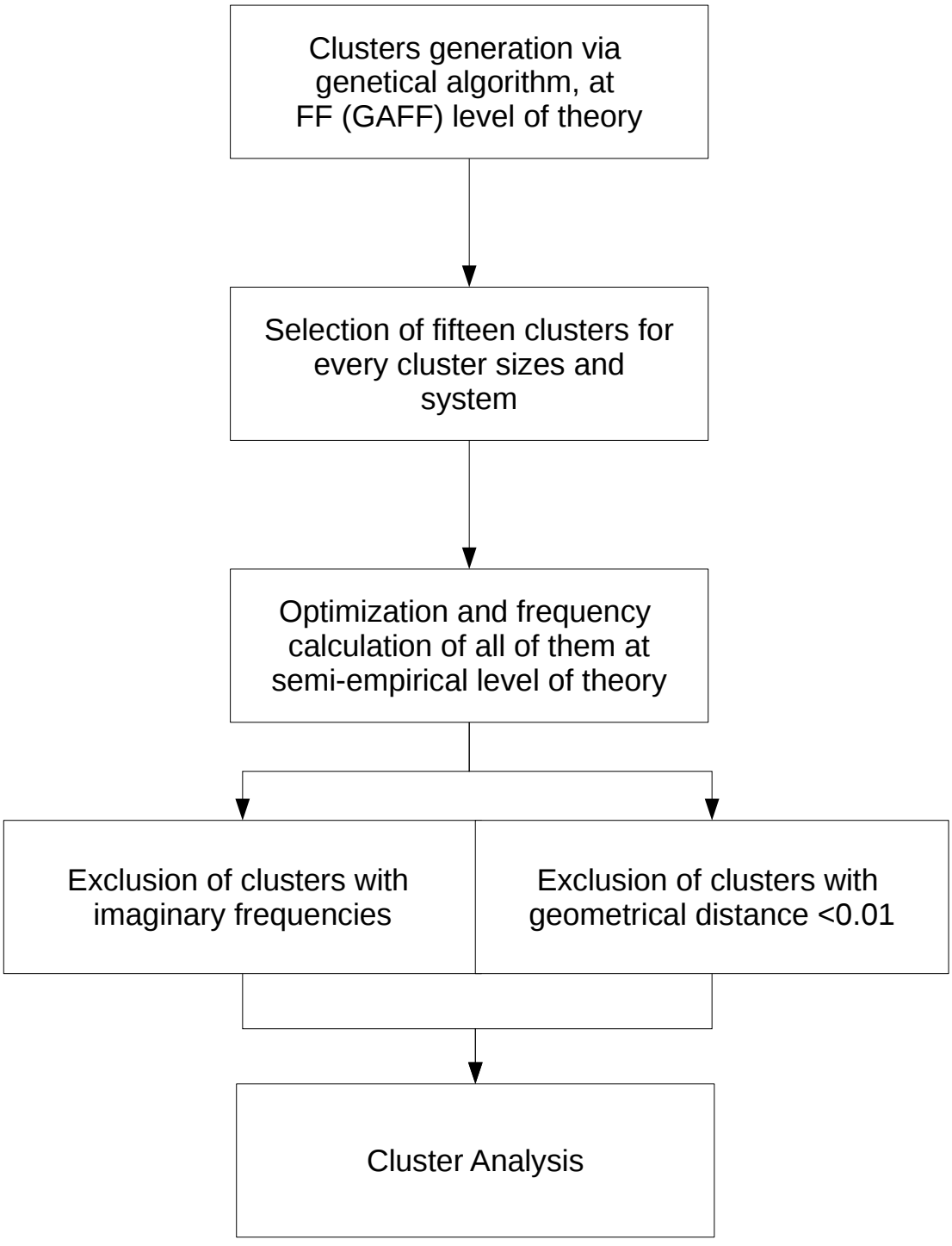

Figure 3.9. Cluster generation procedure.

rameters a_{mf} and b_{xv} were fitted so that the deviation of bQCE results to experimental boiling points and densities taken from literature[148,156–160] become minimal. Different to our earlier works, here, we employed the Nelder–Mead optimization algorithm.[161]

Acknowledgement

B. Kirchner and G. Marchelli would like to express their gratitude to the ETN Socrates (http://etn-socrates.eu/) because this project has received funding from the European Union's EU Framework Programme for Research and Innovation Horizon 2020 under Grant Agreement No 721385.

4. Hydrogen Bonding in HFIP-Acetone and HFIP-Methanol Mixtures

Reprinted (adapted) with permission from
G. Marchelli, J. Ingenmey, O. Hollozcky, A. Chaumont and B. Kirchner.
Paper under review on ChemPhysChem.

Contributions to the manuscript

- Performing the QM calculations, the classical MD simulations, and making the analysis of all the systems.
- Discussing of the results.
- Writing the manuscript.

Summary

In the following chapter, the hydrogen bond networks of binary mixtures of hexafluoroisopropanol with either methanol or acetone are analyzed with a combination of quantum mechanical calculations, classical molecular dynamics (MD) simulations, and the bQCE approach. hexafluroisopropanol is extensively studied in literature,[162–164] and already used in different fields,[164–168] but its intermolecular interactions with acetone or methanol were nonetheless never investigated in detail.[166,169] Since acetone is a hydrogen bond acceptor and methanol is both an acceptor and a donor, they are a good model systems to be combined with hexafluoroisopropanol as these mixtures present a first necessary step to model and simulate more complicated systems. In contrast to to the strategy used in Chapter 3, here the cluster size for both the neat and the mixed system is reduced to 6, but all the clusters are geometrically optimized at the DFT level of theory, improving the results. Since the experimental data to fit the bQCE calculations are not available in this case, classical MD simulations are performed in the temperature range of 298–338 K with a step size of 10 K for the two mixed systems, and the simulated densities are used as input for the bQCE calculations. These calculations are performed with the in-house code Peacemaker 2.8, here upgraded with temperature dependent parameters, as explained in the methodology section. The radial distribution fuctions, the coordination numbers, the angular distribution functions, and the lifetime of the hydrogen bond for both mixtures are evaluated, to fully describe the inter-molecular interactions. In general, both the systems hexafluoroisopropanol/acetone and hexafluoroisopropanol/methanol are showing a highly coordinating structure. The populations at 298 K for the systems are calculated via the bQCE approach, and the most populated clusters are shown and discussed. The mixed clusters appear to be preferred even at small concentrations of hexafluoroisopropanol. Finally, enthalpies and entropies of vaporization are calculated for both the neat and mixed systems, and show a good agreement with the experimental values available in literature.

Hydrogen Bonding and Vaporization Thermodynamics in Hexafluoroisopropanol-Acetone and -Methanol Mixtures. A Joined Cluster Analysis and Molecular Dynamics Study

Gwydyon Marchelli * Johannes Ingenmey*

Oldamur Hollóczki* Alain Chaumont† Barbara Kirchner*

Submitted: 17 August 2021

4.1. Abstract

Binary mixtures of hexafluoroisopropanol with either methanol or acetone are analyzed via classical molecular dynamics simulations and quantum cluster equilibrium calcula-

* Mulliken Center for Theoretical Chemistry, Rheinische Friedrich-Wilhelms-Universität Bonn, Beringstr. 4+6, D-53115 Bonn, Germany

†Université de Strasbourg, CNRS, CMC UMR 7140, Laboratoire MSM, F-67000 Strasbourg, France

tions. In particular, their populations and thermodynamic properties are investigated with the binary quantum cluster equilibrium method, using our in-house code PEACEMAKER 2.8, upgraded with temperature-dependent parameters. A novel approach, where the final density from classical molecular dynamics, has been used to generate the necessary reference isobars. The hydrogen bond network in both type of mixtures at molar fraction of hexafluoroisopropanol of 0.2, 0.5, and 0.8 respectively is investigated via the molecular dynamics trajectories and the cluster results. In particular, the populations show that mixed clusters are preferred in both systems even at 0.2 molar fractions of hexafluoroisopropanol. Enthalpies and entropies of vaporization are calculated for the neat and mixed systems and found to be in good agreement with experimental values.

4.2. Introduction

The investigation of the mechanisms and interactions that regulate both neat fluids as well as their mixtures plays a fundamental role in the design of novel solvents. Over the last decades the interest in developing sustainable chemical processes has grown, and with it the need for new solvents that follow the fundamentals of green chemistry.[6] For example liquid-liquid – i.e. solvent – metal extraction offers a number of advantages compared to other techniques,[170] but the employed solvents are often toxic and expensive to dispose of. The last few years have seen an increasing demand of novel sustainable solvents for metal ions extraction.[171] Another approach is the use of the so-called deep eutectic solvents (DES), which are low-melting eutectics formed by the mixture of two or more substances whose eutectic point temperature is much lower than that of an ideal mixture.[8,138] With properties similar to those of ionic liquids, such as a low vapor pressure, low melting point, high thermal stability,[172,173] and they have come to be known as an economic and eco-friendly alternative for conventional organic solvents. A new kind of DESs, called Type V DESs, has recently been introduced.[12] It is formed by the combination of two non-ionic moieties which establish a strong hydrogen bond network, and has been proven to be more sustainable than traditional organic solvents.[12] In recent works, hydrophobic DES formed by menthol with different organic acids have been proved to present a strong

hydrogen bond between the two components, stronger than the hydrogen bond network in the neat system.[174,175] Different hydrogen bond donors and acceptors have been investigated as components of hydrophobic or Type V DESs,[12] such as decanoic acid and lidocaine,[176] menthol with different natural acids,[177] and 1,1,1,3,3,3-hexafluoroisopropanol (HFIP) with betaine and L-carnitine.[178] HFIP in particular is an extraordinary solvent used in many different applications, including the activation of organic functionalities such as the intramolecular Schmidt reaction using a Lewis acid in HFIP,[165] the activation of carbonyl and epoxide substrates,[164,166] or the activation of hydrogen peroxide in the Baeyer–Villiger oxidation reaction.[167,168] It can also serve as a proton donor in dihydrogen bonding with different transition metal hydrides, as non-classical hydrogen bond.[164,179] Its widespread use is due to a number of beneficial properties, such as its thermal stability, transparency to UV radiation, as well as to its remarkable solvent properties, allowing it to dissolve a wide range of polymers, as well as most common polar and non-polar solutes.[162,163] In aqueous solutions, its acidity range is comparable to the one of formic acid.[164] Furthermore, its low boiling point facilitates its recovery via distillation. However computational studies on HFIP remain sparse. For instance HFIP has been investigated with molecular dynamics by some of the present authors to prove its catalytic effect on C,C coupling reactions on aromatic compounds with positive results.[166] In 2019, Deng *et al.* were the first to study HFIP-based DESs as the non-polar phase in liquid-liquid micro-extractions.[178] To be able to understand the mechanisms behind the formation of novel mixtures it is imperative to study their structure and in particular the hydrogen bond network which may exist in these liquids. From an experimental prospective, hydrogen bonds can be investigated via IR and NMR.[180,181] However, since their experimental detection and analysis can still be challenging and expensive, computational tools may be valuable for this kind of investigation.[182–184] We were able to calculate the activity coefficients of methanol in its binary mixtures with a set of small alcohols, which allowed some insight into how the chain length and branching modify the hydrogen bond network and consequently affect their behavior.[1] Since it is fundamental to study the hydrogen bond network in binary organic solvents, it is interesting to investigate the behavior of HFIP with both an hydrogen bond acceptor (acetone) and a compound able to work

both as hydrogen bond acceptor and donor (methanol). The binary mixtures of HFIP with acetone or methanol have already been investigated experimentally in the past, but so far their liquid structure has never been investigated in detail.[166,169] In the current article, we investigate the intermolecular interactions present in the binary mixtures of HFIP with either solvents. The study is based on a combined computational procedure of both classical molecular dynamics simulations (MD) and quantum chemical calculations. Furthermore, we use the binary quantum cluster equilibrium (bQCE) method to investigate the distribution of intermolecular interaction motifs in the system. The method assigns populations to a set of clusters, enabling the weighting of properties according to the cluster distribution similar to Boltzmann weighting. In contrast to it, however, the bQCE method can weight clusters of different sizes and compositions and considers not only their electronic energies but also the particle volume and inter-cluster interactions. Boltzmann and bQCE weighting were compared in the past by our group in the field of the computational calculation of vibrational circular dichroism spectra of bulk phase, showing the advantages of our method over Boltzmann weighting.[77] For this purpose we use our in-house code PEACEMAKER 2.8, which has proven to be a valuable tool to investigate the thermodynamic properties of both neat and mixed systems.[1,3,4,65,74,75,78,79,132,133] The standard bQCE method involves optimization of two empirical parameters by fitting them to a set of experimental data such as boiling points or isobars; however, even for simple mixtures of organic solvents, these data are often unavailable in the literature. Hence we follow a different approach, namely, the isobars are instead obtained via MD simulations. In the following we will first outline and discuss the computational methods used, after which we will present and investigate the results we have obtained.

4.3. Computational Details

4.3.1. Classical Molecular Dynamics Simulations

Initial configurations of the different systems were generated using the PACKMOL package (version 17.039).[185] Molecules were randomly placed in a cell with an initial cell vector of 40–50 Å, depending on the composition of the system. MD simulations were performed

using the LAMMPS program package (version 11 Aug 2017).[186] OPLS-AA force field parameters were used for methanol (MeOH) and acetone, whereas for HFIP we adopted the force field developed by Fioroni *et al.*, which was optimized to reproduce the experimental density.[187] A Lennard-Jones 6–12 potential was used to describe van der Waals (vdW) interactions. Lorentz–Berthelot mixing rules were used to describe non-bonded interactions.[188] A cutoff of 1 nm was applied for vdW and Coulombic interactions. In the first step the SHAKE algorithm[189] was used to constrain the bonds involving hydrogen atoms and followed by energy minimization. This process was repeated 3–5 times to let the systems mix correctly and eliminate energetic hot spots in order to stabilize the systems. Afterwards, the boxes were deformed to reach a preliminary and fixed cell volume, calculated to reflect a density of 0.8 g/cm^3 for each system. Following this, the systems were simulated for 1.5 ns in the NpT ensemble, using Nosé–Hover thermostat and barostat, to let the volume converge. The cell volumes over the last 0.5 ns were found to remain constant, as can be seen in Fig. S2 in the SI. The system volume was then set to the average volume taken over the last 0.5 ns in the NpT ensemble. A further 1 ns of simulation time in the NVT ensemble was performed to further equilibrate the system. Finally, a production run of 20 ns was performed in the NVT ensemble using the same conditions as during equilibration. The time step was set to 0.5 fs for the pre-equilibration processes (shake, minimization, and deformation of the box) and increased to 1 fs afterwards. The simulations were analyzed with our in-house trajectory analysis code Travis.[144,190] The angular distribution functions (ADFs) were calculated using the cone correction included in Travis with a cut off of 250 pm as maximum distance between the reference and observed molecules.[191] Along with the Radial Distribution Functions (RDFs), the coordination numbers (CN) are calculated as well ($CN = \rho_{bulk} \int g(r) r^2 dr$), where $g(r)$ is the RDF's intensity and ρ_{bulk} is the bulk density of the system. Please note that, since the RDF is strictly dependent on the number of molecules that respect the given condition, the intensity of the systems cannot be compared. The peak's position, however, is not dependent on the number of molecules and they can be compared. Hydrogen bond lifetimes are analyzed using the dimer existence auto correlation function (DACF) implemented in the Travis code with the default curve fitting and approximations included in the code

and described in literature.[192] For this analysis, the distance condition of 350 pm for the O–O distance and an angular condition of 135°–180° for the O-H–O angle were applied.

4.3.2. Cluster Generation

The construction of a cluster set that is representative of the investigated system is a crucial step in the bQCE procedure and has been discussed in previous works.[1,3,4,45,129] As a first step, to find clusters, we performed a global minimum structure search for each cluster size and composition by running the genetic optimization algorithm OGOLEM[103,104] at the force field level of theory, using the AMBER 2016 program package[152] and the GAFF force field[102] implemented therein. The AMBER/OGOLEM combination is optimized to screen a great number of individual clusters.[1,3,4] The number of individuals per generation was varied between 80 and 240 in accordance to the cluster size to adjust for the increasing complexity. In total, a number of 2000–6000 individuals, i.e. clusters, were generated and evaluated for every possible composition up to a cluster size of six molecules. As the search for the global minimum structure by a genetic algorithm is performed on the classical force field level and the enormous configuration space poses a great challenge, the obtained structures are not necessarily identical to the global minimum on the quantum chemical level of theory. Instead, they can be understood as good candidate solutions to the global minimum and generally represent stable clusters that cover a range of enthalpically or entropically favored configurations. In addition, many of the obtained structures are expected to collapse towards the same geometry during quantum chemical optimization. Therefore, we select a number of ten clusters evenly distributed in the energetic range of the final generation for subsequent quantum chemical optimization for each cluster size. These clusters were then optimized at the BP86/def2-TVZP[193] level of theory with Turbomole (version 7.41) and an energy convergence threshold of 10^{-9}.[194] The BP86 functional is proven to deliver good structural parameters results and, if combined with a basis set triple-ζ, to reproduce with good accuracy the measured vibrational fundamentals.[195,196] The London dispersion energy was taken into account by applying the D3 dispersion correction.[197,198] Frequency calculations were performed for all clusters and those with imaginary frequencies were excluded. To avoid duplicate clusters in the cluster

set, the structural similarity of all optimized clusters is quantified by their geometrical distance[153] d:

$$d(\mathcal{P},\mathcal{P}') = \left[\left(\frac{I_\mathrm{A} - I_{\mathrm{A}'}}{I_\mathrm{A}}\right)^2 + \left(\frac{I_\mathrm{B} - I_{\mathrm{B}'}}{I_\mathrm{B}}\right)^2 + \left(\frac{I_\mathrm{C} - I_{\mathrm{C}'}}{I_\mathrm{C}}\right)^2\right]^{\frac{1}{2}}, \tag{4.1}$$

wherein I and I' are the principal moments of inertia of the clusters $\mathcal{P}$ and $\mathcal{P}'$, respectively. Clusters $\mathcal{P}'$ with a geometrical distance of $d(\mathcal{P},\mathcal{P}') < 0.01$ were removed from the cluster set. At the end of this procedure, 10 clusters of neat HFIP, 11 of neat acetone, 13 of neat methanol, 45 of the mixed HFIP–acetone system and 73 of HFIP–methanol were ready to be analyzed and to be included as inputs for the further bQCE calculations. Their interaction energy, size, and composition are tabulated in the supporting information. In the following, clusters will be given unique labels of the form hXsY–Z, where h stands for HFIP, s can be either acetone (a) or methanol (m), X is the number of monomers of HFIP, Y is the number of monomers of s, and Z is a label to differentiate clusters of the same composition.

The bQCE Method

The theory of bQCE methods has been extensively detailed in several earlier works.[3,27,45,65] Through this method, we are able to calculate the cluster distribution and the thermodynamic properties of the system (for instance vaporization enthalpies) for a selected temperature range. Here, only a short overview of the bQCE method will be presented. As a first step, a system of non-interacting clusters in thermodynamic equilibrium is considered. Each cluster in that system is built up from either one (neat systems) or two (binary systems) monomers.

In thermodynamic equilibrium these clusters can transform into each other. We can write the equilibrium reaction between the clusters as

$$i(\mathcal{P})\mathrm{C}_1 + j(\mathcal{P})\mathrm{C}_2 \rightleftharpoons \mathrm{C}_\mathcal{P}, \tag{4.2}$$

where $i(\mathcal{P})$ and $j(\mathcal{P})$ are the number of monomers of each component C_1 and C_2 that form the cluster $\mathcal{P}$. The system's total partition function Q^tot at volume V and temperature

T is given by

$$Q^{\mathrm{tot}}(\{N_{\mathcal{P}}\}, V, T) = \prod_{\mathcal{P}=1}^{N} \frac{1}{N_{\mathcal{P}}!} \left[q_{\mathcal{P}}^{\mathrm{tot}}(V,T)\right]^{N_{\mathcal{P}}}, \tag{4.3}$$

where $q_{\mathcal{P}}^{\mathrm{tot}}$ is the partition function of the single cluster $\mathcal{P}$ and $\{N_{\mathcal{P}}\}$ is the full set of total cluster populations $N_{\mathcal{P}}$. This cluster partition function can be evaluated as product of partition functions corresponding to the different degrees of freedom:

$$q_{\mathcal{P}}^{\mathrm{tot}}(V,T) = q_{\mathcal{P}}^{\mathrm{trans}}(V,T) q_{\mathcal{P}}^{\mathrm{rot}}(T) q_{\mathcal{P}}^{\mathrm{vib}}(T) q_{\mathcal{P}}^{\mathrm{elec}}(T). \tag{4.4}$$

Here, $q_{\mathcal{P}}^{\mathrm{trans}}$ is the translational, $q_{\mathcal{P}}^{\mathrm{rot}}$ the rotational, and $q_{\mathcal{P}}^{\mathrm{vib}}$ the vibrational partition function. They are calculated from standard equations for the particle in a box, rigid rotator, and harmonic oscillator, respectively.[27,149] The electronic partition function $q_{\mathcal{P}}^{\mathrm{elec}}$ is calculated from the adiabatic binding energy $\Delta_{\mathrm{bind}} E_{\mathcal{P}}^{\mathrm{elec}}$ of the cluster.[150]

Until here, we considered our system to consist of non-interacting clusters. However, in order to describe a liquid, not only the binding energy within a cluster but also the inter-cluster interactions must be considered. First, in order to take the volume into account that is taken up by the clusters themselves and is inaccessible to translation, an exclusion volume V_{ex} must be subtracted from the phase volume V in $q_{\mathcal{P}}^{\mathrm{trans}}$. The exclusion volume is calculated as

$$V_{\mathrm{ex}} = b_{\mathrm{xv}} \sum_{\mathcal{P}=1}^{N} N_{\mathcal{P}} v_{\mathcal{P}}, \tag{4.5}$$

wherein b_{xv} is the empirical exclusion volume parameter to correctly scale the cluster volume $v_{\mathcal{P}}$, which is sensitive to the choice of the volume method and the atomic radii used therein. In previous works, b_{xv} was treated as temperature independent.[1,3,4,65,74] Here, we introduce a linear temperature dependence of b_{xv}

$$b_{\mathrm{xv}}(T) = T \cdot \beta_{\mathrm{xv}} + b_{\mathrm{xv}}^{0}, \tag{4.6}$$

where β_{xv} is the exclusion volume expansion coefficient and b_{xv}^{0} is the base of the intercept. A similar approach was used in the past by Kelterer and coworkers.[199]

Finally, the inter-cluster interactions must be taken into account. The electronic partition function $q_{\mathcal{P}}^{\mathrm{elec}}$ is extended by a volume dependent mean-field-like correction term:

$$q_{\mathcal{P}}^{\mathrm{elec}}(V,T) = \exp\left\{-\frac{\Delta_{\mathrm{int}}E_{\mathcal{P}}^{\mathrm{elec}} - [i(\mathcal{P}) + j(\mathcal{P})]\frac{a_{\mathrm{mf}}}{V}}{k_{\mathrm{B}}T}\right\}, \tag{4.7}$$

where k_{B} is the Boltzmann constant and the mean-field parameter a_{mf} is an empirical parameter, that scales the strength of the inter-cluster interactions.

When performing a bQCE calculation, the empirical parameters b_{xv}^{0}, β_{xv}, and a_{mf} are chosen such that the deviation from a given reference property, such as densities and phase transition temperatures, is minimized. In earlier works, a simple grid sampling algorithm was used to optimize the empirical parameters. With the introduction of a third parameter β_{xv} this method is no longer feasible. Here, the Differential Evolution algorithm[99] as implemented in the SciPy library[100] for PYTHON 3.4 is interfaced with the PEACEMAKER 2.8 code to find the best solution. The script is available upon request.

4.4. Results and Discussion

Here, we will discuss the results of our investigation of the binary mixtures of HFIP with acetone and methanol, respectively. These were obtained by employing the bQCE method to a set of quantum chemically optimized clusters depicting different binding motifs, that are representative for the specific interactions in each system. Instead of employing experimental data, in this work, we use isobars obtained from a set of classical molecular dynamics simulations of the mixed systems that we conducted at different temperatures and mixture compositions as detailed in the computational details section.

4.4.1. Classical Molecular Dynamics Simulations

Classical molecular dynamics simulations of both mixed systems HFIP/acetone and HFIP/methanol were carried out at defined temperatures ranging from 298.15–338.15 K in intervals of 10 K. These simulations were repeated at different compositions with mole fractions of HFIP of 0.2, 0.5, and 0.8. The results are listed in Tab. 4.1 for HFIP/methanol (top) and HFIP/acetone (bottom). Both binary mixtures show similar behavior. Due to the high density of HFIP, the density increases with the mole fraction of HFIP but decreases with rising temperature. In addition, Tab. 4.1 lists the experimental densities of

Table 4.1. **Top**: Calculated densities ρ^{calc} of the HFIP/methanol mixture in g/cm^3 at different temperatures and mole fractions.
Bottom: Experimental[169] densities ρ^{exp} and calculated densities ρ^{calc} of the HFIP/acetone mixture in g/cm^3 at different temperatures and mole fractions.

HFIP/MeOH

$\mathbf{x_{HFIP}}$	ρ^{exp}_{298}	ρ^{calc}_{298}	ρ^{calc}_{308}	ρ^{calc}_{318}	ρ^{calc}_{328}	ρ^{calc}_{338}
0.2	–	1.044	1.028	1.013	0.993	0.975
0.5	–	1.290	1.270	1.252	1.232	1.216
0.8	–	1.513	1.492	1.471	1.446	1.427

HFIP/Acetone

$\mathbf{x_{HFIP}}$	ρ^{exp}_{298}	ρ^{calc}_{298}	ρ^{calc}_{308}	ρ^{calc}_{318}	ρ^{calc}_{328}	ρ^{calc}_{338}
0.2	0.996	0.971	0.957	0.943	0.927	0.914
0.5	1.274	1.140	1.124	1.101	1.089	1.066
0.8	1.479	1.320	1.298	1.273	1.251	1.231

the HFIP/acetone mixture at 298.15 K, which were measured by Evans *et al.* using a single neck capillary tube pycnometer.[169] No experimental density could be found for the system HFIP/methanol. Our calculated densities for the system HFIP/acetone deviate by 2.5%, 10.5%, and 10.8% from the experimentally measured values at mole fractions 0.2, 0.5, and 0.8, respectively. This deviation can have an impact on the thermodynamic properties of mixing calculated via the bQCE approach, however we demonstrate in the supporting information (SI) that a deviation in this range only slightly affects the cluster population and thermodynamic properties such as entropies and enthalpies of vaporization. Approximated thermodynamics properties of mixing are included in the SI for sake of completeness.

In order to characterize the hydrogen bonds present in the mixtures, additional analyses were carried out including Radial Distribution Functions (RDFs), Coordination Numbers (CNs), and Angle Distribution Functions (ADFs) of the simulated systems at 298.15 K averaged over 19.8 ns of production run.

Fig. 4.1 shows (from top to bottom) the RDF, the CN, and ADF of the O-H$\cdots$O hydrogen bond between HFIP and acetone (left side) and between HFIP and HFIP (right side). Please note, HFIP is treated as the reference molecule. The observed molecule

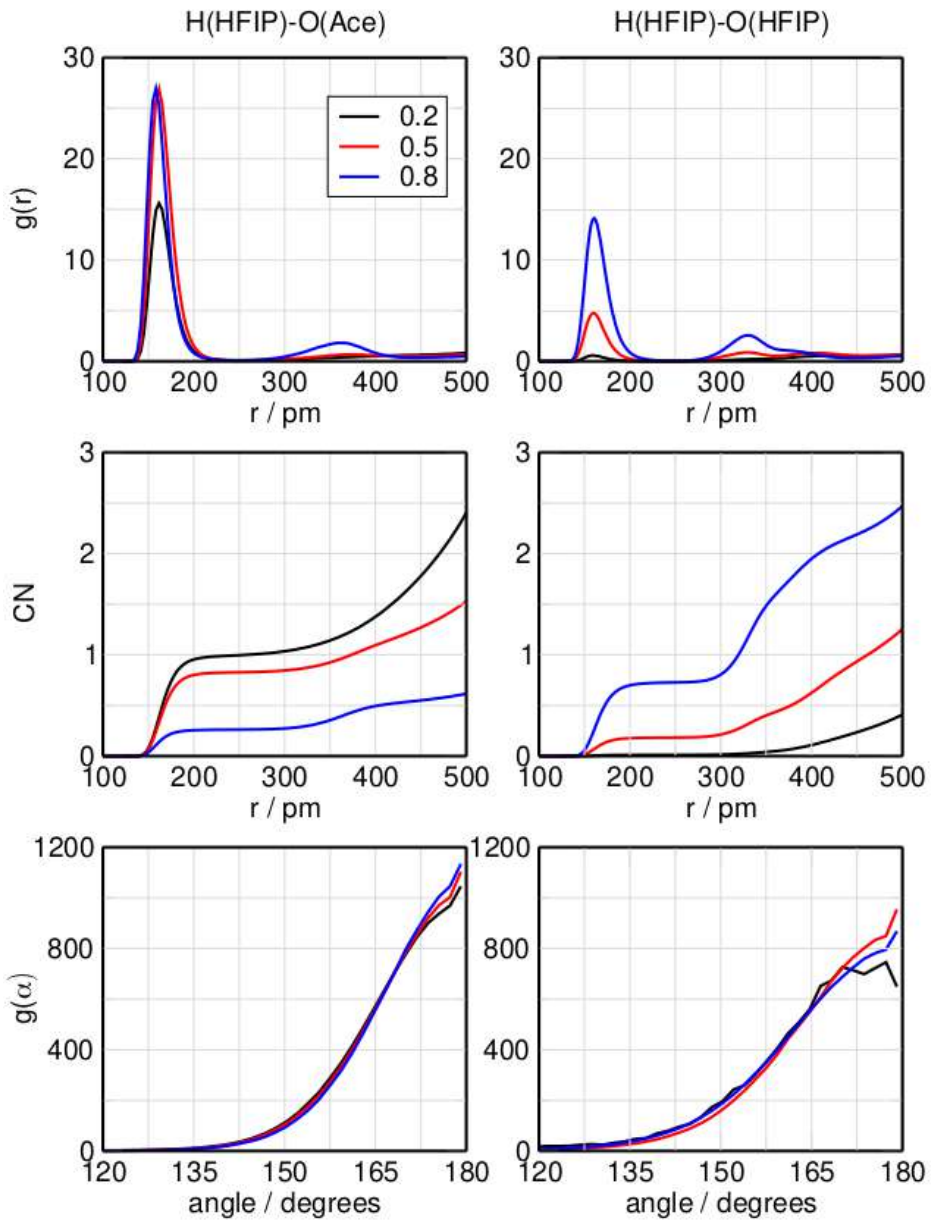

Figure 4.1. Radial distribution function, coordination number, and angular distribution function of the hydrogen bond for the system HFIP/acetone increasing the molar fraction of HFIP at 298.15 K with HFIP bond donor and acetone acceptor (left) or HFIP (right).

can be either acetone or another molecule of HFIP. The reference atom is the hydrogen of the hydroxy group, and the observed atom is the oxygen of the observed molecule. First, the inter-species hydrogen bond between HFIP and acetone will be considered. A sharp peak is present in the RDF at 161 pm at mole fractions of 0.2 and 0.5. The bond length decreases to 159 pm at a mole fraction of 0.8. An additional peak emerges around

350 pm at high concentrations of HFIP. The coordination number (CN) displayed in Fig. 4.1 provides insight into the average number of molecules participating in a hydrogen bond. A single hydrogen bond is possible between the two molecules. At a distance of 250 pm, which is the location of the first minimum in the RDF and can be considered the maximum hydrogen bond length, the CN is 1.0 for the mole fraction of 0.2, meaning all the possible hydrogen bonds are filled by this interaction. With an increasing mole fraction of HFIP of 0.5 and 0.8, the CN decreases to 0.83 and to 0.26, respectively. In the RDF of the same-species hydrogen bond between two molecules of HFIP, a peak is present at 164 pm, which becomes sharper as the mole fraction of HFIP increases. At mole fractions of 0.5 and 0.8 an additional peak is visible at 326 pm, indicating an involved hydrogen bond network. From the CN plot, it is immediately clear that inter-species interactions are preferred over neat ones at mole fractions of 0.2 and 0.5, whereas same-species interactions become predominant at a mole fraction of 0.8. In particular, at a mole fraction of 0.2 same-species interactions are almost absent with a CN close to 0, but the CN increases to 0.17 and 0.73 at mole fractions of 0.5 and 0.8, respectively. This is due to a smaller number of acetone molecules able to be coordinated by the HFIP, forcing the same-species interaction to happen more frequently. The CNs for different binding motifs sum up neatly to 1.0, excluding the possibility of a significant presence of non-associated monomeric species in the system. Considering the CNs at 450 pm, which is the location of the second minimum in the RDFs, the inter-species interactions are preferred with a value of 1.3 against 0.9 of the H(HFIP)-O(HFIP) interaction at a mole fraction of 0.5. However at a mole fraction of 0.8 the situation is different, with the same-species interaction winning over the mixed ones with CNs of 2.2 and 0.6, respectively. A third peak is not visible at larger distances (RDFs up to 15 Å are included in the SI). This might indicate circular configurations of neat HFIPs are present and maybe even preferred over chains at this mole fraction; however, this argument cannot exclude the presence of these linear formations. The bottom panels in Fig. 4.1 show the ADFs of the hydrogen bond angle. Both the inter-species and same-species hydrogen bonds show similar behavior and a clear preference for a linear arrangement.

In contrast to the HFIP/acetone mixture, both compounds in the HFIP/methanol

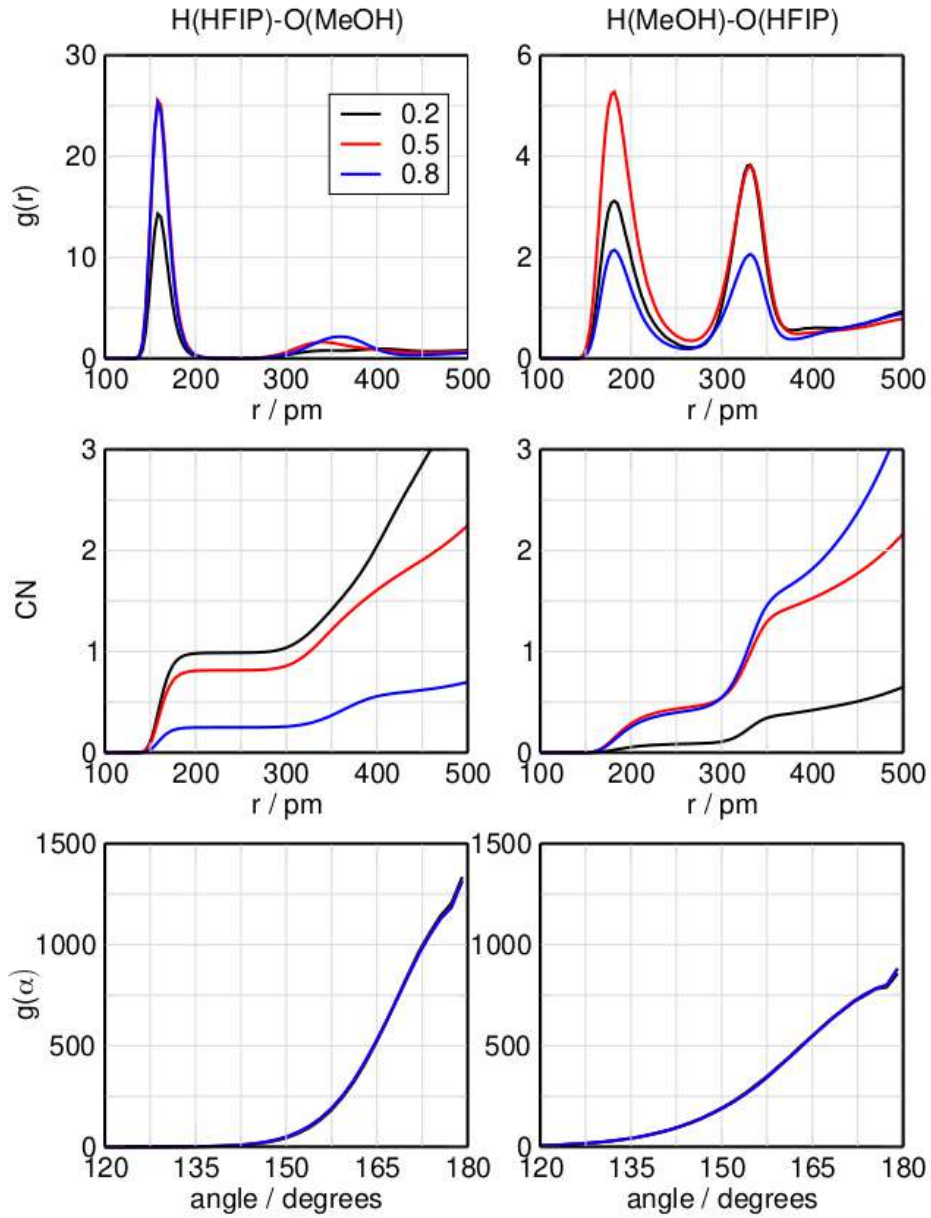

Figure 4.2. Radial distribution function, coordination number, and angular distribution function of the hydrogen bond for the system HFIP/methanol increasing the molar fraction of HFIP at 298.15 K with HFIP bond donor and MeOH acceptor (left), or MeOH donor and HFIP acceptor (right).

can act as hydrogen bond donor or acceptor. Fig. 4.2 shows the RDFs of the interspecies hydrogen bond length with HFIP acting as donor and acceptor, respectively. Looking at the (H)HFIP-(O)MeOH interaction first, the average hydrogen bond length is located at 160 pm. A second peak emerges at 340 pm as the mole fraction increases from 0.2 to 0.5, showing the possible presence of MeOH in the second structure coordination

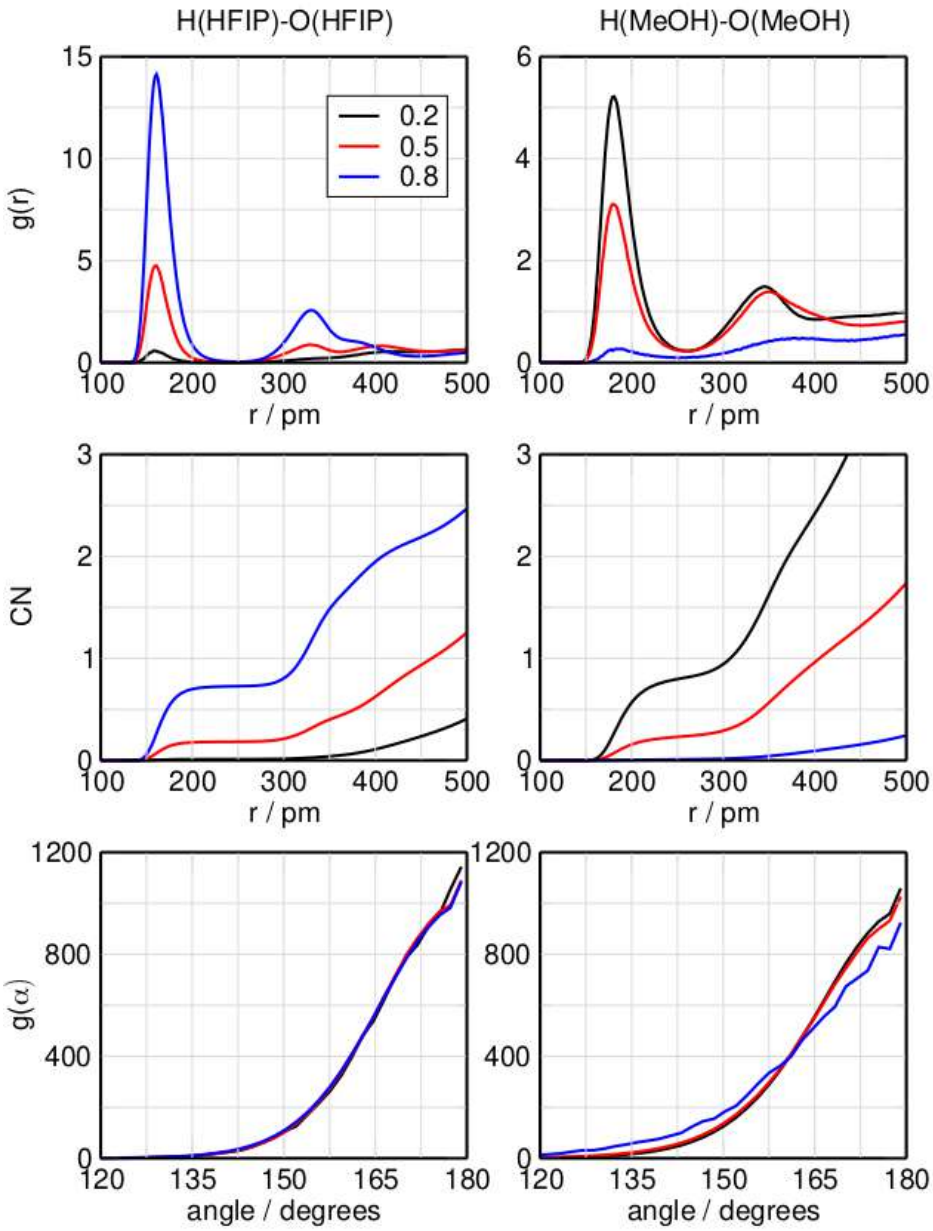

Figure 4.3. Radial distribution function, coordination number, and angular distribution function of the hydrogen bond for the system HFIP/methanol increasing the molar fraction of HFIP at 298.15 K, with HFIP donor and acceptor (left) or MeOH donor and acceptor (right).

shell of HFIP. This peak shifts to a slightly larger distance of 360 pm at higher HFIP concentrations. Here, the CNs are 0.98, 0.82, and 0.25 at mole fractions 0.2, 0.5, and 0.8 respectively, showing a similar behavior with an increasing concentration of HFIP as in the HFIP/acetone system. The ADFs show a similar preference for linear hydrogen bonds as observed for the HFIP/acetone mixture. Moving on to the (H)MeOH-(O)HFIP

interaction, which has HFIP acting as hydrogen bond acceptor and methanol as donor, it is immediately clear that interactions of this kind are much less prevalent in the mixture than hydrogen bonds of the opposite direction. At all three mole fractions two peaks are present at 181 pm and 333 pm, showing the first and second solvation shell of HFIP, respectively. The larger distance of 181 pm shows that the hydrogen bond donated by methanol is weaker than that donated by HFIP. Their position remains the same independent of the mixture's compisition. The left and right side of Fig. 4.3 show the RDF, CN, and ADF of the same-species hydrogen bonds shared between two molecules of HFIP and two molecules of methanol, respectively. The RDF of the (H)HFIP-(O)HFIP hydrogen bond shows a prominent peak at 161 pm and, similar to the same interaction in the mixture HFIP/acetone, as well as an additional peak at 324 pm at mole fractions of 0.5 and 0.8. Also similar to the previous mixture, the CN plot shows that only at mole fractions greater than 0.5 this interaction becomes predominant. In the RDF of the (H)MeOH-(O)MeOH interaction a peak is present at 180 pm, which decreases in intensity as the content of HFIP rises. A second peak at 340 pm can be observed at mole fractions of 0.2 and 0.5. This peak is still weakly present at 0.8 around 380 pm. With an increasing mole fraction of HFIP, the same-species interaction of methanol with itself are concentrated in the first solvation shell, with a second solvation shell being present but less populated. The CN suggests that the MeOH-MeOH hydrogen bond is more significant in the equimolar mixture than the HFIP-HFIP hydrogen bond. As for the previous system, the CN values for the biding motifs sum up to 1. The CNs of the different interaction motifs sum up neatly to 1.0, which shows that non-associated monomeric species aren't present in significant amounts. Considering the CNs at 400 pm, which is the location of the second minimum in the RDFs shown in Figs. 4.2 and 4.3, it is possible to get some insight over the geometric structures of these interactions, as for the previous system. At a mole fraction of HFIP of 0.2, the CNs the inter-species interactions H(HFIP)-O(MeOH) and H(MeOH)-O(HFIP) are 2.0 and 0.4, respectively, whereas the CN of the same-species interaction H(MeOH)-O(MeOH) is 2.4. The same-species interaction between two molecules of HFIP is negligible. The situation is different at a mole fraction of 0.5, where the CNs of both the mixed interactions show similar values of 1.6 for H(HFIP)-O(MeOH) and 1.5 for H(MeOH)-O(HFIP). The same-

species hydrogen bonds formed by pairs of HFIP or methanol have a CN of 0.6 and 1.0, respectively. At a mole fraction of 0.8, the CN of the H(HFIP)-O(MeOH) interaction drops to 0.6 and the CN of the H(HFIP)-O(HFIP) interaction has a value of 2.0. For this reason it is possible to assume that at this mole fraction, the neat interaction of HFIP with itself is dominant; however, a high CN of 1.8 for the H(MeOH)-O(HFIP) interaction suggests the presence of clusters where a single or several methanol molecules are coordinated by a larger number of HFIP molecules. As for the HFIP/acetone system, circular clusters seem to be a good description of the system; however, linear oligomers cannot be ruled out, and there is proof in literature of chain configuration in pure methanol.[200]

Overall, all the ADFs of this mixture at all mole fractions show that linear interactions are preferred.

The lifetimes τ of the hydrogen bonds in both mixtures were calculated as explained in the computational details and are presented in Tab. 4.2. A longer lifetime means a stronger bond, as it requires more time to break. In the top part of the table, the lifetimes of hydrogen bonds for the system HFIP/Acetone are listed. The H(HFIP)-O(Ace) hydrogen bond has a lifetime of 9 ps, whereas the same-species H(HFIP)-(O)HFIP hydrogen bond has a significantly shorter lifetime of 3 ps. With an increasing mole fraction of HFIP, the lifetimes of the inter-species hydrogen bonds increase, meanwhile the same-species interaction remains stable. In the bottom part of Tab. 4.2, the hydrogen bond lifetimes for the system HFIP/MeOH are presented. All four interaction types are considered. At a mole fraction of 0.2, the inter-species H(HFIP)-O(MeOH) hydrogen bond has a lifetime of 48 ps and it indicates this interactions as the preferred one in this system. With an increasing mole fraction of HFIP, the lifetime of this hydrogen bond decreases. The (H)MeOH-(O)MeOH hydrogen bond lifetimes are in good agreement with both experimental and calculated data from literature.[37,201,202] H(MeOH)-O(HFIP) is confirmed to be weaker than the other inter-species interaction.

4.4.2. Cluster Analysis

Multiple clusters are optimized following the procedure described in the computational details section above to build the cluster sets which serve as input for the bQCE method.

Table 4.2. Lifetimes of the hydrogen bonds in both HFIP/acetone and HFIP/MeOH increasing the molar fraction of HFIP at 298.15 K.

HFIP/Acetone			
	τ/ps(0.2)	τ/ps(0.5)	τ/ps(0.8)
H(HFIP)-O(Ace)	9	11	16
H(HFIP)-O(HFIP)	3	4	4
HFIP/MeOH			
	τ/ps(0.2)	τ/ps(0.5)	τ/ps(0.8)
H(HFIP)-O(MeOH)	48	45	43
H(MeOH)-O(HFIP)	2	2	2
H(HFIP)-O(HFIP)	11	11	11
H(MeOH)-O(MeOH)	4	4	2

One of the most important features of the bQCE method is that it assigns populations to all clusters in the cluster set. The goal is to find the equilibrium distribution of all clusters so that they reproduce the reference isobars. The monomer-normalized population gives a measure of the importance of specific clusters and interaction motifs in the system. These populations are available for each temperature in the investigated temperature range.

In Fig. 4.4 the most populated clusters in neat systems of pure HFIP, methanol, and acetone are shown for the temperature of 298.15 K. In the HFIP system, the tetramers h4-1 and h4-5 dominate the neat solvent, with populations of 0.57 and 0.37, respectively. In acetone the cyclic trimer a3-1 is the highest populated cluster with a population of 0.71. However, a significant amount of acetone molecules in the system exist in the form of non-associated monomers. The methanol system is dominated by ring formations, where the cyclic pentamers m5-1, m5-10, and hexamer m6-11 are the preferred geometries with values 0.37, 0.28, and 0.26 respectively.

Figures 4.5 and 4.6 show visualizations of the most populated clusters in the binary mixtures HFIP/acetone and HFIP/methanol at 298.15 K, respectively. Since dozens of clusters have been considered for both systems, here only the most populated ones are presented. Cartesian coordinates and visualizations of all cluster geometries are available in the supporting information. Focusing on Fig. 4.5 first, at the mole fraction 0.2 the neat

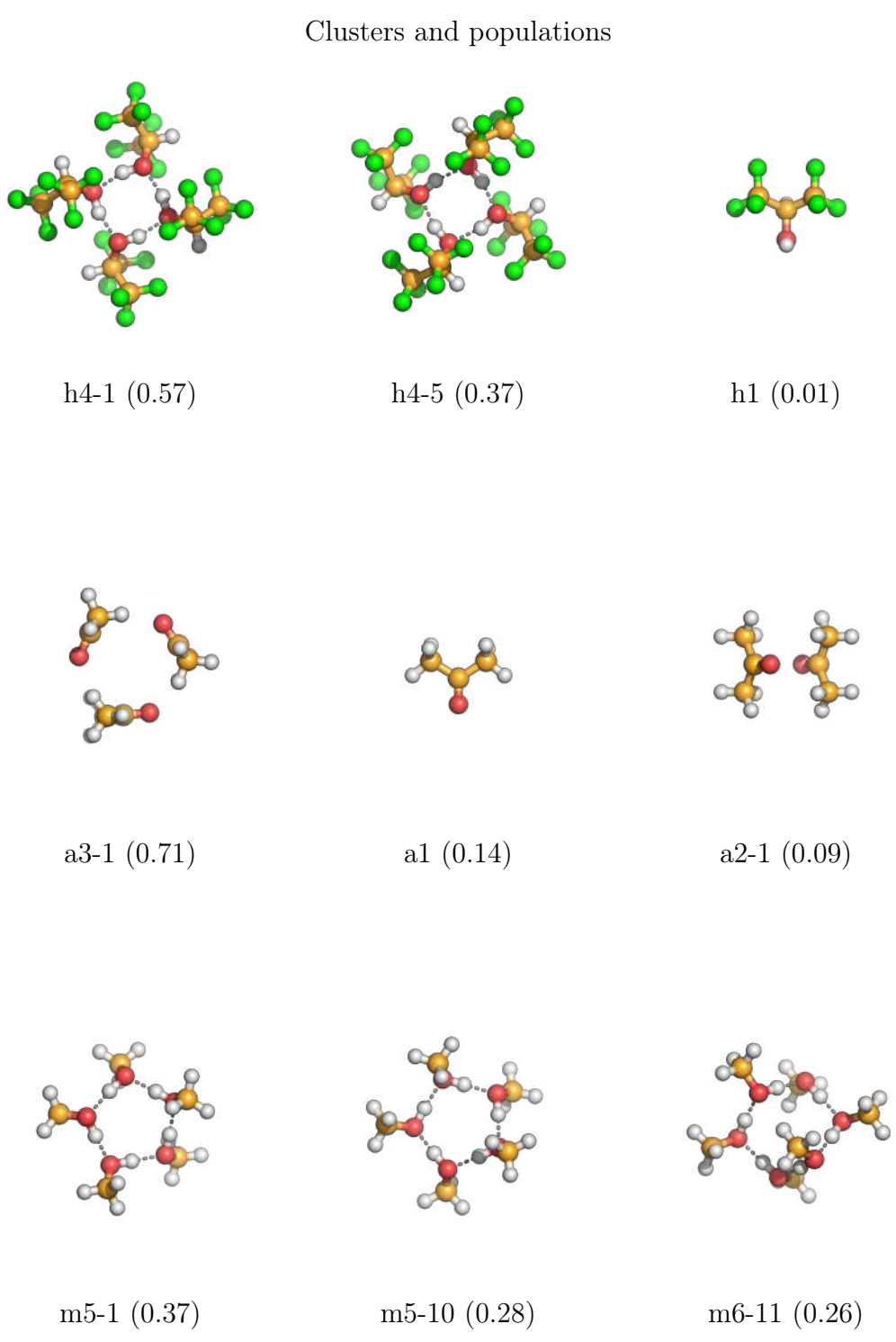

Figure 4.4. Structures and relative populations of the most populated clusters of the neat systems acetone (a), HFIP (h), methanol (m) at 298.15 K.

acetone trimer a3-1, which consists of three acetone molecules arranged in a triangular ring structure, is the most populated cluster with a value of 0.33, followed by the mixed

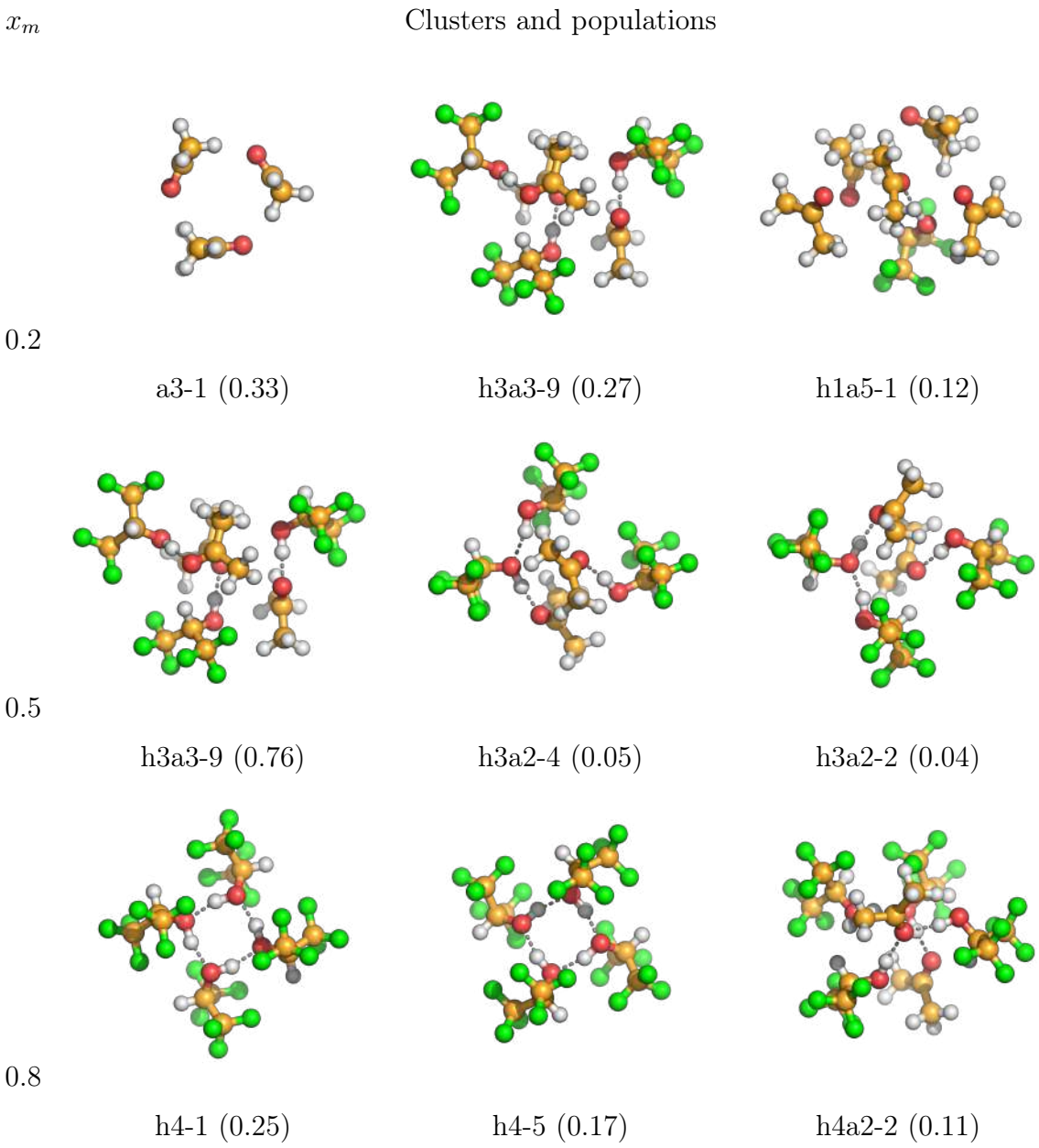

Figure 4.5. Structures and relative populations of the most populated clusters of the system HFIP/acetone at the molar fraction of HFIP 0.2, 0.5, 0.8 at 298.15 K.

hexamer h3a3-9 with 0.27. The same cluster, which can be described as aggregation of three alternating hydrogen bonded HFIP/acetone dimers, is the most populated cluster in the equimolar mixture of HFIP and acetone with a population of 0.76. Please note that clusters with compositions that differ from the system's molar composition can be populated as the bQCE method will automatically find a cluster distribution that is consistent with the system's molar composition. In agreement with the CNs measured

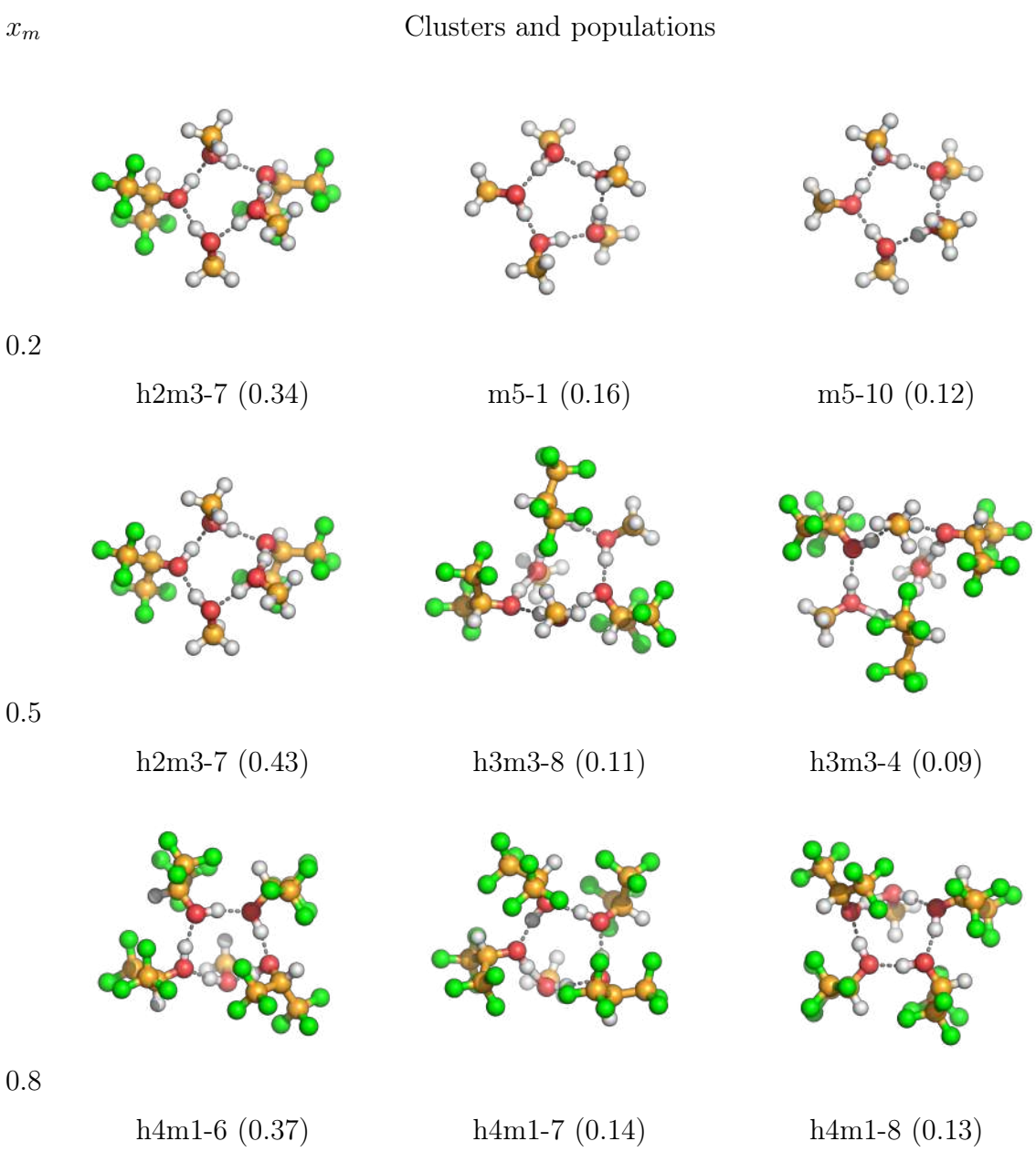

Figure 4.6. Structures and relative populations of the most populated clusters of the system HFIP/methanol at the molar fraction of HFIP 0.2, 0.5, 0.8 at 298.15 K.

from MD simulations of the same system (Fig. 4.1), there are no same-species bonds of HFIP in this cluster.

In contrast, at the higher mole fraction of 0.8, the neat HFIP tetramers are the most populated, which feature four HFIP molecules arranged in a quadratic ring of hydrogen bonds, each acting as both acceptor and donor. This indicates a mixture in which at lower concentrations of HFIP the inter-species hydrogen bond between HFIP and acetone is the

most common interaction, in agreement with the CN plots in Fig. 4.1. There is a good agreement between the CN at 400 pm and the RDF of the neat HFIP interactions and the most populated clusters at this mole fraction; already the classical simulation suggests the presence of neat HFIP rings at a mole fraction of 0.8. The distance between one H atom and the O atom on the molecule opposite to it in the tetramer is 327 pm, really close to the second RDF peak for the same-species interaction at 326 pm in Fig. 4.1. At higher concentrations of HFIP, cooperative effects between multiple HFIP molecules become more important and the system is dominated by hydrogen bonded ring formations, while mixed interactions are still significant.

In Fig. 4.6 the most populated clusters of the HFIP/methanol mixture are displayed. At low concentration of HFIP, the highly coordinated hydrogen bond ring formations of the neat methanol pentamers dominate the system. But already at the low mole fraction of 0.2, the mixed h2m3-7 cluster, which contains hydrogen bonded HFIP and methanol molecules forming a ring in an alternating pattern, is highly populated. The possible presence of these kind of clusters was already suggested when discussing Figs. 4.2 and 4.3. The significance of the mixed h2m3-7 cluster carries over to the equimolar mixture, where it is still the highest populated cluster and more populated than the stoichiometrically favored clusters h3m3-8 and h3m3-4, which are the second and third highest populated clusters. At high concentrations of HFIP, and in contrast to the HFIP/acetone mixture, the system is dominated by the mixed clusters h4m1-6, h4m1-7, and h4m1-8. This is in good agreement with the conclusions drawn from Figs. 4.2 and 4.3.

Overall, there is a good agreement for both systems between the classical MD simulations and the populations calculated via the bQCE approach.

For now, the most significant clusters were considered only at room temperature. However, as the temperature changes other cluster formations might emerge and begin to dominate the bulk structure. The bQCE model provides such information and allows insight into the temperature dependence of the cluster equilibrium distribution in the selected temperature range of 298.15–338.15 K. Here, we will take a look at the populations of neat and mixed clusters and their evolution with temperature, which are shown in Figs. 4.7 and 4.8 for different mole fractions of HFIP in the mixtures HFIP/acetone

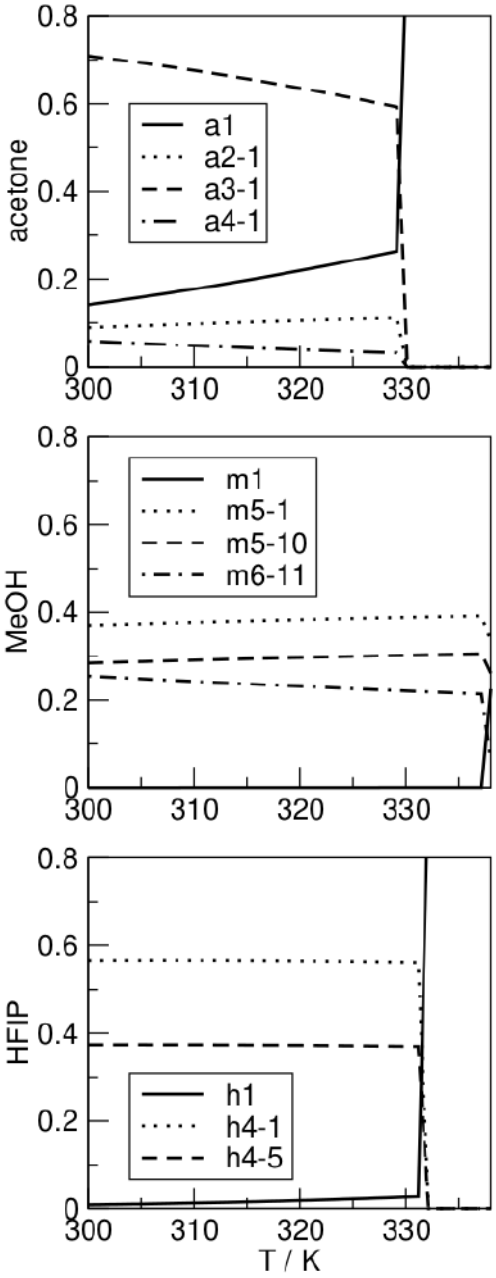

Figure 4.7. Populations of neat acetone (a), MeOH (m), and HFIP (h) (from top to bottom) in the temperature range of 298.15-338.15 K.

and HFIP/methanol, where their population is significant (higher than 0.05). The top panel in Fig. 4.7 shows the cluster populations in neat acetone. The trimeric a3-1 cluster dominates the system, but with rising temperature its population decreases in favor of the acetone monomer. In the center panel, cluster populations in the methanol system

are presented. The pentamers m5-1 and m5-10 together with the hexamer m6-11 dominate the system until the boiling point is reached. Several research groups investigated neat methanol with the QCE approach. A recent work from Teh and coworkers,[203] which extensively investigates methanol cluster populations with both DFT and MP2 geometry optimization, states the most populated cluster is the octamer, which is not investigated in this article due to the computational time required, as explained in the computational details section. An older work by Kelterer and coworkers[199] finds instead that the most populated cluster size is the hexamer, followed by the pentamer, regardless that also clusters up to the octamer were investigated. The differences between those works and this article can be imputed to the geometry optimization and frequency calculation at different levels of theory,[203] or to a different procedure to generate the clusters.[199] However, there is a general agreement that multi-molecular cyclic clusters are preferred until the boiling point, while in the gas phase the monomer dominates the population. In the bottom panel, the cluster populations in neat HFIP show that the tetramers h4-1 and h4-5 dominate the system until the boiling point.

Fig. 4.8 shows the cluster populations in the mixed systems at different mole fractions of HFIP. At low concentrations of HFIP, the neat acetone trimer is the preferred cluster at 298.15 K, whereas the monomer population increases significantly with rising temperature. This is due to the breaking of the enthalpically favored inter-species hydrogen bonds (calculated interaction energy of -53.6 kJ/mol) and the rise of entropically favored small clusters such as the acetone dimer (calculated interaction energy of -26.8 kJ/mol) and the non-associated acetone monomer. Pure HFIP clusters are not populated even at higher temperature. Instead, HFIP is bound in mixed clusters, of which the hexamer h3a3-9 is the most populated. In the equimolar HFIP/acetone mixture, the hexamer h3a3-9 is highly populated at 298.15 K, but with rising temperature decreases in population in favor of the acetone monomer and smaller mixed clusters dominated by HFIP. At high concentrations of HFIP, neat acetone clusters are almost absent. Meanwhile, the tetrameric neat HFIP clusters h4-1 and h4-5 are significantly populated, which is in agreement with earlier observations of the emergence of cooperativity effects at high HFIP concentrations. With rising temperature, the population of mixed clusters increases.

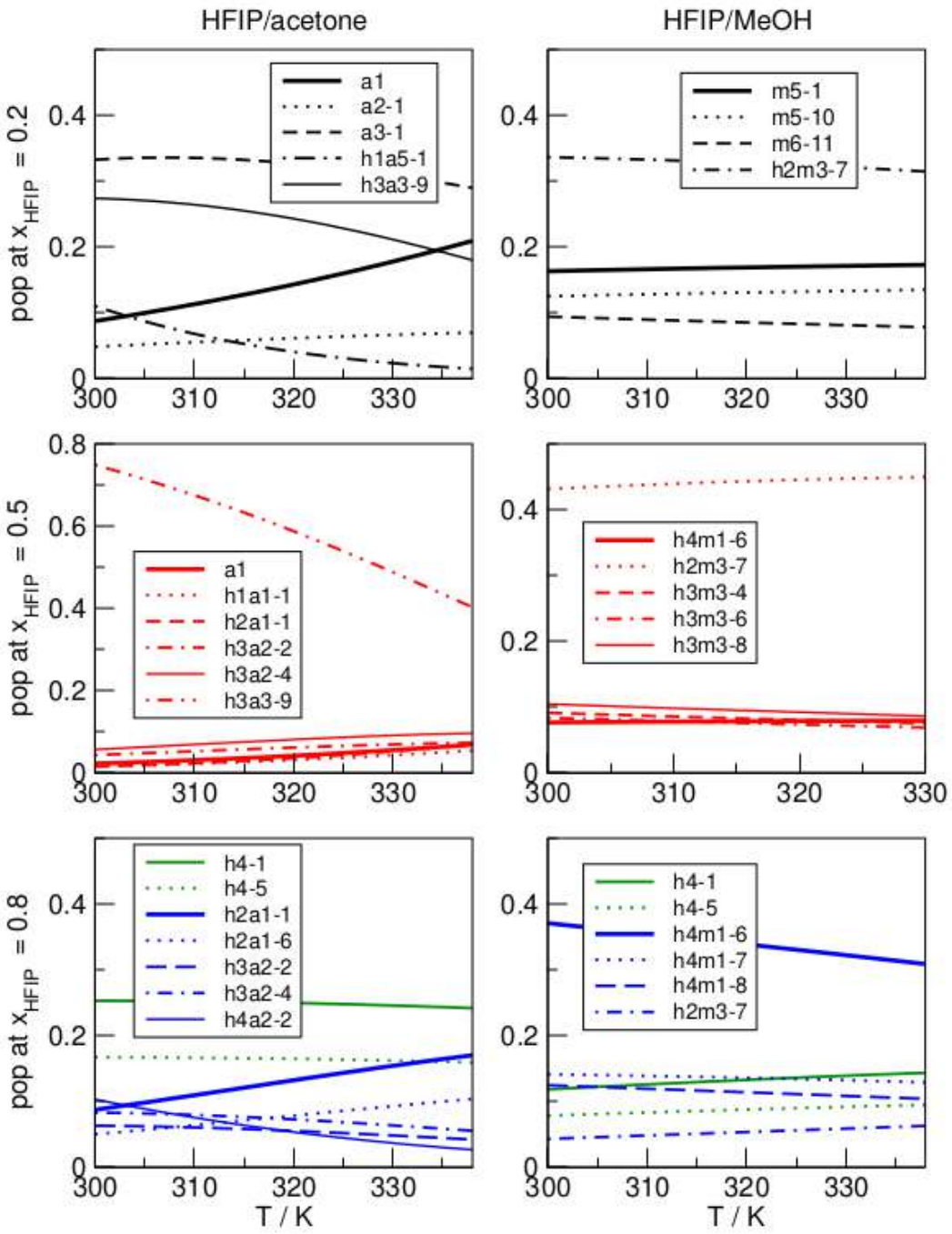

Figure 4.8. Populations of acetone (a), HFIP (h), MeOH (m) and mixed clusters at (from top to bottom) 0.2, 0.5, and 0.8 HFIP molar fraction, in the temperature range of 298.15-338.15 K.

The right column of Fig. 4.8 shows the cluster populations in the HFIP/methanol. In contrast to the other mixture, the methanol-dominated mixed cluster h2m3-7 is more populated at low concentrations of HFIP and the populations are nearly constant over

Table 4.3. Hydrogen bond distances, angles, and interaction energy of different dimers ΔE at the BP86/TZVP level of theory in kJ/mol. The hydrogen bond donor is written before the acceptor.

Dimer	ΔE	r(pm)	$\alpha(^\circ)$
$(HFIP)_2$	-21.6	184	168.74
$(MeOH)_2$	-23.6	183	169.78
$(Ace)_2$	-23.1	–	–
HFIP-MeOH	-36.8	170	175.44
MeOH-HFIP	-12.8	201	165.52
HFIP-Ace	-37.6	170	170.46

temperature. The equimolar mixture is again composed mainly by mixed clusters, in particular the methanol-dominated h2m3-7, whereas neat clusters are absent. At high concentrations of HFIP, the HFIP-dominant mixed cluster h4m1-6 dominates the system, but with rising temperature its population decreases in favor of pure HFIP clusters. Neat HFIP clusters are significantly populated, but less than in the HFIP/acetone mixture.

For both systems, the formation of close inter-species interactions is favored over interactions of the same species. This behavior is more pronounced for the HFIP/methanol mixture.

To complete the quantum cluster equilibrium analysis, the interaction energies, the hydrogen bond lengths, and the hydrogen bond angles of the dimers, are presented in Tab. 4.3, wherein for mixed dimers the first named species is the hydrogen bond donor and the last named species is the hydrogen bond acceptor. It is apparent that the interaction energies of the mixed dimers, where HFIP acts as the donor, are significantly stronger than that of any neat dimer. Both the bond lengths and interaction energies of the isolated dimers indicate the importance of inter-species interactions over same-species interactions if HFIP is the hydrogen bond donor, in line with the MD results presented before, where there are exclusively H(HFIP)-O(Ace) and H(HFIP)-O(MeOH) interactions at mole fractions of HFIP of 0.2 and 0.5.

4.4.3. Thermodynamic Properties of Neat and Mixed Systems

Through calculating the system's total partition function based on the equilibrium distribution of a set of representative clusters, the bQCE method grants access to the absolute thermodynamic functions such as the Gibbs energy G, enthalpy H, and entropy S at any investigated temperature. Using the bQCE method, we can thus calculate properties such as the enthalpy and entropy of vaporization ΔH_{vap} and ΔS_{vap} as simple difference of the liquid phase and a gas phase reference. Already in earlier works we were able to establish our procedure of using a so-called QCE^0 calculation, wherein a_{mf} is set to 0 removing all inter-cluster interactions, as gas phase reference.[1,4,81] Tab. 4.4 compare the calculated vaporization enthalpies and entropies of the neat systems to their experimental reference values at room temperature and the boiling point. Overall, good to excellent agreement with the experimental reference is achieved for all systems. This is true both at room temperature and at boiling points of the solvents. In all cases, $\Delta_{\mathrm{vap}}H$ is slightly overestimated, possibly indicating an over-stabilization of the liquid phase. The largest deviation is observed for methanol at its boiling point. A likely explanation is the experimentally observed aggregation of methanol molecules to small clusters in the gas phase,[204] which is not properly sampled by the QCE^0 calculation, as the monomers are populated with 99%. This is in agreement with our already published calculated $\Delta_{\mathrm{vap}}H$ of 39.33 kJ/mol of methanol at room temperature presented in a previous work, calculated at the same level

Table 4.4. Calculated and experimental enthalpy $\Delta_{\mathrm{vap}}H$ (kJ/mol) and entropy $\Delta_{\mathrm{vap}}S$ (J/mol K) of vaporization of the neat substances at 298.15 K and at the boiling point temperature. Experimental values, where present, were taken from the NIST Chemistry WebBook.[147]

Solvent	T	$\Delta^{calc}_{\mathrm{vap}}H$	$\Delta^{exp}_{\mathrm{vap}}H$	$\Delta^{calc}_{\mathrm{vap}}S$	$\Delta^{exp}_{\mathrm{vap}}S$
Acetone	298.15	32.65	31.27	98.38	95.00
	329.30	30.11	29.10	91.45	88.37
HFIP	298.15	42.25	41.60	126.42	–
	331.35	40.96	–	123.62	–
Methanol	298.15	40.14	37.6	99.45	114.89
	337.70	39.89	35.21	114.23	104.26

Table 4.5. Enthalpies and entropies of vaporization at 298.15 K for the HFIP/Acetone mixture (left) and the HFIP/MeOH mixture (right) at the x_m molar fraction of HFIP. Enthalpies in kJ/mol, entropies in J/(mol K).

	HFIP/Acetone		HFIP/MeOH	
x_m	ΔH_{vap}^{calc}	ΔS_{vap}^{calc}	ΔH_{vap}^{calc}	ΔS_{vap}^{calc}
0.2	43.39	111.75	35.75	102.12
0.5	46.57	125.08	55.62	111.37
0.8	46.01	121.06	42.65	119.51

of theory.[1] Here, we obtain a slightly different value due to the changes in methodology.

Enthalpies and entropies of vaporization at 298.15 K were calculated for the mixed systems as well, see Tab. 4.5. For HFIP/acetone the calculated vaporization enthalpies are higher than those of the neat components, with the highest value calculated for a mole fraction of 0.5. In contrast, the entropies of vaporization are always higher than that of pure acetone, but lower than that of pure HFIP. In HFIP/methanol at a mole fraction of 0.2 the calculated enthalpy of vaporization is lower than those of the neat components. At higher mole fractions, the enthalpy of vaporization is higher than those in either of the neat components, similar to the HFIP/acetone system. The same behavior is observed for the entropy of vaporization.

4.5. Conclusions

The mixtures of HFIP with methanol and acetone were investigated. First, molecular dynamics simulations were performed to get the isobars of the systems for the temperatures 298.15, 308.15, 318.15, 328.15, and 338.15 K at mole fractions of HFIP of 0.2, 0.5, and 0.8, respectively. Then the structure of the hydrogen bond from the simulations were analyzed and discussed. Molecular dynamics simulations and hydrogen bond evaluation from the dimer clusters calculated at DFT level are in good agreement. Together with the population analysis and the evaluation of the most populated clusters, we are presenting two strongly interacting mixtures, with some hints that the HFIP/methanol system presents a stronger hydrogen bond framework. Clusters of up to six molecules

were optimized at DFT level for both the mixtures and the neat systems. The hydrogen bonds of the dimers were analyzed. The calculated clusters, from simulated isobars and experimental data, where available, were used as input for the binary quantum cluster equilibrium method to get the thermodynamic properties. The enthalpies and entropies of vaporization of the neat systems are in good agreement with previous theoretical results and with experimental values. In addition, enthalpies and entropies of vaporization were calculated for the mixed systems.

Acknowledgment

B. Kirchner and G. Marchelli would like to express their gratitude to the ETN Socrates (http://etn-socrates.eu/) because this project has received funding from the European Union's EU Framework Programme for Research and Innovation Horizon 2020 under Grant Agreement No 721385. B. Kirchner and J. Ingenmey thank the DFG under the grant project number 406232243.

5. Conclusions

To investigate the liquid phase, mixtures of solvents in particular, it is imperative to understand and model their behavior and intermolecular interactions. Among them, the hydrogen bond (HB) network that can be formed between an HB donor and an acceptor is the most important one. At the same time, the tools and models currently used to investigate liquids are either computationally expensive or dependent on experimental data; therefore novel approaches must be adopted to address this problem more specifically.

In this thesis the binary Quantum Cluster Equilibrium (bQCE) approach, that relies on the description of the liquid and vapor phase as an ensemble of molecular clusters, has been applied to mixtures of small organic solvents with remarkable results. In Chapter 3, this approach has been applied to the mixture of methanol with small alcohols. A chain length ranging from two to four carbon atoms was considered, as well as the different branching of the isomers, to understand their respective influence on the hydrogen bond network. The semi-empirical extended tight binding method GFN2-xTB[91,92] was used to geometrically optimize thousands of clusters calculated via the genetical algorithm OGOLEM[103,104] interfaced with the AMBER[152] package for molecular dynamics. The resulting clusters were used as inputs for the bQCE calculations, and the activity coefficients of methanol in the alcohols – and viceversa – were calculated from the excess Gibbs energy of mixing. The activity coefficients measure a mixture's deviation from ideality. Increasing the chain length of the solvent, a larger deviation from ideality can be seen; the branching, on the other hand, brings the systems closer to an ideal mixture. These results show clearly that the mixture methanol/*tert*-butanol is closer to an ideal mixture than methanol/*n*-butanol. These studies can be extended to more complex systems, and they are a good indication on how to tune or develop novel mixtures, depending on the properties desired

for the specific problem. The same cluster set used to calculate the thermodynamic properties via the bQCE approach was employed also to determine the average length and angle of the hydrogen bond in the mixture methanol/*tert*-butanol. Combined distribution functions (CDFs) of the distance against the angle were calculated. These CDFs were weighted using the populations calculated with the bQCE approach, giving a more reliable description of the hydrogen bond network of the systems. Additionally, the intensity maximum in the CDFs moves to smaller values, i.e. the average hydrogen bond distance and angle, decreases with increasing molar fraction of methanol. This approach can be applied to bigger systems and the same analysis can be done to describe the intermolecular interactions of a binary system more precisely.

In Chapter 4, the binary mixtures of hexafluoroisopropanol (HFIP) with acetone and methanol were simulated via classical molecular dynamics at different temperatures, and their simulated densities were used as input for the subsequent bQCE calculations. The choice of the solvents was not randomly made: while the previous work aimed to be a benchmark for future steps in the description of the intermolecular interactions in organic solvents, this study's purpose was to describe two systems already known in literature whose inter molecular interactions were never deeply investigated. HFIP is a remarkable solvent used in different fields,[164–168] while acetone is a hydrogen bond acceptor, and methanol is both an acceptor and a donor. Both organic solvent mixtures are described with a combination of bQCE and molecular dynamics, and the results can be considered as a model case study to understand and describe the intermolecular interactions – in particular the hydrogen bond network – of novel solvents mixtures, e.g. deep eutectic solvents, whose interesting properties rely deeply on the hydrogen bond interactions between their components. The two mixtures are simulated with classical molecular dynamics in the temperature range of 298.15–338.15 K with a step of 10 K for molar fractions of HFIP of 0.2, 0.5, and 0.8 in order to calculate their densities. The hydrogen bond network of both systems is analyzed at 298.15 K, considering HFIP the hydrogen bond donor and, for the HFIP/methanol mixture, both donor and acceptor. The coordination numbers – calculated as the integral of the radial distribution function of the hydrogen bonds multiplied by the bulk density – provide insights on the average number of molecules participating

in the hydrogen bond network. In both the mixtures it is clear that there is no significant presence of non-interacting monomers. The situation where HFIP acts as hydrogen bond donor and the respective second compound acts as an acceptor shows to be preferred even at low concentrations of the solvents. Additionally, the analysis of the molecular dynamics trajectories shows that both mixtures are typically found in a long distance interaction structure. A more quantitative approach was desired for this investigation. For this reason the clusters used for the bQCE calculations have been geometrically optimized at DFT level instead of employing semi-empirical methods. The downside of this approach lies in the necessity to downsize the cluster size to a maximum of six molecules due to the increased computational cost. In addition, the bQCE theory has been expanded, as explained in Section 2.2.2, to include temperature dependent parameters. The populations of the neat systems and the mixtures with 0.2, 0.5, and 0.8 molar fractions of HFIP have been calculated. The most populated clusters are presented and the corresponding population plots are reported for a temperature ranging from 298.15 to 338.15 K with a step size of 1 K. The mixed clusters are populated even at low molar fractions of HFIP, in good agreement with the molecular dynamics analysis. Finally, the enthalpies and entropies of vaporization are calculated via the bQCE approach, and the values obtained for the neat systems show a good agreement with the data available in literature. As no experimental data for the mixed systems could be found, this bQCE study presents the first attempt to measure them. Since the systems were first simulated via classical molecular dynamics and the resulting densities have then been used as reference for the bQCE calculations, it is important to remark that no experimental reference data were required in this investigation.

These works are a first step in a wider field. Thanks to the now validated and expanded bQCE approach, the description of the intermolecular interactions is computationally accessible for a multitude of solvents and binary mixtures, such as ionic liquids or deep eutectic solvents (DES). In particular, some HFIP-based type V DESs have already been experimentally investigated, and their structure can now be studied with the approach tested in this thesis. The future developments of the work presented lead in this direction. As molecular dynamics simulations can provide the data needed for the bQCE

calculations, this combination can free the modeling of new solvents from the necessity to rely on experimental reference values, which might be not available from literature. This approach can be found especially useful to develop and investigate novel mixtures in the context of green chemistry.

In conclusion, this thesis presents the results obtained via the bQCE approach, combined with quantum chemical calculations and classical molecular dynamics simulations, on mixtures of organics solvents. Their thermodynamic properties were calculated and their populations at different temperatures are presented. The bQCE theory was expanded to include temperature dependent parameters and a novel approach, combining the model with classical molecular dynamics simulations, was tested. A new protocol to generate the data necessary for the bQCE calculations starting from classical molecular dynamics simulations was developed. The mixtures of HFIP/methanol and HFIP/acetone, already studied in literature but never deeply analyzed before, were successfully investigated with this procedure in order to describe their intermolecular interactions.

Appendix

A. Supporting Information to Chapter 3

A.1. BP86 Data

Table A.1. Calculated and experimental enthalpies of vaporization $\Delta_{\text{vap}}H$ and $\Delta_{\text{vap}}H^{\text{exp}}$ in kJ mol^{-1} for the neat systems at standard conditions. Experimental enthalpies of vaporization are taken from the NIST Chemistry WebBook.[147]

	$\Delta_{\text{vap}}H$	$\Delta_{\text{vap}}H^{\text{exp}}$
methanol	34.11	37.60
ethanol	40.00	42.30
n-propanol	44.41	47.00
iso-propanol	44.18	45.00

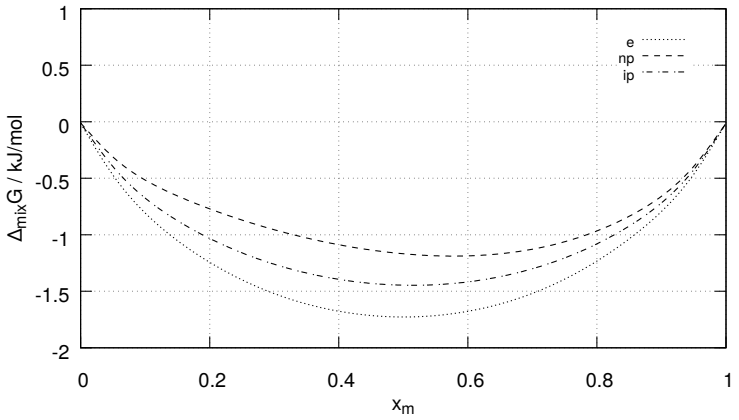

Figure A.1. Calculated Gibbs energies of mixing $\Delta_{\text{mix}}G^{\text{e}}$ for binary mixtures of methanol with ethanol (e), *n*-propanol (np), *iso*-propanol (ip), *n*-butanol (nb), *iso*-butanol (ib), and *tert*-butanol (tb) at 298.15 K. x_m indicates the mole fraction of methanol.

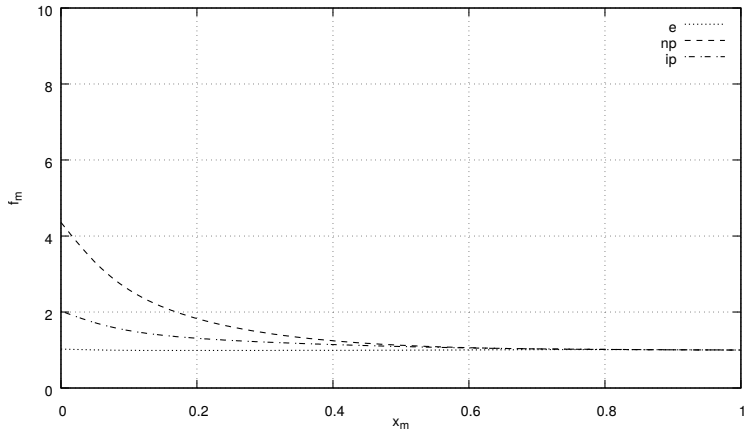

Figure A.2. Activity coefficients of methanol f_m in binary mixtures with ethanol (e), *n*-propanol (np), *iso*-propanol (ip), *n*-butanol (nb), *iso*-butanol (ib), and *tert*-butanol (tb) at 298.15 K. x_m indicates the mole fraction of methanol.

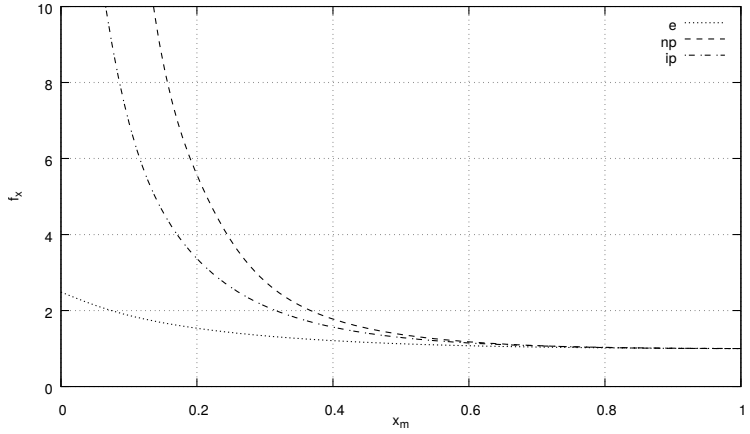

Figure A.3. Activity coefficients f_x of ethanol (e), *n*-propanol (np), *iso*-propanol (ip), *n*-butanol (nb), *iso*-butanol (ib), and *tert*-butanol (tb) in binary mixture with methanol. x_m indicates the mole fraction of methanol.

A.2. Number of Clusters

Table A.2. Number of clusters per size for pure alcohols.

	1	2	3	4	5	6	7	8	9
MeOH	1	2	1	2	2	6	6	11	5
EtOH	1	1	5	3	4	4	3	4	9
n-PrOH	1	1	3	3	5	7	4	3	4
i-PrOH	1	1	1	1	4	7	11	6	7
n-BuOH	1	2	4	1	1	3	6	8	4
i-BuOH	1	3	3	1	3	5	1	2	1
t-BuOH	1	1	1	1	3	1	5	8	7

Table A.3. Number of clusters per size for mixed alcohols.

	EtOH								n-PrOH								i-PrOH							
MeoH	1	2	3	4	5	6	7	8	1	2	3	4	5	6	7	8	1	2	3	4	5	6	7	8
1	1	4	5	6	3	4	3	1	2	3	3	3	1	1	7	4	1	4	2	1	3	11	14	9
2	4	1	3	3	4	5	5		4	2	6	8	3	2	4		3	2	4	3	11	8	10	
3	4	7	2	5	7	6			2	8	4	4	4	2			2	2	6	5	10	11		
4	9	9	6	7	5				4	5	7	4	6				4	6	4	2	12			
5	5	3	7	6					6	6	5	1					5	2	5	7				
6	4	6	5						5	2	2						4	6	5					
7	10	4							6	9							5	6						
8	4								3								4							
	n-BuOH								i-BuOH								t-BuOH							
	1	2	3	4	5	6	7	8	1	2	3	4	5	6	7	8	1	2	3	4	5	6	7	8
1	2	2	2	3	2	1	6	2	1	3	2	2	1	1	4	6	1	1	1	7	7	5	2	7
2	3	3	4	2	6	2	5		3	1	3	2	2	4	6		3	2	3	8	7	10	6	
3	3	5	6	5	4	5			5	4	3	4	4	3			2	3	3	9	9	8		
4	6	1	5	6	1				4	2	7	6	8				3	3	4	8	10			
5	3	2	5	3					6	6	6	3					5	3	11	11				
6	4	4	4						7	7	4						5	6	12					
7	2	5							8	5							6	5						
8	2								7								3							

A.3. Interaction Energies

The interaction energies of all the quantum optimized clusters used in Chapter 3 are available free of charge from the online version of the Supporting Information at:

https://chemistry-europe.onlinelibrary.wiley.com/action/downloadSupplement?doi=10.1002%2Fopen.202000171&file=open202000171-sup-0001-misc_information.pdf

B. Supporting Information to Chapter 4

B.1. Molecular Dynamics Simulations

B.1.1. Force Field Parameters

Table B.1. Force field bond coefficients.

K_r (kcal/(molÅ^2))	r (Å)	Bond type
HFIP		
734.000	1.3600	CT-F
268.000	1.5300	CT-CT
320.000	1.3600	CT-OH
2000.000	1.0900	CT-HC (must be fixed)
2000.000	1.0000	OH-HO (must be fixed)
Acetone		
317.000	1.5220	C - CT
570.000	1.2290	C - O
340.000	1.0900	CT - HC
MeOH		
320.000	1.4100	CT-OH
340.000	1.0900	CT-HC
553.000	0.9600	OH-HO

Table B.2. Force field pair coefficients.

ϵ (kcal/mol)	σ (Å)	atom type
HFIP		
0.097098	3.3611	CT
0.071041	3.1578	F
0.000000	0.0000	HO
0.028321	2.3734	HC
0.203255	2.9548	OH
Acetone		
0.105000	3.7500	C
0.066000	3.5000	CT
0.030000	2.5000	HC
0.210000	2.9600	O
MeOH		
0.066000	3.5000	CT
0.170000	3.1200	OH
0.000000	0.0000	HO
0.030000	2.5000	HC

Table B.3. Force field angle coefficients.

K_r (kcal/(mol rad^2))	r (θ)	Angle type
HFIP		
55.048	107.600	F -CT- F
55.048	111.000	F -CT-CT
55.048	110.000	CT-CT-CT
55.048	111.000	CT-CT-OH
55.048	109.500	CT-CT-HC
47.548	109.500	OH-CT-HC
47.548	109.500	CT-OH-HO
Acetone		
70.000	116.000	CT - C - CT
80.000	120.400	O - C - CT
35.000	109.500	C - CT - HC
33.000	107.800	HC - CT - HC
MeOH		
50.000	109.500	OH-CT-HC
35.000	109.500	HC-CT-HC
55.000	108.500	CT-OH-HO

Table B.4. Force field dihedral coefficients.

HFIP					
all dihedrals set as harmonic 0 1 0					
Acetone					
Style	V1	V2	V3	V4	torsion type
opls	0.000	0.000	0.275	0.000	CT - C - CT - HC
opls	0.000	0.000	0.000	0.000	O - C - CT - *
MeOH					
opls	0.000	0.000	4.500	0.000	HO-OH-CT-HC

Table B.5. Force field charges.

q (Coulomb)	atom type
HFIP	
0.60000	CT
-0.20000	F
-0.07000	CT
-0.59500	OH
0.17000	HC
0.49500	HO
Acetone	
0.47000	C
-0.18000	CT
0.06000	HC
-0.47000	O
MeOH	
0.14500	CT
-0.68300	OH
0.41800	HO
0.04000	HC

B.1.2. Number of Molecules in the Molecular Dynamics Simulations

Table B.6. Number of molecules of neat and mixed simulated systems at each molar fraction of HFIP.

System	x_m	HFIP molecules	Ace molecules	MeOH molecules
HFIP	–	350	–	–
MeOH	–	–	–	1720
Ace	–	–	950	–
HFIP/Ace	0.2	100	400	–
HFIP/Ace	0.5	210	210	–
HFIP/Ace	0.8	280	70	–
HFIP/MeOH	0.2	192	–	768
HFIP/MeOH	0.5	480	–	480
HFIP/MeOH	0.8	768	–	192

B.1.3. Cell Volumes

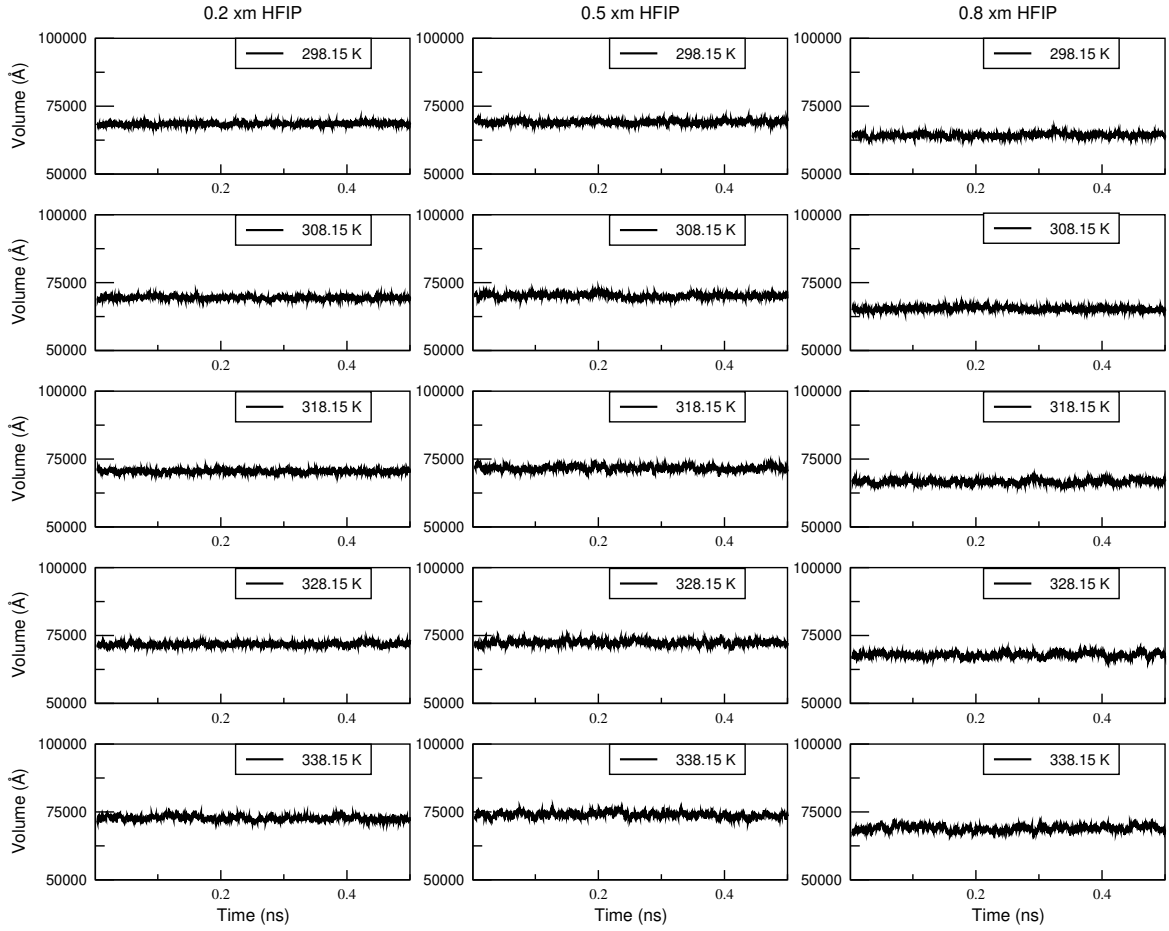

Figure B.1. Cell volume with respect to the simulation time in the last 0.5 ns of npt run for the systems HFIP/acetone

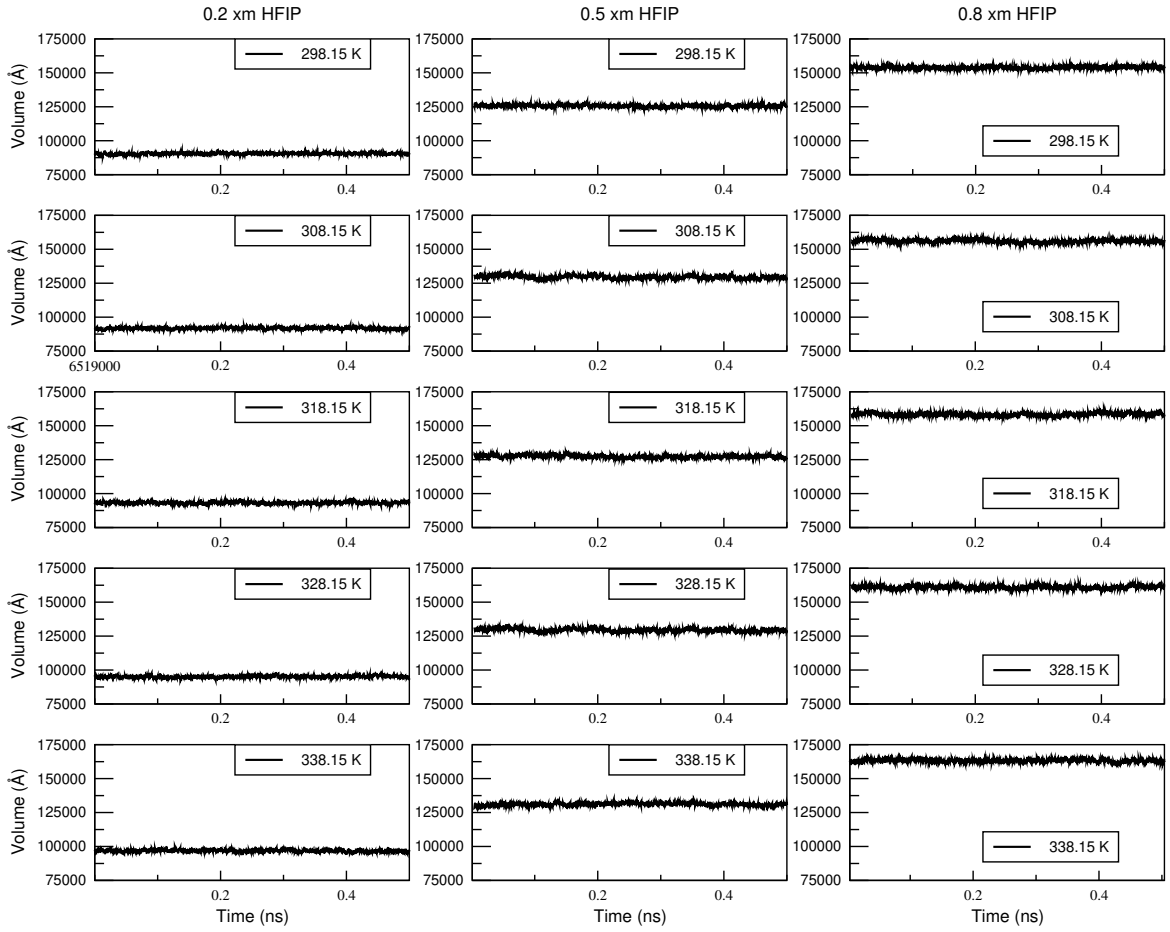

Figure B.2. Cell volume with respect to the simulation time in the last 0.5 ns of npt run for the systems HFIP/methanol

B.1.4. Neat Systems

Table B.7. Experimental densities ρ^{exp} and calculated densities ρ^{calc} of the neat systems HFIP, MeOH, and acetone in g/cm^3. The densities are calculated from molecular dynamics simulations, at the same conditions as described in the computational details.

System	$\rho_{298}^{\mathrm{exp}}$	$\rho_{298}^{\mathrm{calc}}$
HFIP	1.596	1.521
MeOH	0.792	0.753
Acetone	0.784	0.777

B.1.5. Molecular Dynamics Analysis at Different Temperatures

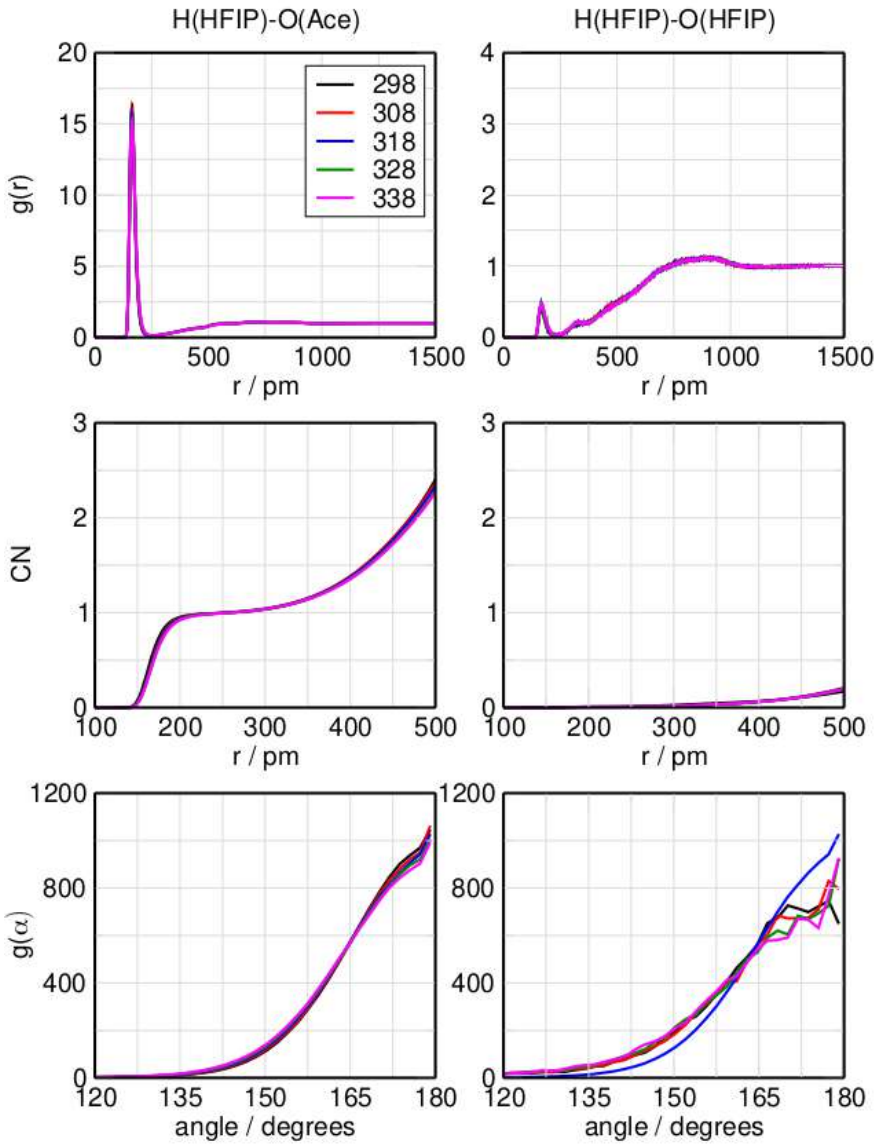

Figure B.3. Radial distribution function, numbers of integral, and angular distribution function of the hydrogen bond for the system HFIP/acetone at molar fraction of HFIP 0.2 at the temperatures 298.15 K, 308.15 K, 318.15 K, 328.15 K, and 338.15 K with HFIP bond donor and acetone acceptor (left) or HFIP (right).

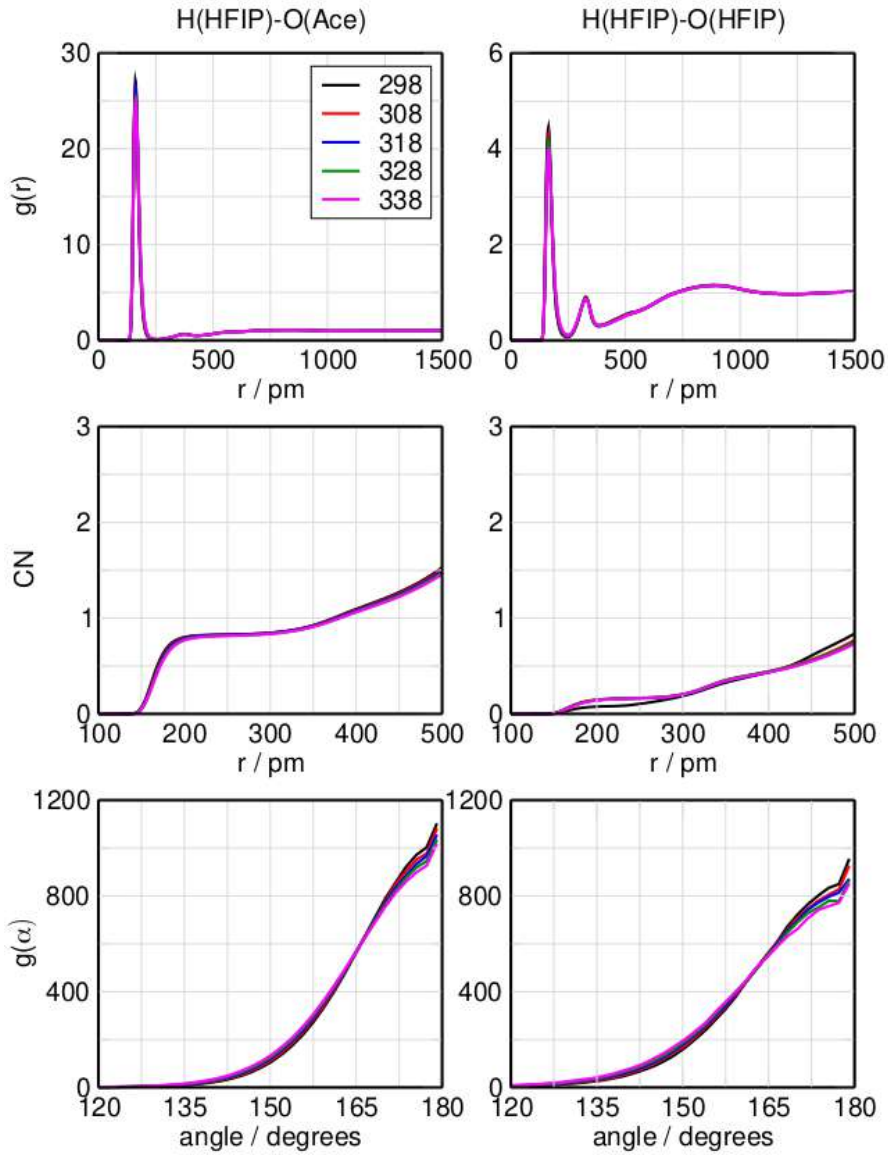

Figure B.4. Radial distribution function, numbers of integral, and angular distribution function of the hydrogen bond for the system HFIP/acetone at molar fraction of HFIP 0.5 at the temperatures 298.15 K, 308.15 K, 318.15 K, 328.15 K, and 338.15 K with HFIP bond donor and acetone acceptor (left) or HFIP (right).

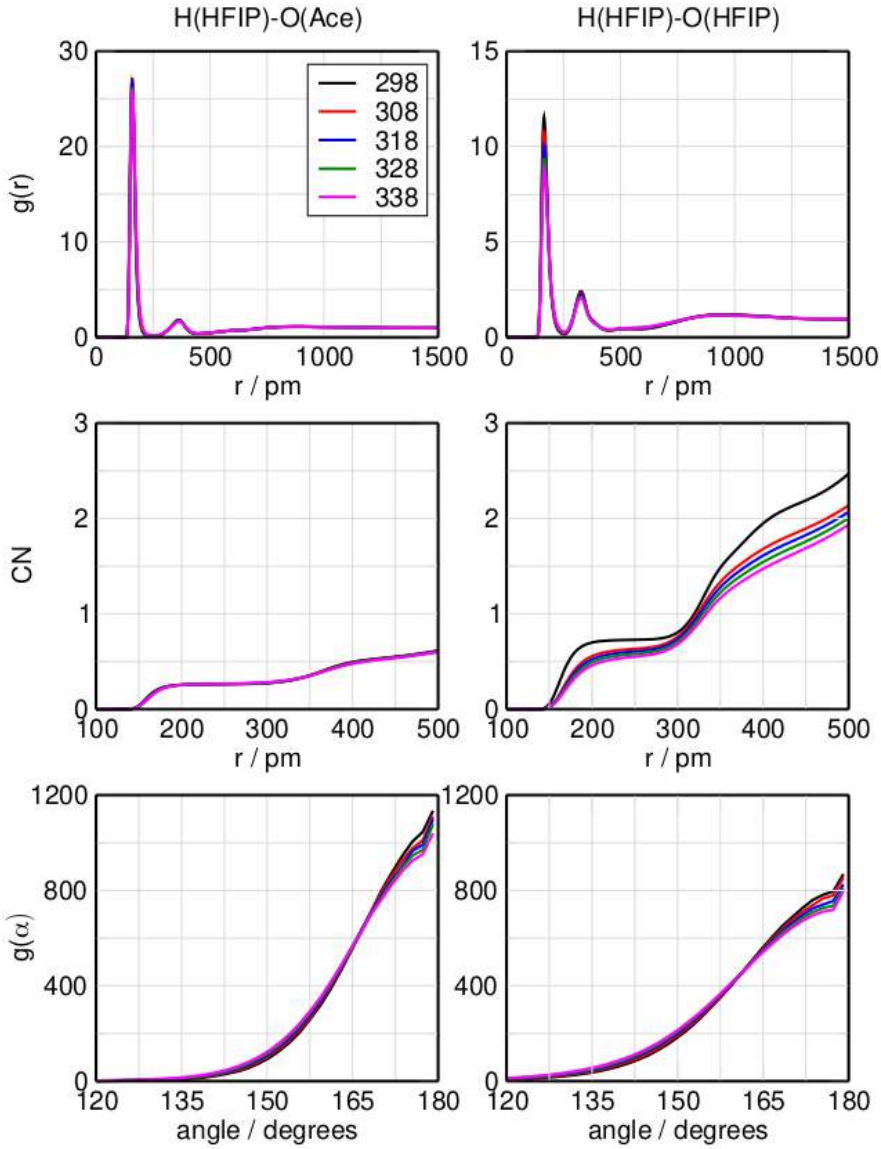

Figure B.5. Radial distribution function, numbers of integral, and angular distribution function of the hydrogen bond for the system HFIP/acetone at molar fraction of HFIP 0.8 at the temperatures 298.15 K, 308.15 K, 318.15 K, 328.15 K, and 338.15 K with HFIP bond donor and acetone acceptor (left) or HFIP (right).

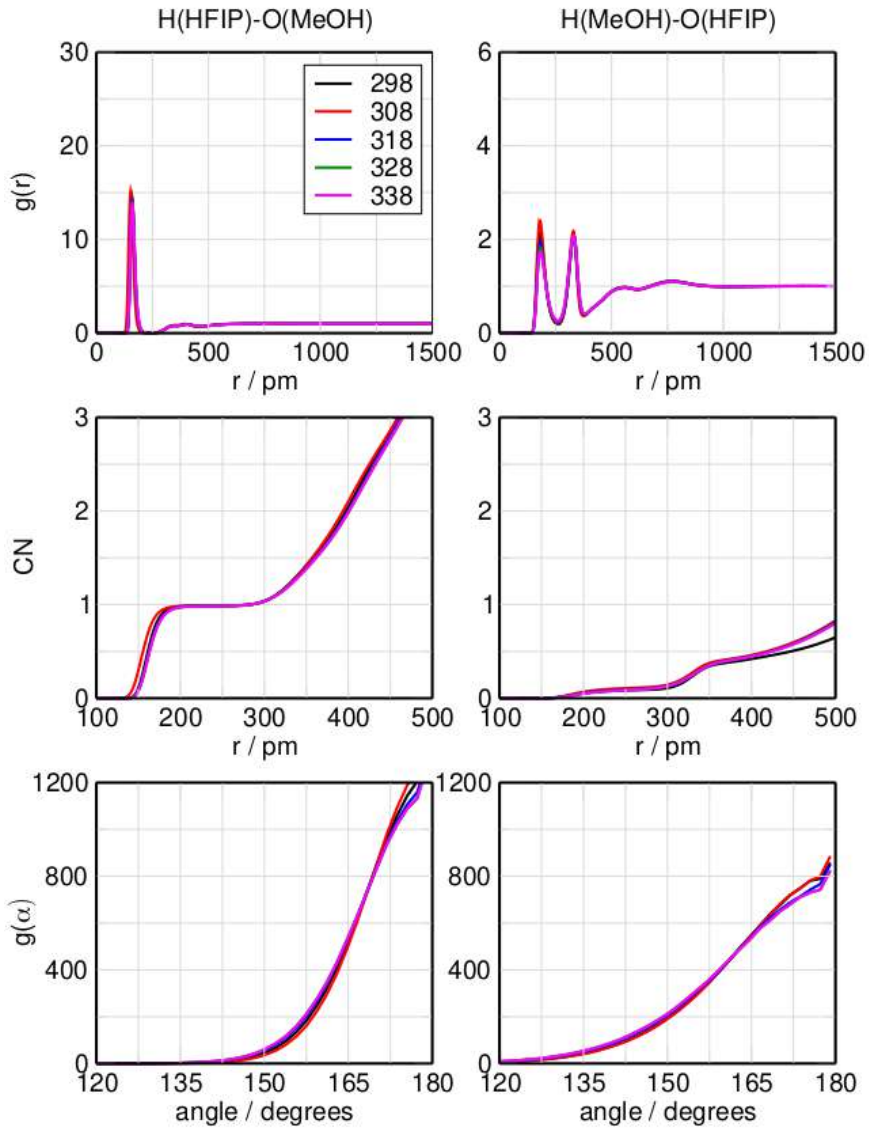

Figure B.6. Radial distribution function, numbers of integral, and angular distribution function of the hydrogen bond for the system HFIP/methanol at molar fraction of HFIP 0.2 at the temperatures 298.15 K, 308.15 K, 318.15 K, 328.15 K, and 338.15 K with HFIP bond donor and MeOH acceptor (left), or MeOH donor and HFIP acceptor (right).

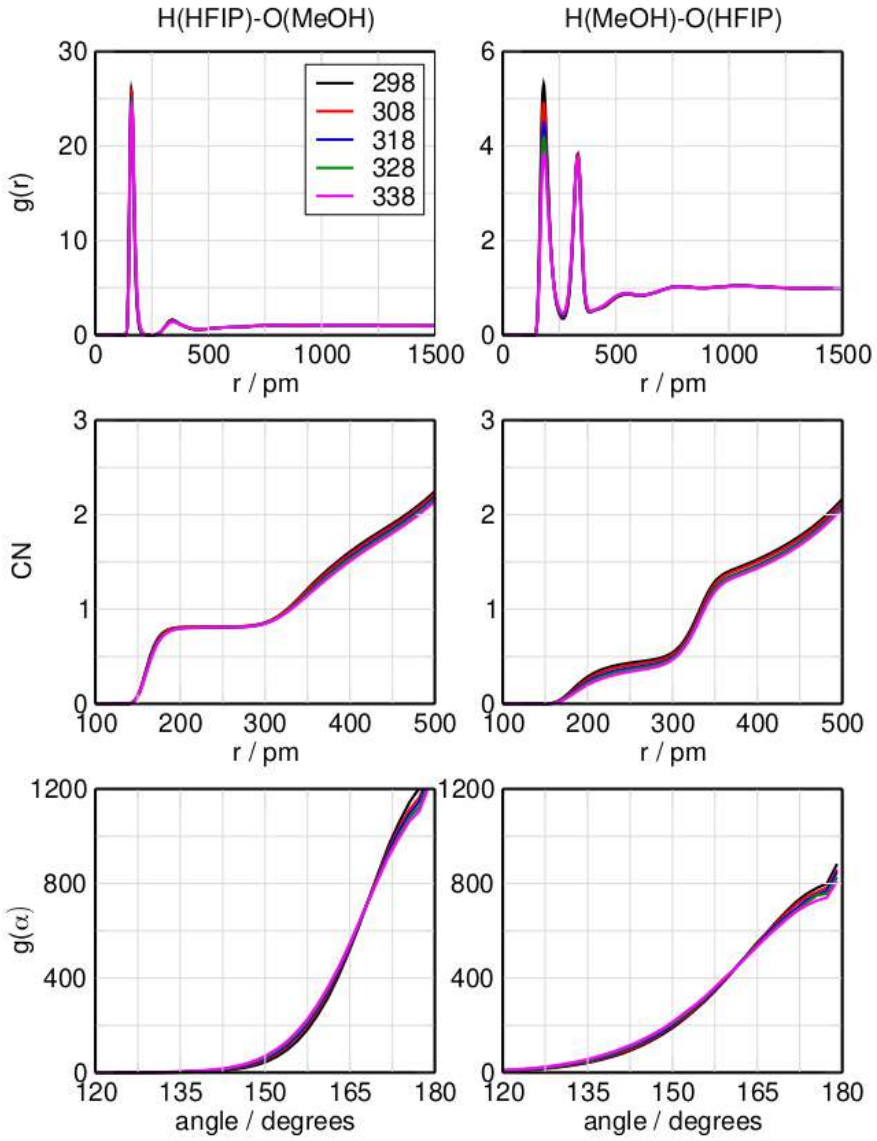

Figure B.7. Radial distribution function, numbers of integral, and angular distribution function of the hydrogen bond for the system HFIP/methanol at molar fraction of HFIP 0.5 at the temperatures 298.15 K, 308.15 K, 318.15 K, 328.15 K, and 338.15 K with HFIP bond donor and MeOH acceptor (left), or MeOH donor and HFIP acceptor (right).

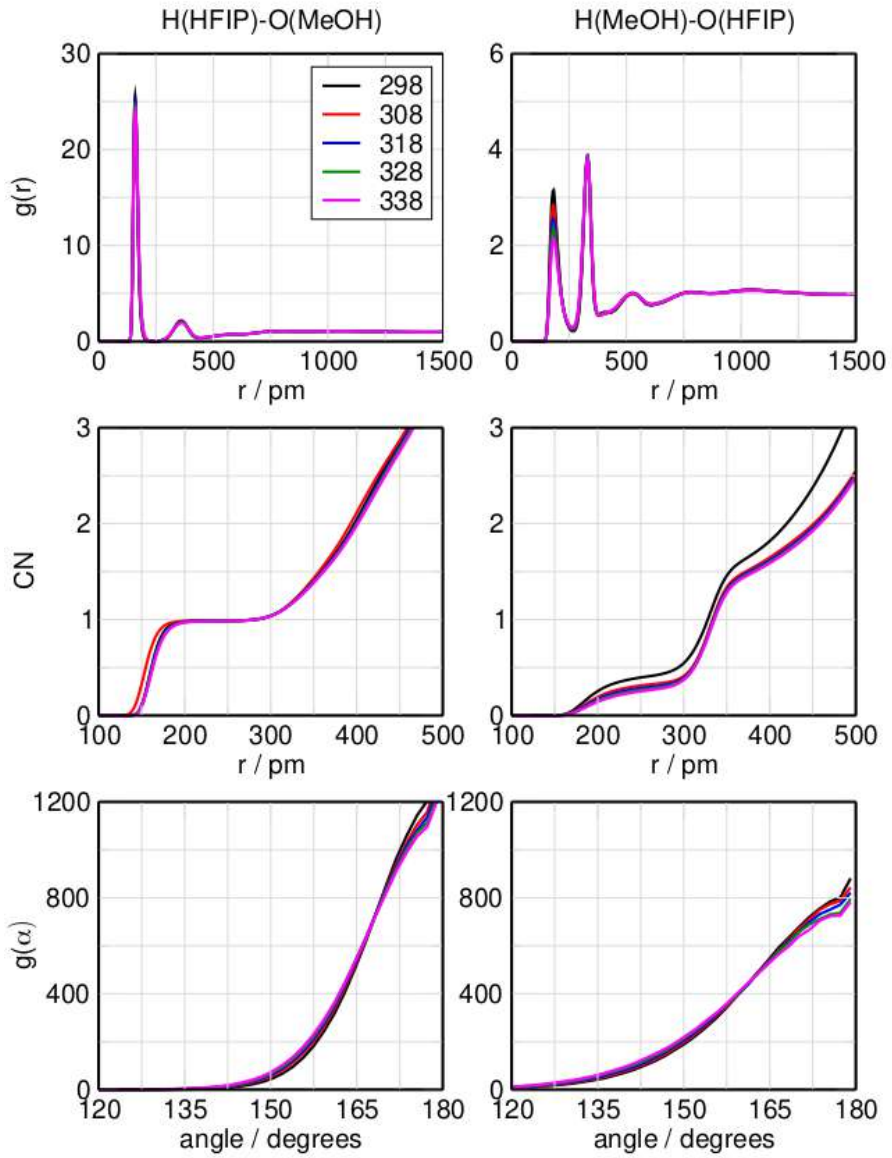

Figure B.8. Radial distribution function, numbers of integral, and angular distribution function of the hydrogen bond for the system HFIP/methanol at molar fraction of HFIP 0.8 at the temperatures 298.15 K, 308.15 K, 318.15 K, 328.15 K, and 338.15 K with HFIP bond donor and MeOH acceptor (left), or MeOH donor and HFIP acceptor (right).

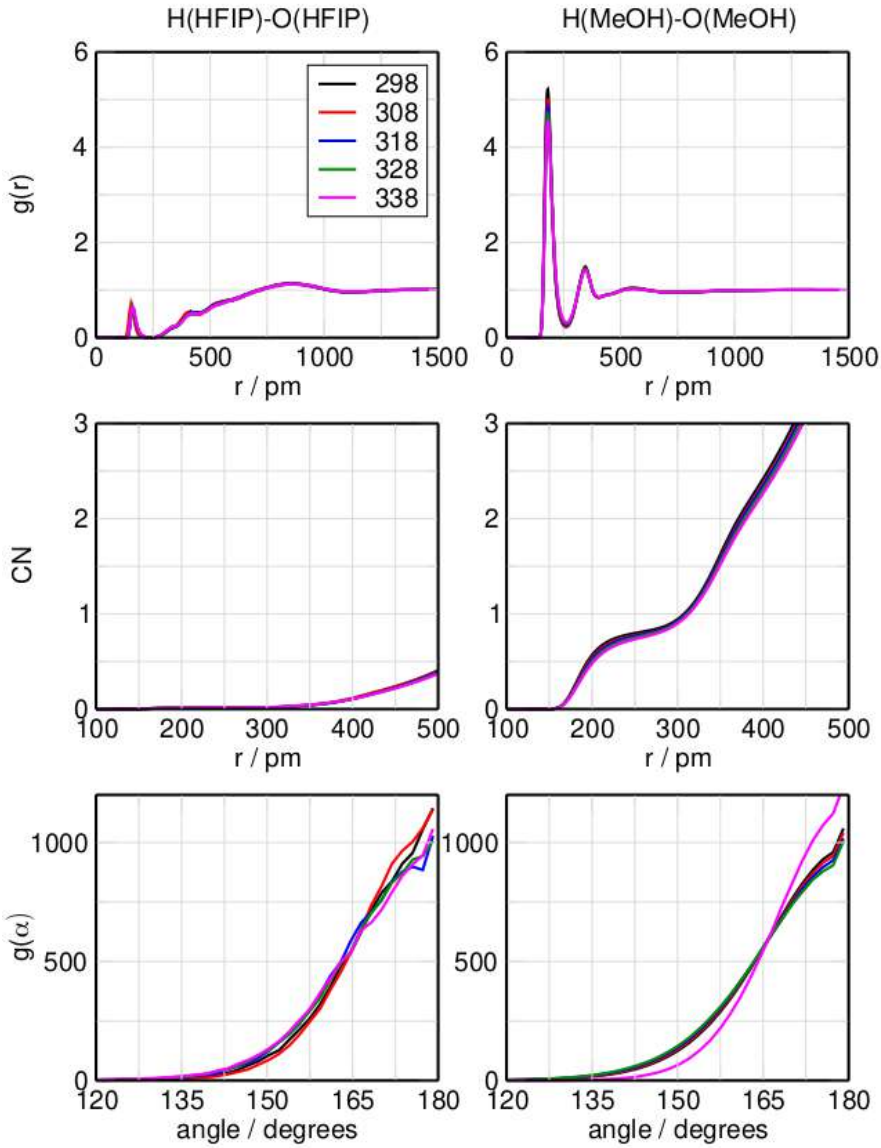

Figure B.9. Radial distribution function, numbers of integral, and angular distribution function of the hydrogen bond for the system HFIP/methanol at molar fraction of HFIP 0.2 at the temperatures 298.15 K, 308.15 K, 318.15 K, 328.15 K, and 338.15 K with HFIP donor and acceptor (left) or MeOH donor and acceptor (right).

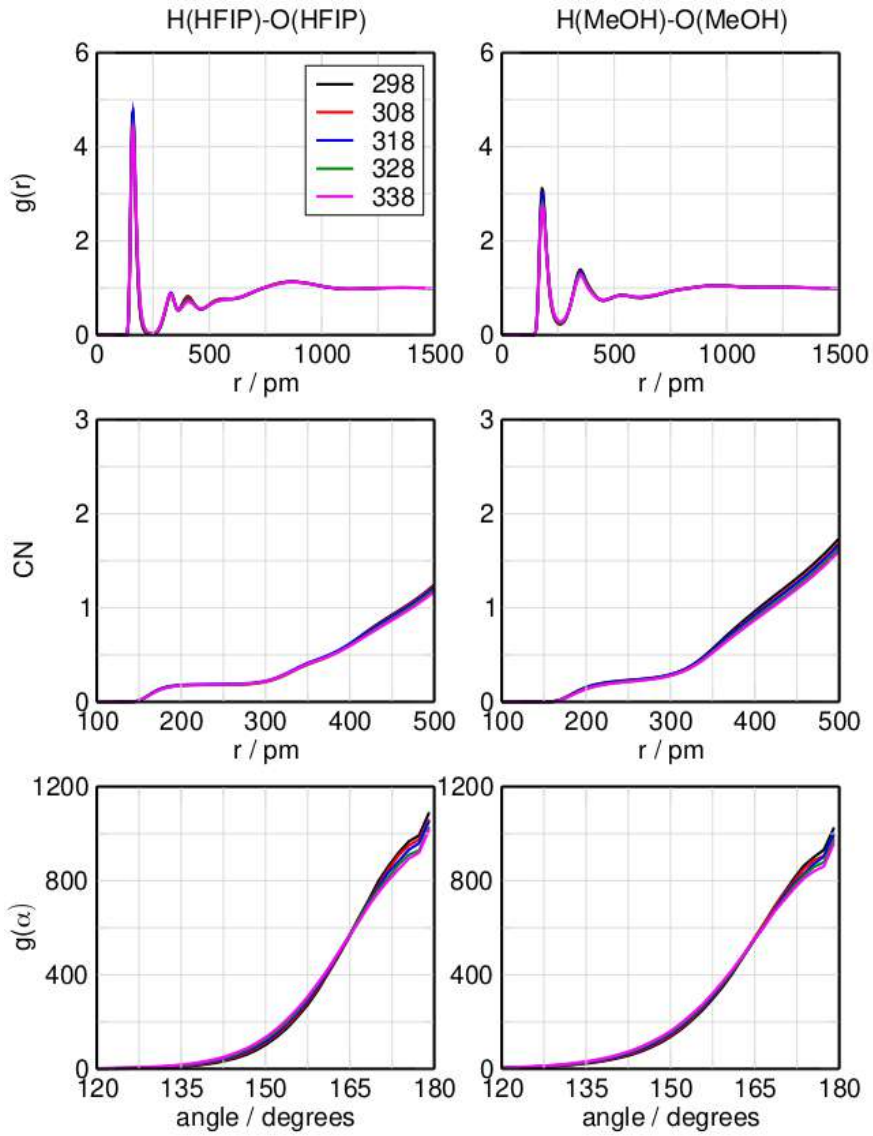

Figure B.10. Radial distribution function, numbers of integral, and angular distribution function of the hydrogen bond for the system HFIP/methanol at molar fraction of HFIP 0.5 at the temperatures 298.15 K, 308.15 K, 318.15 K, 328.15 K, and 338.15 K with HFIP donor and acceptor (left) or MeOH donor and acceptor (right).

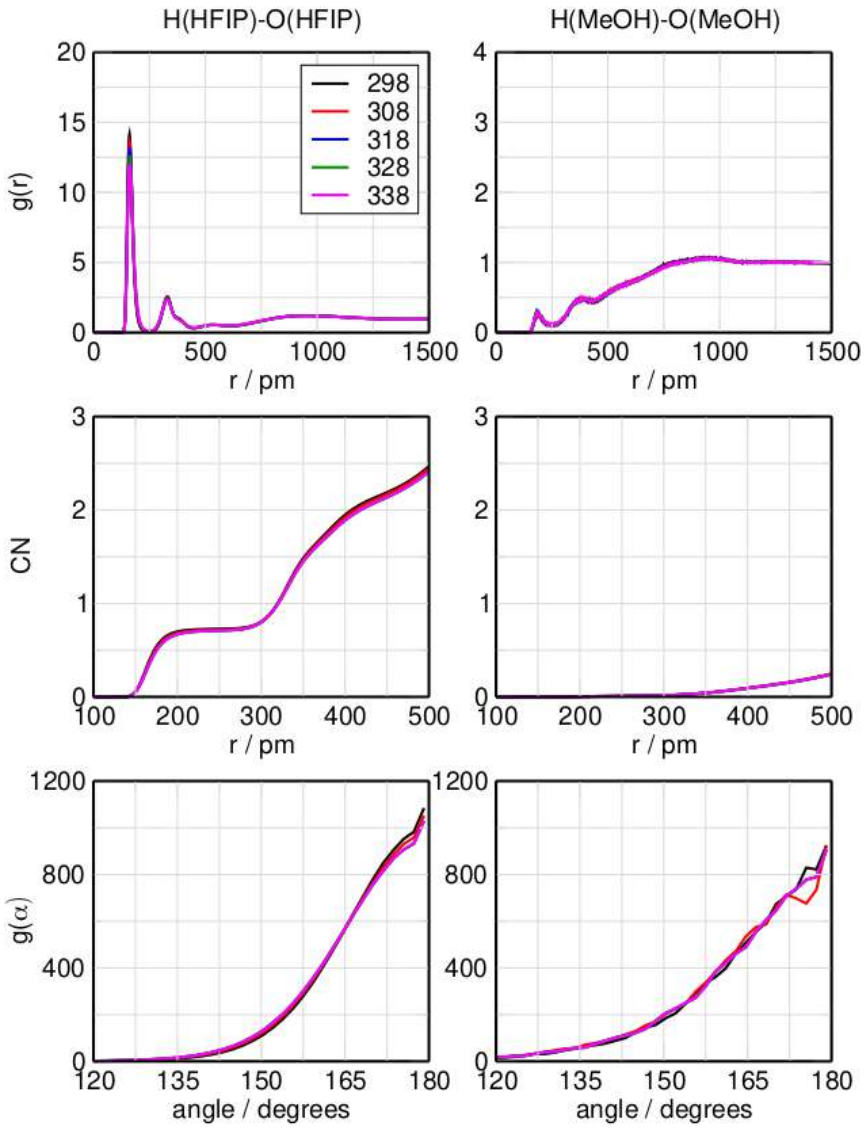

Figure B.11. Radial distribution function, numbers of integral, and angular distribution function of the hydrogen bond for the system HFIP/methanol at molar fraction of HFIP 0.8 at the temperatures 298.15 K, 308.15 K, 318.15 K, 328.15 K, and 338.15 K with HFIP donor and acceptor (left) or MeOH donor and acceptor (right).

B.2. Clusters Interaction Energies

Table B.8. Interaction energies E_{int} and interaction energies per monomer E_{int}/m of the system HFIP, in kJ/mol.

cluster	size	E_{int}	E_{int}/m
h2-10	2	-25.2	-12.6
h3-1	3	-62.4	-20.8
h3-2	3	-62.3	-20.8
h3-6	3	-56.2	-18.7
h3-10	3	-61.6	-20.5
h4-1	4	-129.0	-32.2
h4-5	4	-129.0	-32.3
h5-1	5	-169.1	-33.8
h6-1	6	-207.6	-34.6
h6-2	6	-207.5	-34.6

Table B.9. Interaction energies E_{int} and interaction energies E_{int}/m per monomer of the system acetone, in kJ/mol.

cluster	size	E_{int}	E_{int}/m
a2-1	2	-26.8	-13.4
a3-1	3	-53.6	-17.9
a4-1	4	-81.2	-20.3
a5-1	5	-114.7	-22.9
a5-8	5	-111.0	-22.2
a6-1	6	-143.8	-24.0
a6-4	6	-139.2	-23.2
a6-5	6	-139.9	-23.3
a6-8	6	-138.7	-23.1
a6-9	6	-135.3	-22.6
a6-10	6	-137.7	-23.0

Table B.10. Interaction energies E_{int} and interaction energies E_{int}/m per monomer of the system methanol, in kJ/mol.

cluster	size	E_{int}	E_{int}/m
m2-1	2	-27.4	-13.7
m2-14	2	-27.4	-13.7
m3-1	3	-86.5	-28.8
m4-1	4	-152.3	-38.1
m4-7	4	-149.0	-37.2
m5-1	5	-201.3	-40.3
m5-10	5	-201.0	-40.2
m6-1	6	-246.6	-41.1
m6-2	6	-248.9	-41.5
m6-3	6	-248.8	-41.5
m6-4	6	-249.0	-41.5
m6-6	6	-247.5	-41.3
m6-11	6	-247.7	-41.3

Table B.11. Interaction energies E_{int} and interaction energies E_{int}/m per monomer of the system HFIP/acetone, in kJ/mol.

cluster	size	HFIP	Ace	E_{int}	E_{int}/m	cluster	size	HFIP	Ace	E_{int}	E_{int}/m
h1a1-1	2	1	1	-43.6	-21.8	h2a4-2	6	2	4	-190.3	-31.7
h1a1-2	2	1	1	-38.0	-19.0	h2a4-9	6	2	4	-181.1	-30.2
h1a2-10	3	1	2	-71.0	-23.7	h3a1-1	4	3	1	-120.1	-30.0
h1a3-1	4	1	3	-108.2	-27.0	h3a1-4	4	3	1	-120.0	-30.0
h1a3-9	4	1	3	-108.2	-27.0	h3a1-10	4	3	1	-120.1	-30.0
h1a3-10	4	1	3	-108.2	-27.0	h3a2-1	5	3	2	-174.6	-34.9
h1a4-1	5	1	4	-134.1	-26.8	h3a2-2	5	3	2	-174.6	-34.9
h1a4-4	5	1	4	-138.4	-27.7	h3a2-4	5	3	2	-174.6	-34.9
h1a4-5	5	1	4	-138.5	-27.7	h3a2-10	5	3	2	-172.8	-34.6
h1a5-1	6	1	5	-180.9	-30.2	h3a3-4	6	3	3	-202.0	-33.7
h1a5-3	6	1	5	-173.6	-28.9	h3a3-7	6	3	3	-202.1	-33.7
h1a5-4	6	1	5	-165.5	-27.6	h3a3-8	6	3	3	-207.0	-34.5
h1a5-7	6	1	5	-175.1	-29.2	h3a3-9	6	3	3	-221.1	-36.9
h2a1-1	3	2	1	-84.1	-28.0	h4a1-1	5	4	1	-166.0	-33.2
h2a1-6	3	2	1	-82.8	-27.6	h4a1-3	5	4	1	-166.0	-33.2
h2a1-10	3	2	1	-85.2	-28.4	h4a1-4	5	4	1	-166.3	-33.3
h2a2-1	4	2	2	-117.1	-29.3	h4a1-5	5	4	1	-166.2	-33.2
h2a2-4	4	2	2	-117.2	-29.3	h4a1-6	5	4	1	-166.2	-33.2
h2a2-6	4	2	2	-117.1	-29.3	h4a2-1	6	4	2	-228.4	-38.1
h2a2-7	4	2	2	-117.1	-29.3	h4a2-2	6	4	2	-228.2	-38.0
h2a2-10	4	2	2	-117.2	-29.3	h5a1-1	6	5	1	-204.4	-34.1
h2a3-1	5	2	3	-164.8	-33.0	h5a1-3	6	5	1	-203.5	-33.9
h2a4-1	6	2	4	-187.2	-31.2						

Table B.12. Interaction energies E_{int} and interaction energies E_{int}/m per monomer of the system HFIP/methanol, in kJ/mol.

cluster	size	HFIP	MeOH	E_{int}	E_{int}/m	cluster	size	HFIP	MeOH	E_{int}	E_{int}/m
h1m1-1	2	1	1	-42.7	-21.3	h2m3-1	5	2	3	-197.7	-39.5
h1m1-3	2	1	1	-42.7	-21.3	h2m3-2	5	2	3	-197.7	-39.5
h1m1-6	2	1	1	-42.7	-21.3	h2m3-6	5	2	3	-197.7	-39.5
h1m2-1	3	1	2	-85.0	-28.3	h2m3-7	5	2	3	-204.5	-40.9
h1m2-2	3	1	2	-85.0	-28.3	h2m3-8	5	2	3	-199.8	-40
h1m2-6	3	1	2	-85.0	-28.3	h2m4-1	6	2	4	-256.6	-42.8
h1m2-7	3	1	2	-84.2	-28.1	h2m4-4	6	2	4	-251.2	-41.9
h1m2-8	3	1	2	-84.2	-28.1	h2m4-6	6	2	4	-256.7	-42.8
h1m3-1	4	1	3	-150.6	-37.6	h2m4-7	6	2	4	-252.8	-42.1
h1m3-2	4	1	3	-150.6	-37.7	h3m1-1	4	3	1	-121.6	-30.4
h1m3-3	4	1	3	-147.8	-37	h3m1-6	4	3	1	-121.6	-30.4
h1m3-4	4	1	3	-150.6	-37.7	h3m1-7	4	3	1	-120.4	-30.1
h1m3-5	4	1	3	-150.6	-37.7	h3m2-1	5	3	2	-194.6	-38.9
h1m3-6	4	1	3	-150.6	-37.7	h3m2-3	5	3	2	-195.2	-39.0
h1m3-7	4	1	3	-150.9	-37.7	h3m2-4	5	3	2	-194.0	-38.8
h1m3-8	4	1	3	-150.9	-37.7	h3m2-7	5	3	2	-190.1	-38.0
h1m4-1	5	1	4	-202.8	-40.6	h3m2-8	5	3	2	-191.0	-38.2
h1m4-2	5	1	4	-202.8	-40.6	h3m3-1	6	3	3	-249.6	-41.6
h1m4-4	5	1	4	-202.8	-40.6	h3m3-3	6	3	3	-246.9	-41.1
h1m4-5	5	1	4	-202.8	-40.6	h3m3-4	6	3	3	-246.9	-41.1
h1m4-6	5	1	4	-202.8	-40.6	h3m3-8	6	3	3	-246.9	-41.1
h1m4-7	5	1	4	-201.9	-40.4	h4m1-1	5	4	1	-160.5	-32.1
h1m4-8	5	1	4	-199.5	-39.9	h4m1-2	5	4	1	-182.4	-36.5
h1m5-1	6	1	5	-256.5	-42.8	h4m1-6	5	4	1	-185.1	-37.0
h1m5-2	6	1	5	-255.6	-42.6	h4m1-7	5	4	1	-183.4	-36.7
h1m5-3	6	1	5	-255.6	-42.6	h4m1-8	5	4	1	-185.1	-37.0
h1m5-6	6	1	5	-255.7	-42.6	h4m2-1	6	4	2	-224.8	-37.5
h2m1-1	3	2	1	-78.6	-26.2	h4m2-2	6	4	2	-225.7	-37.6
h2m1-6	3	2	1	-78.6	-26.2	h4m2-4	6	4	2	-225.7	-37.6
h2m2-1	4	2	2	-123.5	-30.9	h4m2-6	6	4	2	-225.6	-37.6
h2m2-3	4	2	2	-123.5	-30.9	h4m2-7	6	4	2	-231.2	-38.5
h2m2-5	4	2	2	-123.5	-30.9	h4m2-8	6	4	2	-230.2	-38.4
h2m2-6	4	2	2	-122.1	-30.5	h5m1-2	6	5	1	-219.1	-36.5
h2m2-7	4	2	2	-122.1	-30.5	h5m1-5	6	5	1	-219.0	-36.5
h2m2-8	4	2	2	-122.1	-30.5	h5m1-6	6	5	1	-219.0	-36.5

B.3. Thermodynamic Properties of the Neat Systems

Table B.13. Enthalpies of vaporization ΔH_{vap} at 298.15 K for the neat substances calculated at experimental density, and with the decrease of 1%,5%, 10% in kJ/mol.

Solvent	ΔH_{vap}^{exp}	ΔH_{vap}	$\Delta H_{vap}^{99\%}$	$\Delta H_{vap}^{95\%}$	$\Delta H_{vap}^{90\%}$
Acetone	31.27	32.65	32.69	32.84	33.03
HFIP	41.60	42.25	42.26	42.30	42.37
Methanol	37.60	40.14	40.15	40.18	40.22

As can be seen in table in B.13, with small variations of the density for each system, the enthalpy of vaporization remains constant within 0.02-0.1 % (1 %), 0.1-0.5 % (5 %) and 0.3-1 (10 %) .

B.4. Activity Coefficients of Mixed Systems

Table B.14. Activity coefficients f_{HFIP} and f_{Acetone}, Gibbs energy G_{mix}, enthalpy H_{mix} and entropy S_{mix} of mixing for the system HFIP/acetone at 298.15 K increasing the molar fraction of HFIP.

x_{m}	G_{mix}	H_{mix}	S_{mix}	f_{HFIP}	f_{Acetone}
0.00	0.00	0.00	0.00	0.000	1.000
0.20	-7.85	-10.30	-8.22	0.011	0.110
0.50	-7.24	-11.96	-15.81	0.171	0.068
0.80	-6.97	-7.77	-2.68	0.153	0.017
1.00	0.00	0.00	0.00	1.000	0.000

Via binary quantum cluster approach we are able to calculate the Gibbs energy of mixing G_{mix}, the enthalpy of mixing H_{mix}, and the entropy of mixing S_{mix}. As explained in 3 the activity coefficients can be calculated from the excess Gibbs energy of mixing G^{e}. Since no experimental boiling point is present in literature for the mixture HFIP acetone and HFIP methanol, with the exception of the boiling point at 0.5 molar fraction of HFIP for the system HFIP acetone, the isobars calculated via molecular dynamics are used as input for the calculations. Since there is not experimental value of activity coefficient nor

Table B.15. Activity coefficients f_{HFIP} and f_{MeOH}, Gibbs energy G_{mix}, enthalpy H_{mix} and entropy S_{mix} of mixing for the system HFIP/methanol at 298.15 K increasing the molar fraction of HFIP.

x_{m}	G_{mix}	H_{mix}	S_{mix}	f_{HFIP}	f_{MeOH}
0.00	0.00	0.00	0.00	0.000	1.000
0.20	-1.38	-1.55	-0.55	0.000	300.720
0.50	-19.49	-21.27	-5.98	0.001	0.003
0.80	-3.77	-4.53	-2.54	124.264	0.000
1.00	0.00	0.00	0.00	1.000	0.000

the other properties in literature, our results are to be considered as qualitatively and not quantitatively. In tables B.14 and B.15 the calculated G_{mix}, H_{mix}, S_{mix} and activity coefficients are shown for the systems HFIP acetone and HFIP methanol respectively. In both cases the strong negative values of G_{mix} means the systems are strongly interactive, and the activity coefficients shows strong interactions of one solvent within the other one.

B.5. Calculated Boiling Point of Neat and Mixed Systems

Table B.16. Experimental and calculated boiling points of the neat and mixed systems.

System	x_m	T_{bol}^{calc} (K)	T_{bol}^{exp} (K)
HFIP	1.0	342	331
MeOH	0.0	438	337
Ace	0.0	392	329
HFIP-ACE	0.2	385	–
HFIP-ACE	0.5	382	367
HFIP-ACE	0.8	369	–
HFIP-MeOH	0.2	338	–
HFIP-MeOH	0.5	449	–
HFIP-MeOH	0.8	349	–

At each investigated temperature the Peacemaker code performs two full QCE iterations with either a gas-like or liquid-like initial volume guess, respectively. The iterations will typically converge to different solutions of the population and volume polynomial, one resembling the gas-phase state and one resembling the liquid-phase state. At each temperature, the Gibbs energies of gas and liquid phase are compared. When the Gibbs energy of the gas phase becomes lower than that of the liquid phase, the Newton-Raphson algorithm is used to find the temperature at which $G(g) - G(l) = 0$. This temperature is then treated as the QCE boiling point.

B.6. Cluster Pictures

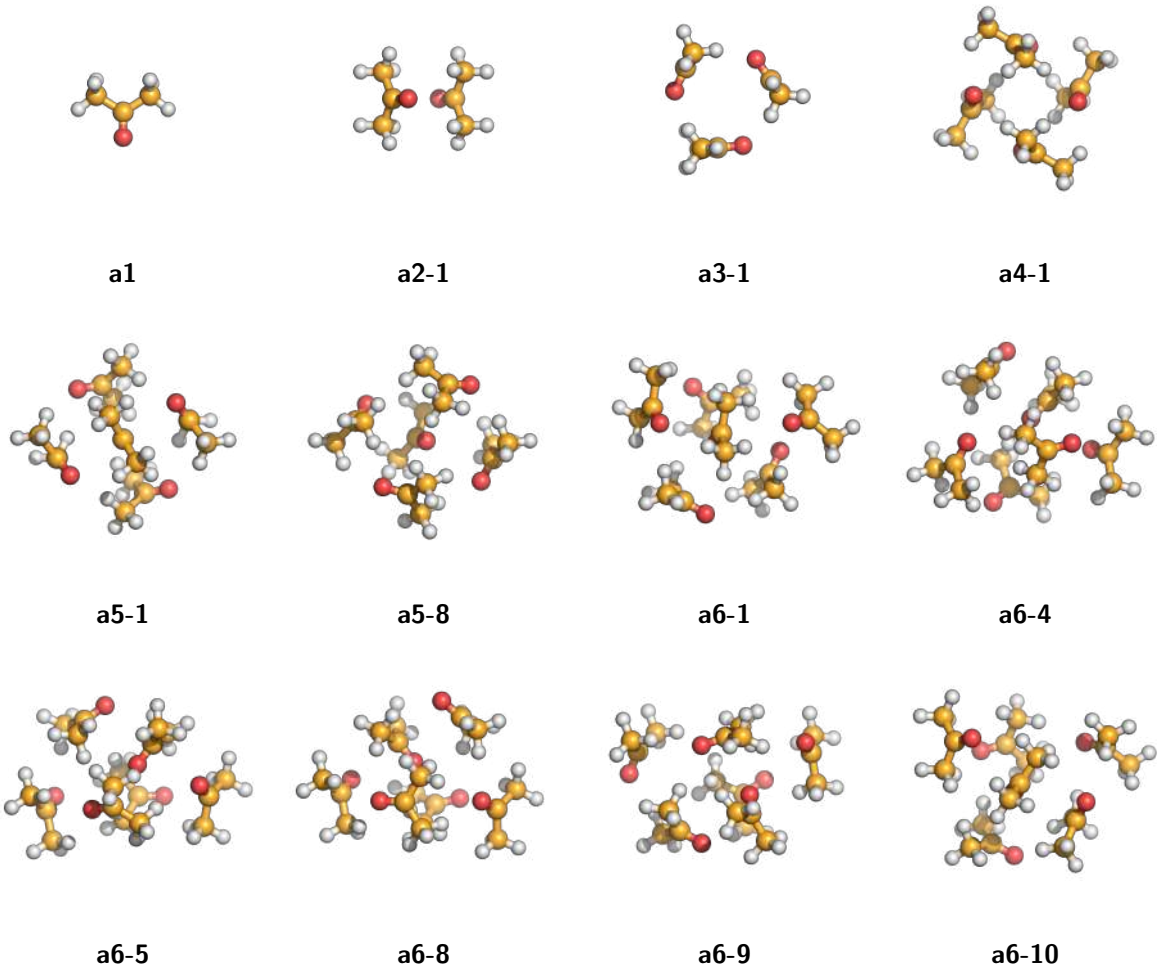

Figure B.12. Pure acetone clusters after BP86/TZVP optimization.

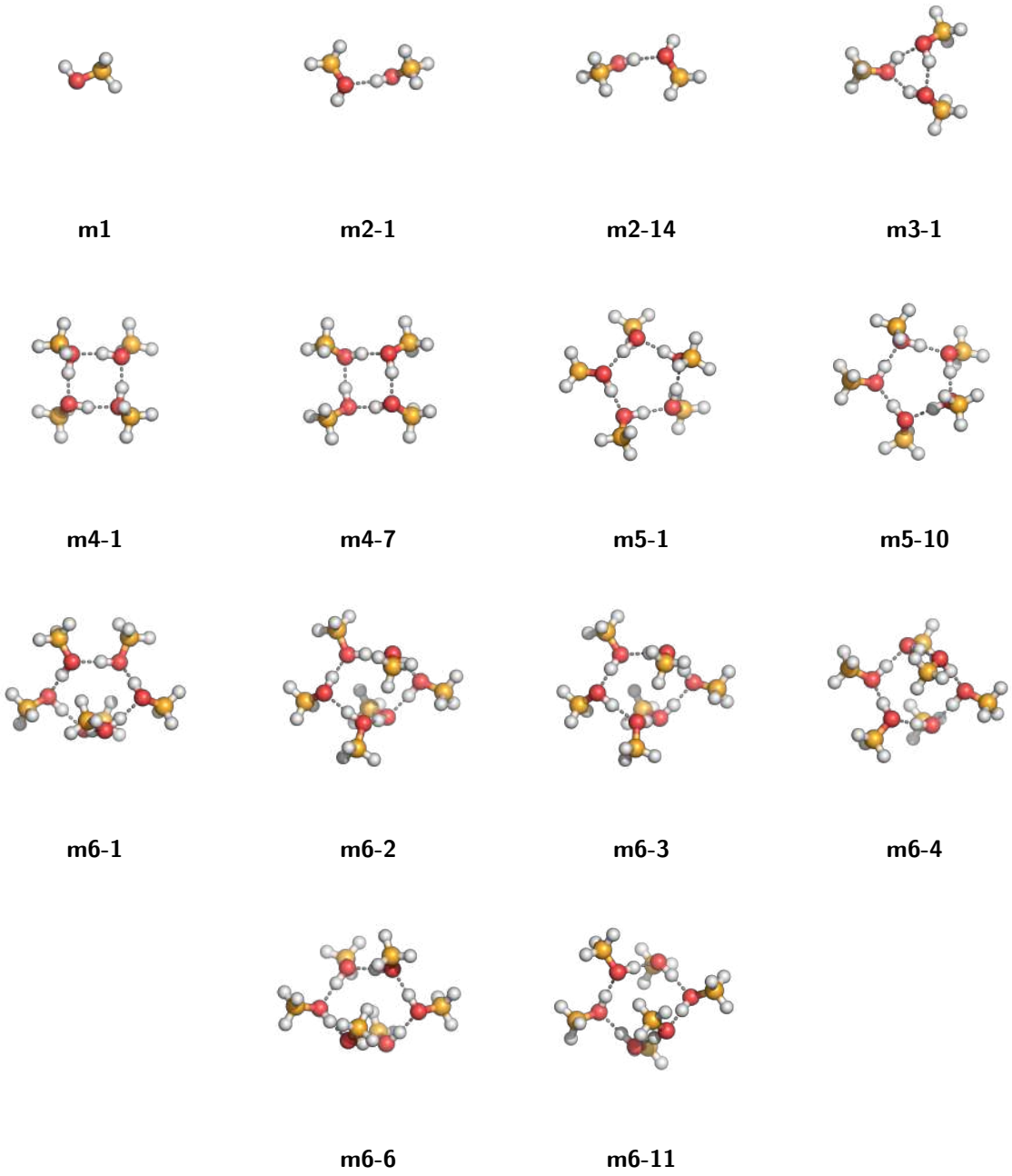

Figure B.13. Pure methanol clusters after BP86/TZVP optimization.

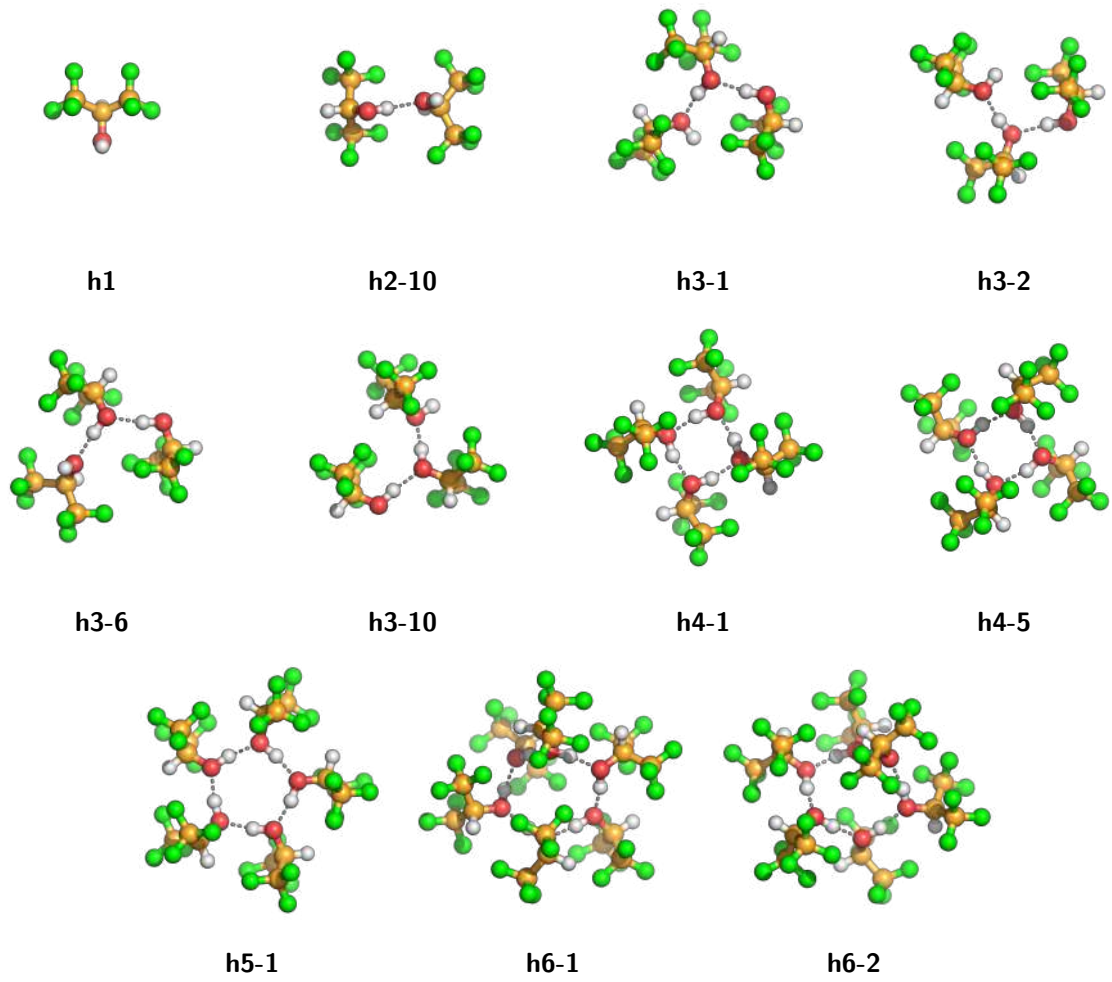

Figure B.14. Pure HFIP clusters after BP86/TZVP optimization.

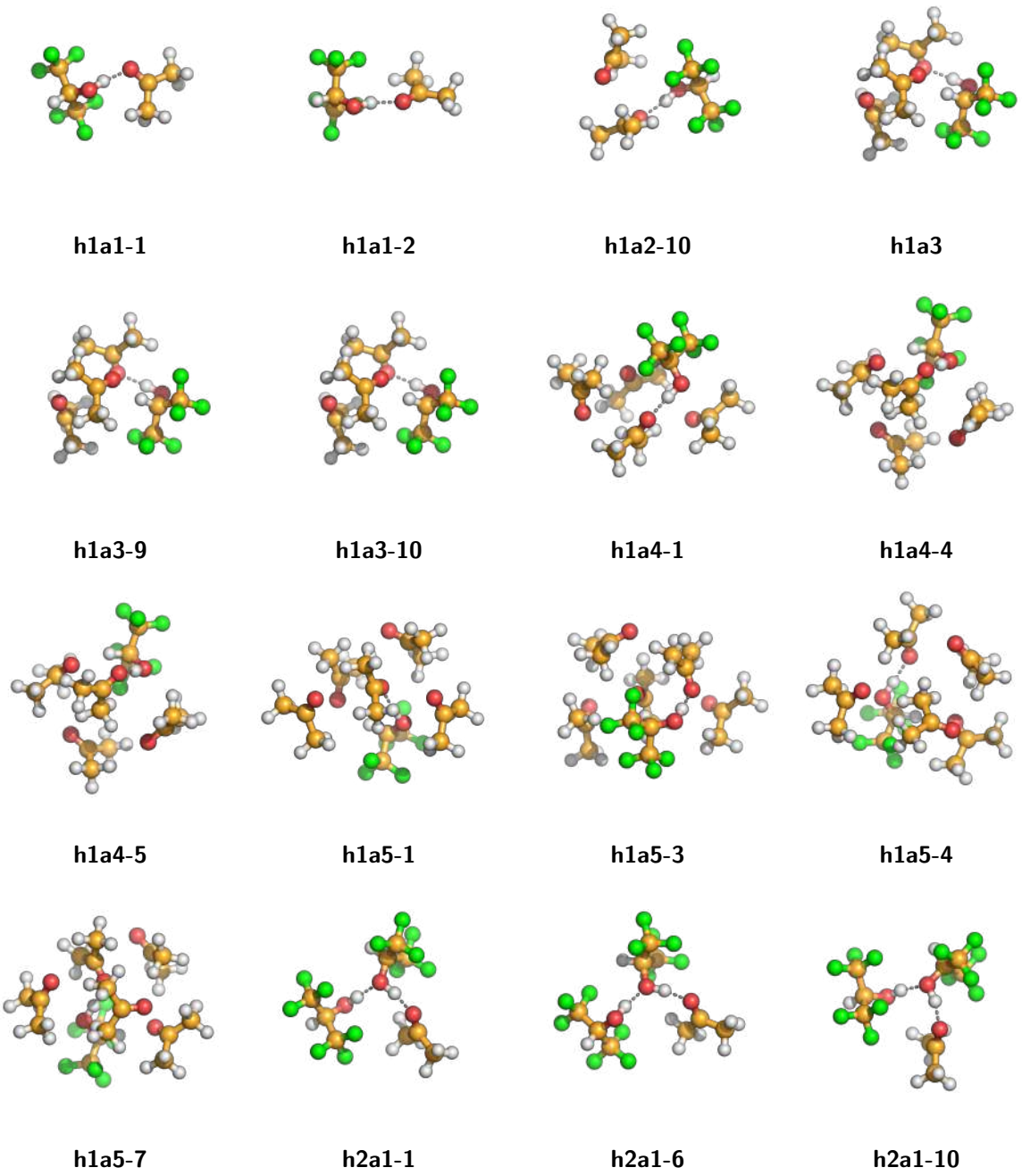

Figure B.15. HFIP/acetone clusters after BP86/TZVP optimization (1/3).

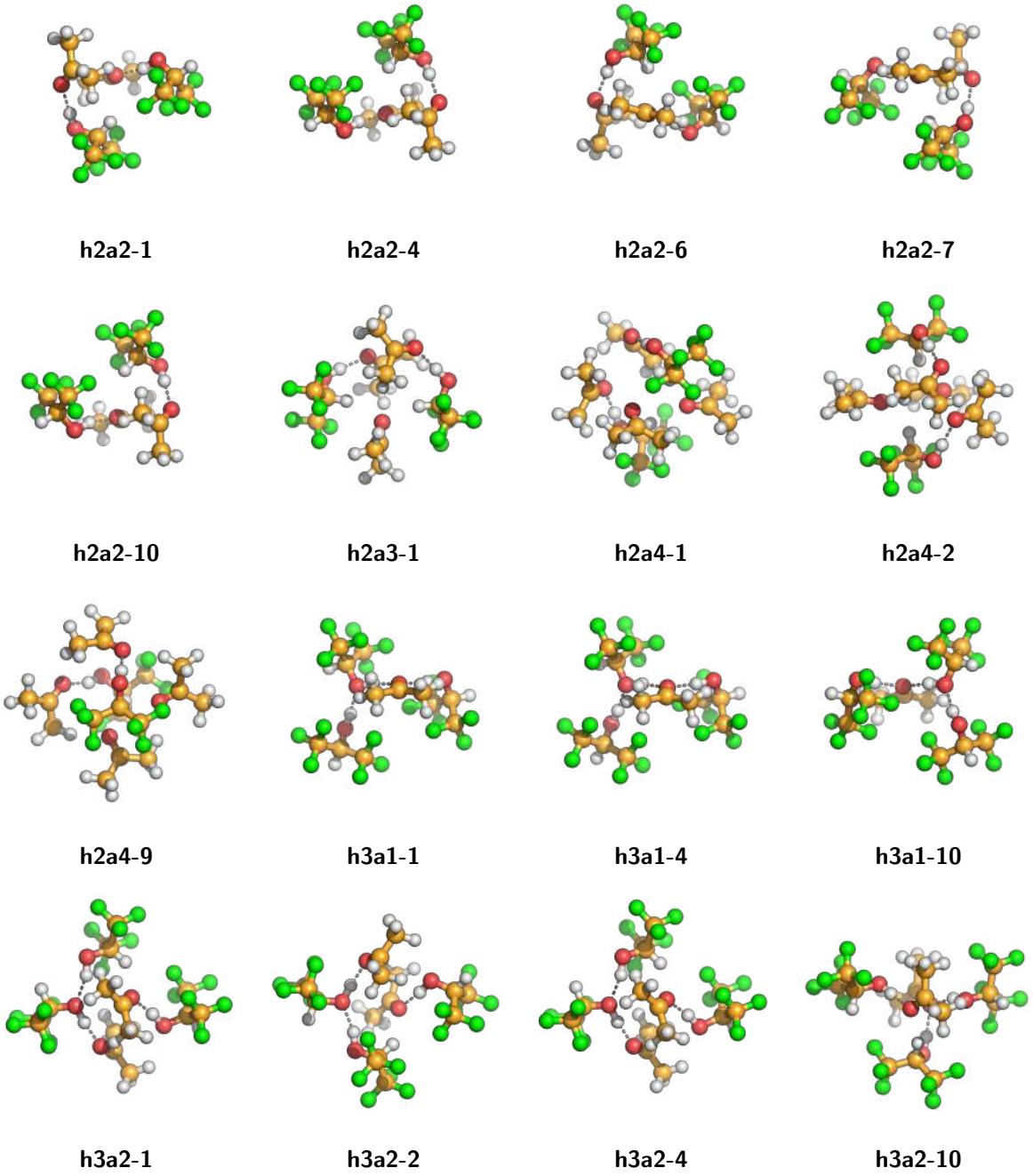

Figure B.16. HFIP/acetone clusters after BP86/TZVP optimization (2/3).

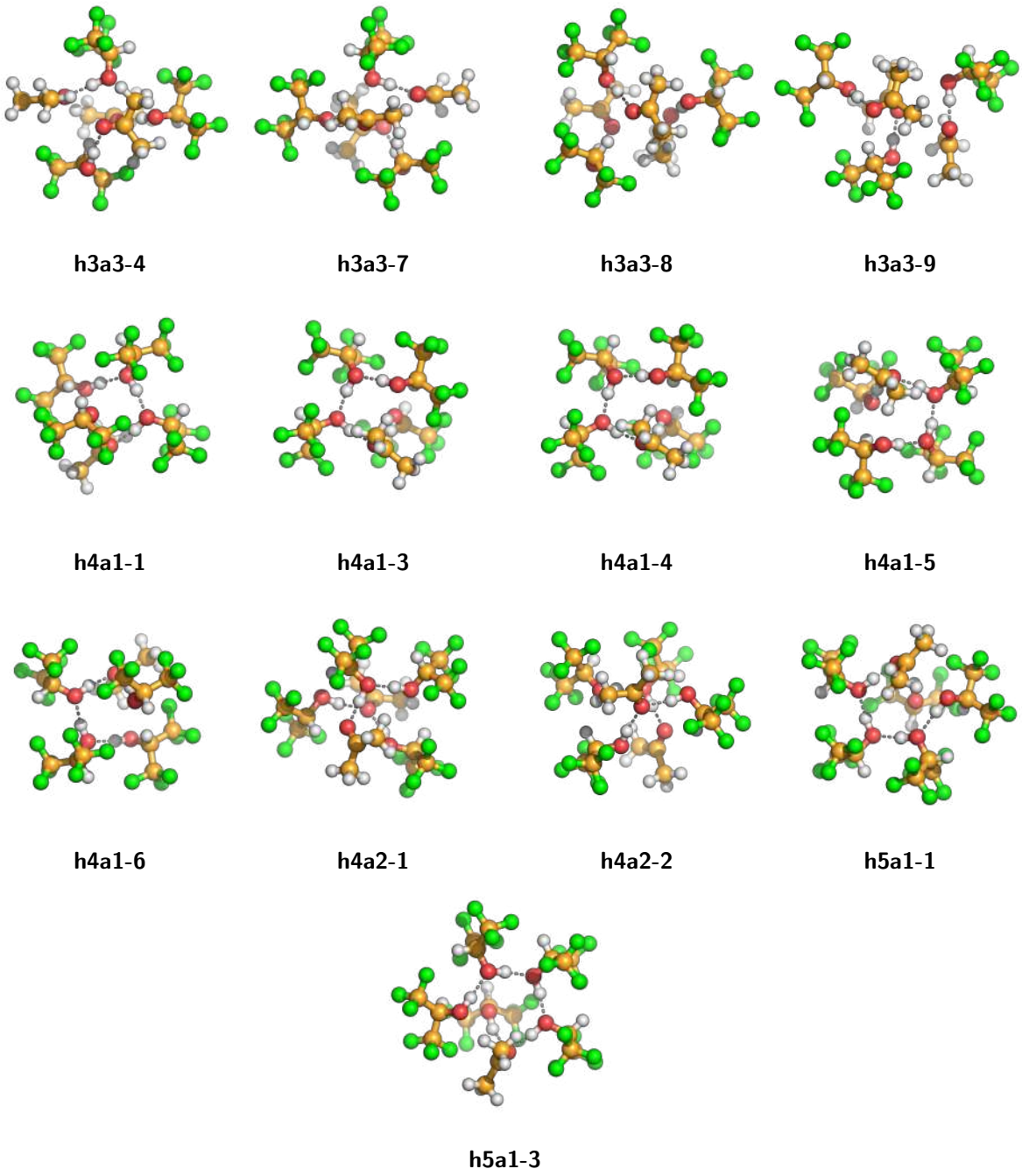

Figure B.17. HFIP/acetone clusters after BP86/TZVP optimization (3/3).

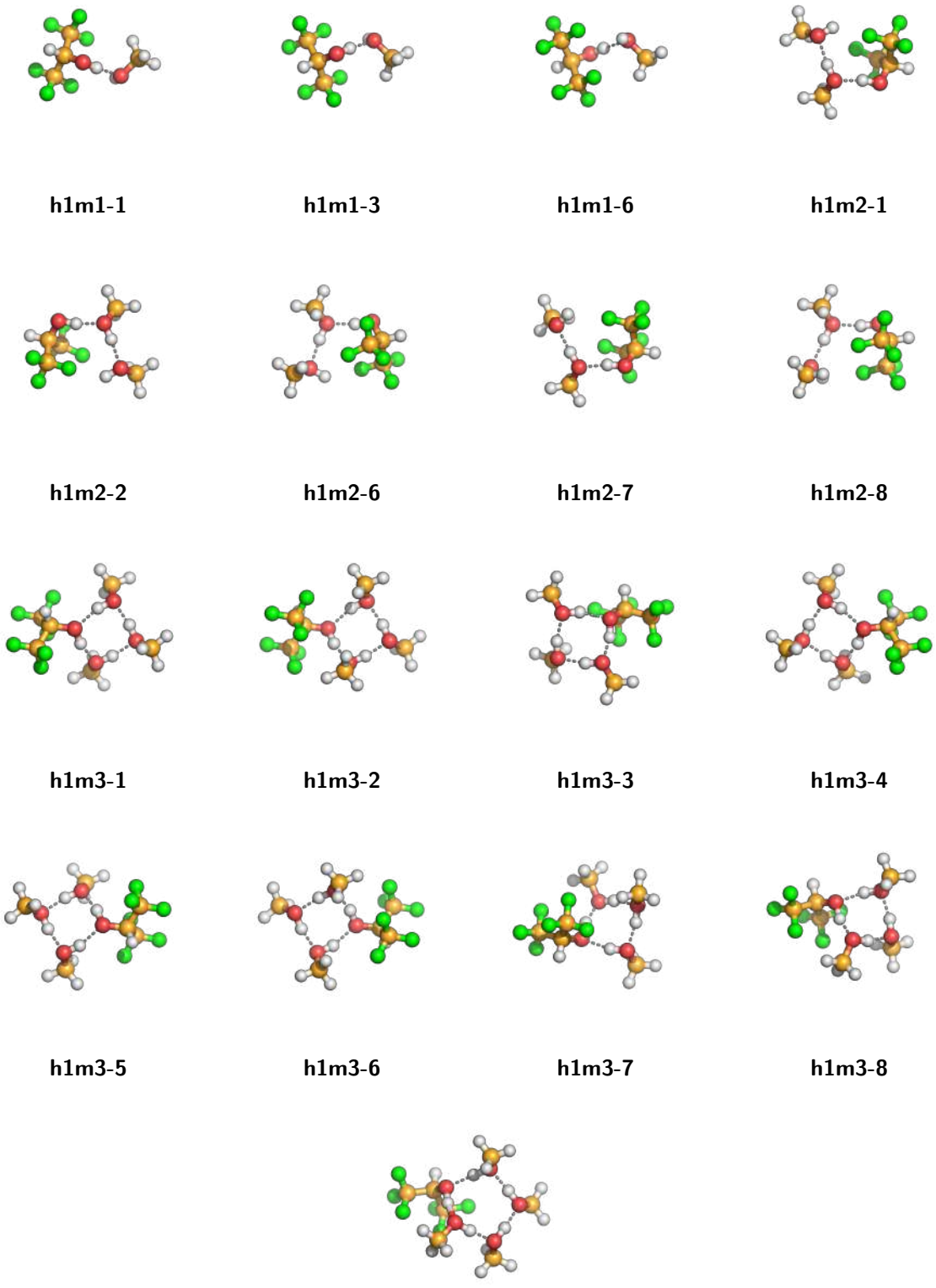

Figure B.18. HFIP/methanol clusters after BP86/TZVP optimization (1/4).

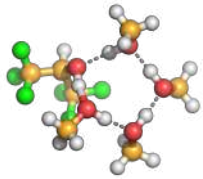

h1m4-2

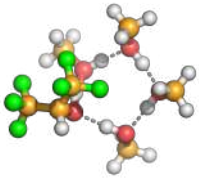

h1m4-4

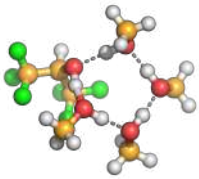

h1m4-5

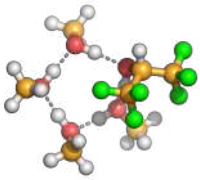

h1m4-6

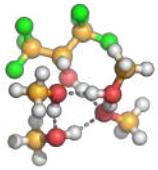

h1m4-7

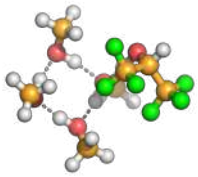

h1m4-8

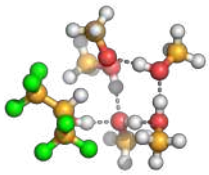

h1m5-1

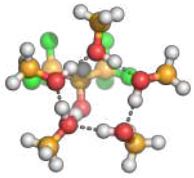

h1m5-2

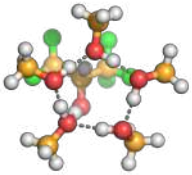

h1m5-3

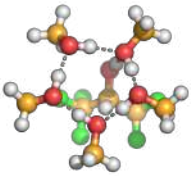

h1m5-6

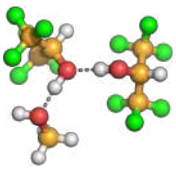

h2m1-1

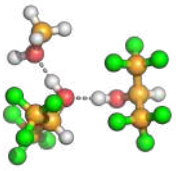

h2m1-6

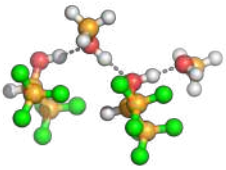

h2m2-1

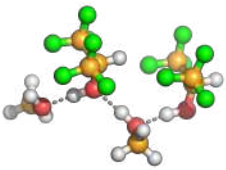

h2m2-3

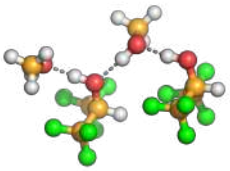

h2m2-5

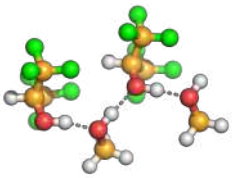

h2m2-6

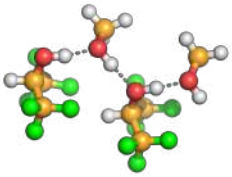

h2m2-7

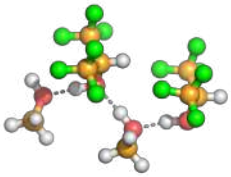

h2m2-8

Figure B.19. HFIP/methanol clusters after BP86/TZVP optimization (2/4).

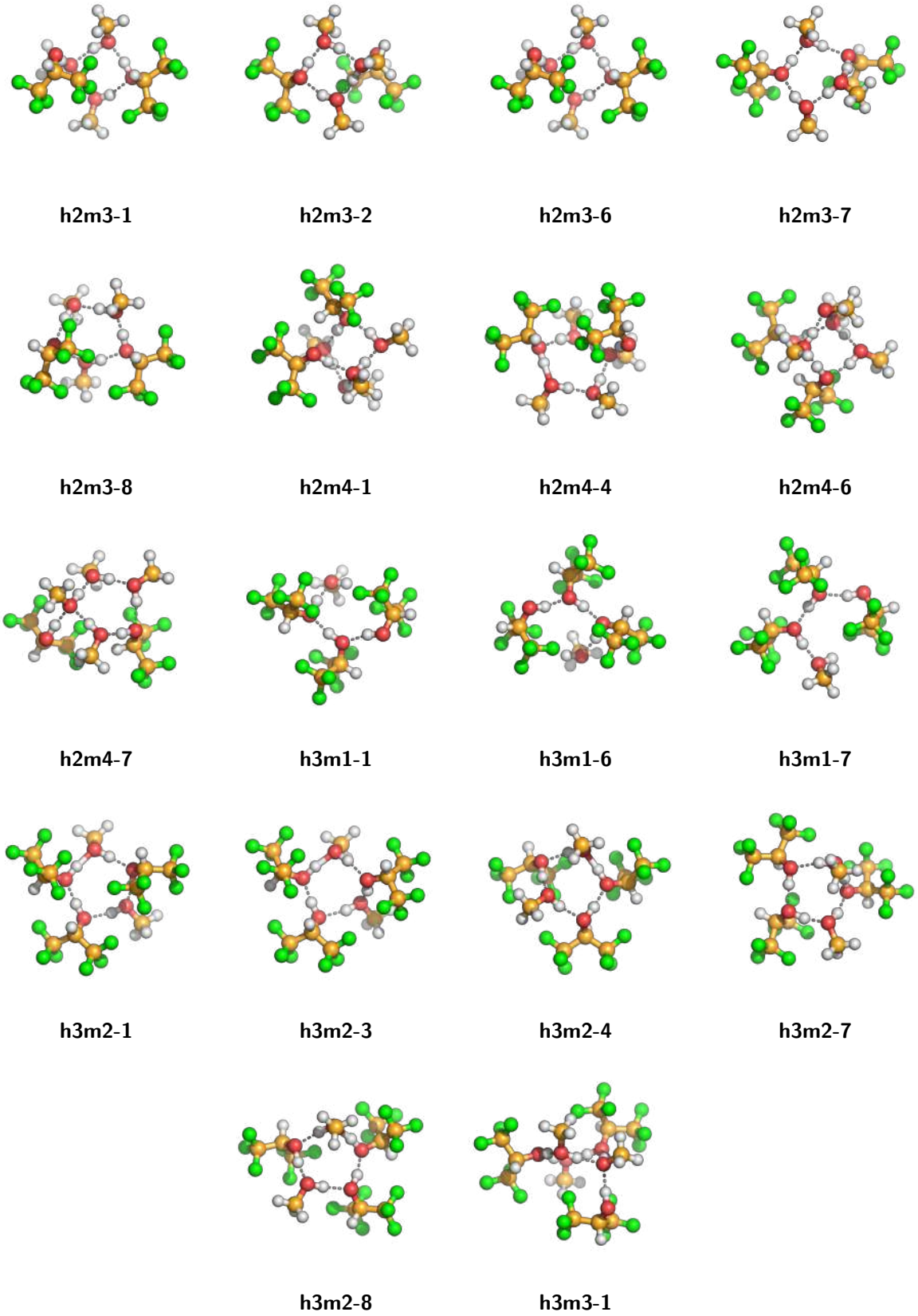

Figure B.20. HFIP/methanol clusters after BP86/TZVP optimization (3/4).

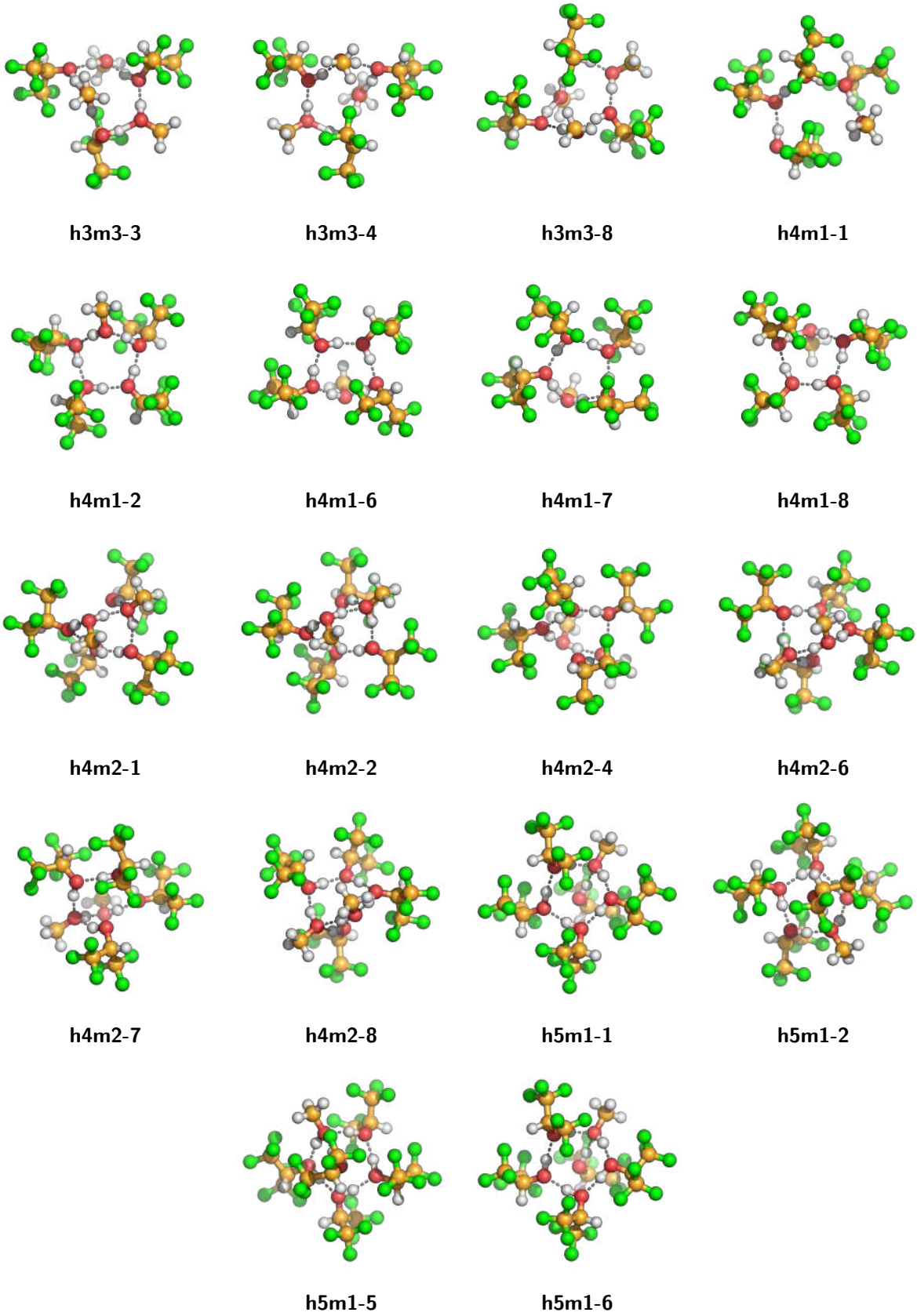

Figure B.21. HFIP/methanol clusters after BP86/TZVP optimization (4/4).

B.7. Cluster Structures

The quantum chemically optimized clusters used in Chapter 4 are available upon request from the authors.

Bibliography

[1] G. Marchelli, J. Ingenmey and B. Kirchner, *ChemistryOpen*, 2020, **9**, 774.

[2] G. Marchelli, J. Ingenmey, O. Hollóczki, A. Chaumont and B. Kirchner, *ChemPhysChem*, 2021.

[3] M. von Domaros, E. Perlt, J. Ingenmey, G. Marchelli and B. Kirchner, *SoftwareX*, 2018, **7**, 356–359.

[4] J. Ingenmey, J. Blasius, G. Marchelli, A. Riegel and B. Kirchner, *J. Chem. Eng. Data*, 2019, **64**, 255–261.

[5] H. Rodríguez, *Ionic liquids for better separation processes*, Springer, 2015.

[6] P. Anastas and N. Eghbali, *Chem. Soc. Rev.*, 2010, **39**, 301–312.

[7] R. D. Rogers and K. R. Seddon, *Science*, 2003, **302**, 792–793.

[8] E. L. Smith, A. P. Abbott and K. S. Ryder, *Che. Rev.*, 2014, **114**, 11060–11082.

[9] A. P. Abbott, D. Boothby, G. Capper, D. L. Davies and R. K. Rasheed, *J. Am. Chem. Soc.*, 2004, **126**, 9142–9147.

[10] M. R. S. J. Foreman, S. Holgersson, C. McPhee and M. S. Tyumentsev, *New J. Chem.*, 2018, **42**, 2006–2012.

[11] M. A. Martins, S. P. Pinho and J. A. Coutinho, *J. Solut. Chem.*, 2019, **48**, 962–982.

[12] D. O. Abranches, M. A. Martins, L. P. Silva, N. Schaeffer, S. P. Pinho and J. A. Coutinho, *Chem. Commun.*, 2019, **55**, 10253–10256.

[13] B. M. Ladanyi and M. S. Skaf, *Annu. Rev. Phys. Chem.*, 1993, **44**, 335–368.

[14] E. Guardia, J. Marti, J. A. Padro, L. Saiz and A. V. Komolkin, *J. Mol. Liq.*, 2002, **96**, 3–17.

[15] I. Bakó, Á. Bencsura, K. Hermannson, S. Bálint, T. Grósz, V. Chihaia and J. Oláh, *Phys. Chem. Chem. Phys.*, 2013, **15**, 15163–15171.

[16] S. Scheiner *et al.*, *Hydrogen bonding: a theoretical perspective*, Oxford University Press on Demand, 1997.

[17] W. M. Latimer and W. H. Rodebush, *J. Am. Chem. Soc.*, 1920, **42**, 1419–1433.

[18] T. Steiner, *Angew. Chem. Int. Ed.*, 2002, **41**, 48–76.

[19] E. Arunan, G. R. Desiraju, R. A. Klein, J. Sadlej, S. Scheiner, I. Alkorta, D. C. Clary, R. H. Crabtree, J. J. Dannenberg, P. Hobza, H. G. Kjaergaard, A. C. Legon, B. Mennucci and D. J. Nesbitt, *Pure Appl. Chem.*, 2011, **83**, 1637–1641.

[20] F. H. Stillinger, *Science*, 1980, **209**, 451–457.

[21] A. Luzar, S. Svetina and B. Žekš, *Chem. Phys. Lett.*, 1983, **96**, 485–490.

[22] A. Luzar, *J. Chem. Phys.*, 1989, **91**, 3603–3613.

[23] B. Santra, R. A. DiStasio Jr, F. Martelli and R. Car, *Mol. Phys.*, 2015, **113**, 2829–2841.

[24] K. A. Petterson, R. S. Stein, M. D. Drake and J. D. Roberts, *Magn. Reson. Chem.*, 2005, **43**, 225–230.

[25] M. Chalaris and J. Samios, *J. Phys. Chem. B*, 1999, **103**, 1161–1166.

[26] R. Ghanghas, A. Jindal and S. Vasudevan, *J. Phys. Chem. B*, 2018, **122**, 9757–9762.

[27] B. Kirchner, *J. Chem. Phys.*, 2005, **123**, 204116.

[28] P. Golub, T. Borzda, I. Doroshenko and V. Pogorelov, *J. Spectrosc. Dyn.*, 2012, **2**, 20.

[29] K. S. Vahvaselkä, R. Serimaa and M. Torkkeli, *J. Appl. Crystallogr.*, 1995, **28**, 189–195.

[30] J. Lehtola, M. Hakala and K. Hamalainen, *J. Phys. Chem. B*, 2010, **114**, 6426–6436.

[31] G. W. Stewart and R. M. Morrow, *Phys. Rev.*, 1927, **30**, 232.

[32] A. Mikusińska-Planner, *Acta Crystallogr. A*, 1977, **33**, 433–437.

[33] R. Kumar, J. R. Schmidt and J. L. Skinner, *J. Chem. Phys.*, 2007, **126**, 05B611.

[34] M. Tomšic, A. Jamnik, G. Fritz-Popovski, O. Glatter and L. Vlcek, *J. Phys. Chem. B*, 2007, **111**, 1738–1751.

[35] A. K. Soper, *J. Condens. Matter Phys.*, 2007, **19**, 335206.

[36] C. J. Benmore and Y. L. Loh, *J. Chem. Phys.*, 2000, **112**, 5877–5883.

[37] M. Matsumoto and K. E. Gubbins, *J. Chem. Phys.*, 1990, **93**, 1981–1994.

[38] A. Perera, F. Sokolić and L. Zoranić, *Phys. Rev. E*, 2007, **75**, 060502.

[39] E. Tsuchida, Y. Kanada and M. Tsukada, *Chem. Phys. Lett.*, 1999, **311**, 236–240.

[40] I. M. Svishchev and P. G. Kusalik, *J. Phys. Chem.*, 1994, **100**, 5165–5171.

[41] D. Mendeleev, *Liebigs Ann.*, 1861, **119**, 1–11.

[42] F. Weinhold, *J. Chem. Phys.*, 1998, **109**, 367–372.

[43] R. Ludwig, F. Weinhold and T. C. Farrar, *J. Phys. Chem. A*, 1997, **101**, 8861–8870.

[44] R. Ludwig, F. Weinhold and T. C. Farrar, *J. Chem. Phys.*, 1997, **107**, 499–507.

[45] M. Brüssel, E. Perlt, S. B. C. Lehmann, M. von Domaros and B. Kirchner, *J. Chem. Phys.*, 2011, **135**, 194113.

[46] F. Weinhold, *J. Chem. Phys.*, 1998, **109**, 373–384.

[47] R. Ludwig and F. Weinhold, *J. Chem. Phys.*, 1999, **110**, 508–515.

[48] R. Ludwig and F. Weinhold, *Phys. Chem. Chem. Phys.*, 2000, **2**, 1613–1619.

[49] R. Ludwig, *ChemPhysChem*, 2007, **8**, 938–943.

[50] A. Lenz and L. Ojamäe, *J. Chem. Phys.*, 2009, **131**, 134302.

[51] F. Weinhold, *J. Phys. Chem. B*, 2014, **118**, 7792–7798.

[52] S. B. C. Lehmann, C. Spickermann and B. Kirchner, *J. Chem. Theory Comput.*, 2009, **5**, 1650–1656.

[53] M. Brüssel, E. Perlt, M. von Domaros, M. Brehm and B. Kirchner, *J. Chem. Phys.*, 2012, **137**, 164107.

[54] R. Ludwig, *Phys. Chem. Chem. Phys.*, 2002, **4**, 5481–5487.

[55] C. Spickermann, S. B. C. Lehmann and B. Kirchner, *J. Chem. Phys.*, 2008, **128**, 244506.

[56] S. B. C. Lehmann, C. Spickermann and B. Kirchner, *J. Chem. Theory Comput.*, 2009, **5**, 1640–1649.

[57] R. Ludwig, F. Weinhold and T. C. Farrar, *Mol. Phys.*, 1999, **97**, 465–477.

[58] M. Huelsekopf and R. Ludwig, *J. Mol. Liq.*, 2000, **85**, 105–125.

[59] M. Huelsekopf and R. Ludwig, *J. Mol. Liq.*, 2002, **98–99**, 163–171.

[60] R. Ludwig, *ChemPhysChem*, 2005, **6**, 1369–1375.

[61] R. Ludwig, *ChemPhysChem*, 2005, **6**, 1376–1380.

[62] G. Matisz, W. M. Fabian, A.-M. Kelterer and S. Kunsági-Máté, *J. Mol. Struc.-THEOCHEM*, 2010, **956**, 103–109.

[63] G. Matisz, A.-M. Kelterer, W. M. F. Fabian and S. Kunsági-Máté, *J. Phys. Chem. B*, 2011, **115**, 3936–3941.

[64] M. Huelsekopf and R. Ludwig, *Magn. Reson. Chem.*, 2001, **39**, S127–S134.

[65] M. von Domaros, S. Jähnigen, J. Friedrich and B. Kirchner, *J. Chem. Phys.*, 2016, **144**, 064305.

[66] E. Perlt, J. Friedrich, M. von Domaros and B. Kirchner, *ChemPhysChem*, 2011, **12**, 3474–3482.

[67] C. Spickermann, E. Perlt, M. von Domaros, M. Roatsch, J. Friedrich and B. Kirchner, *J. Chem. Theory Comput.*, 2011, **7**, 868–875.

[68] J. Friedrich, E. Perlt, M. Roatsch, C. Spickermann and B. Kirchner, *J. Chem. Theory Comput.*, 2011, **7**, 843–851.

[69] M. von Domaros and E. Perlt, *J. Chem. Phys.*, 2017, **146**, 124114.

[70] R. Ludwig, F. Weinhold and T. C. Farrar, *Ber. Bunsenges. Phys. Chem.*, 1998, **102**, 197–204.

[71] R. Ludwig, F. Weinhold and T. C. Farrar, *Ber. Bunsenges. Phys. Chem.*, 1998, **102**, 205–212.

[72] M. A. Wendt, F. Weinhold and T. C. Farrar, *J. Chem. Phys.*, 1998, **109**, 5945–5947.

[73] M. J. Hansen, M. A. Wendt and F. Weinhold, *Mol. Phys.*, 2003, **101**, 1147–1153.

[74] J. Blasius, J. Ingenmey, E. Perlt, M. von Domaros, O. Hollóczki and B. Kirchner, *Angew. Chem. Int. Ed.*, 2019, **58**, 3212–3216.

[75] E. Perlt, M. von Domaros, B. Kirchner, R. Ludwig and F. Weinhold, *Sci. Rep.*, 2017, **7**, 10244.

[76] B. Kirchner, J. Blasius, L. Esser and W. Reckien, *Adv. Theory Simul.*, 2020, 2000223.

[77] J. Blasius and B. Kirchner, *J. Phys. Chem. B*, 2020, **124**, 7272–7283.

[78] G. Matisz, A.-M. Kelterer, W. M. F. Fabian and S. Kunsági-Máté, *Phys. Chem. Chem. Phys.*, 2015, **17**, 8467–8479.

[79] J. Ingenmey, M. von Domaros and B. Kirchner, *J. Chem. Phys.*, 2017, **146**, 154502.

[80] R. Ludwig, J. Behler, B. Klink and F. Weinhold, *Angew. Chem. Int. Ed.*, 2002, **41**, 3199–3202; *Angew. Chem.*, 2002, **114**, 3331–3335.

[81] J. Ingenmey, M. von Domaros, E. Perlt, S. P. Verevkin and B. Kirchner, *J. Chem. Phys.*, 2018, **148**, 193822.

[82] E. Perlt, M. von Domaros, B. Kirchner, R. Ludwig and F. Weinhold, *Sci. Rep.*, 2017, **7**, 1–10.

[83] P. Hohenberg and W. Kohn, *Phys. Rev.*, 1964, **136**, B864.

[84] D. B. Cook, *Handbook of computational quantum chemistry*, Courier Corporation, 2005.

[85] M. Born and R. Oppenheimer, *Ann. Phys.*, 1927, **389**, 457–484.

[86] D. R. Hartree, *Math. Proc. Camb. Philos. Soc.*, 1928, **24**, 89–110.

[87] V. Fock, *Z. Phys.*, 1930, **61**, 126–148.

[88] W. Kohn and L. J. Sham, *Phys. Rev.*, 1965, **140**, A1133.

[89] J. P. Perdew and K. Schmidt, Density Functional Theory and its Application to Materials, 2001, pp. 1–20.

[90] S. Grimme and P. R. Schreiner, *Angew. Chem. Int. Ed.*, 2018, **57**, 4170–4176.

[91] C. Bannwarth, S. Ehlert and S. Grimme, *J. Chem. Theory Comput.*, 2019, **15**, 1652–1671.

[92] S. Grimme, C. Bannwarth and P. Shushkov, *J. Chem. Theory Comput.*, 2017, **13**, 1989–2009.

[93] M. Gaus, Q. Cui and M. Elstner, *J. Chem. Theory Comput.*, 2011, **7**, 931–948.

[94] E. Caldeweyher, C. Bannwarth and S. Grimme, *J. Chem. Phys.*, 2017, **147**, 034112.

[95] E. Caldeweyher, S. Ehlert, A. Hansen, H. Neugebauer, S. Spicher, C. Bannwarth and S. Grimme, *J. Chem. Phys.*, 2019, **150**, 154122.

[96] F. Weinhold, *J. Chem. Phys.*, 1998, **109**, 367–372.

[97] T. J. Ypma, *SIAM Rev.*, 1995, **37**, 531–551.

[98] R. Townsend, *Implementation of an ISO/IEC 1539-2:2000 Conforming Iso_varying_string Module*, 2009, `http://www.astro.wisc.edu/~townsend/static.php?ref=iso-varying-string`.

[99] R. Storn and K. Price, *J. Glob. Optim.*, 1997, **11**, 341–359.

[100] P. Virtanen, R. Gommers, T. E. Oliphant, M. Haberland, T. Reddy, D. Cournapeau, E. Burovski, P. Peterson, W. Weckesser, J. Bright, S. J. van der Walt, M. Brett, J. Wilson, K. J. Millman, N. Mayorov, A. R. J. Nelson, E. Jones, R. Kern, E. Larson, C. J. Carey, İ. Polat, Y. Feng, E. W. Moore, J. VanderPlas, D. Laxalde, J. Perktold, R. Cimrman, I. Henriksen, E. A. Quintero, C. R. Harris, A. M. Archibald, A. H. Ribeiro, F. Pedregosa, P. van Mulbregt and SciPy 1.0 Contributors, *Nat. Methods*, 2020, **17**, 261–272.

[101] W. L. Jorgensen, D. S. Maxwell and J. Tirado-Rives, *J. Am. Chem. Soc.*, 1996, **118**, 11225–11236.

[102] J. Wang, R. M. Wolf, J. W. Caldwell, P. A. Kollman and D. A. Case, *J. Comput. Chem.*, 2004, **25**, 1157–1174.

[103] J. M. Dieterich and B. Hartke, *Mol. Phys.*, 2010, **108**, 279–291.

[104] J. M. Dieterich and B. Hartke, *J. Comput. Chem.*, 2011, **32**, 1377–1385.

[105] H. A. Lorentz, *Ann. Phys.*, 1881, **248**, 127–136.

[106] D. Berthelot, *C. R. Acad. Sci.*, 1898, **126**, 1703–1706.

[107] R. D. Offeman, S. K. Stephenson, G. H. Robertson and W. J. Orts, *Ind. Eng. Chem. Res.*, 2005, **44**, 6797–6803.

[108] S. M. Sarathy, P. Oßwald, N. Hansen and K. Kohse-Höinghaus, *Prog. Energ. Combust.*, 2014, **44**, 40 – 102.

[109] M. Amin, M. Ali, H. Kamal, A. Youssef and M. Akl, *Hydrometallurgy*, 2010, **105**, 115 – 119.

[110] G. H. Morrison and H. Freiser, *Anal. Chem.*, 1964, **36**, 93–116.

[111] Y. Marcus, *Chem. Rev.*, 1963, **63**, 139–170.

[112] V. G. Mayorov and A. I. Nikolaev, *Hydrometallurgy*, 2002, **66**, 77–83.

[113] J. W. Roddy, *Ind. Eng. Chem. Process Des. Dev.*, 1981, **20**, 104–108.

[114] C. L. Munson and C. J. King, *Ind. Eng. Chem. Process Des. Dev.*, 1984, **23**, 109–115.

[115] H. Schaal, T. Häber and M. A. Suhm, *J. Phys. Chem. A*, 2000, **104**, 265–274.

[116] R. A. Provencal, R. N. Casaes, K. Roth, J. B. Paul, C. N. Chapo, R. J. Saykally, G. S. Tschumper and H. F. Schaefer, *J. Phys. Chem. A*, 2000, **104**, 1423–1429.

[117] F. Kollipost, K. Papendorf, Y.-F. Lee, Y.-P. Lee and M. A. Suhm, *Phys. Chem. Chem. Phys.*, 2014, **16**, 15948–15956.

[118] F. J. Lovas, S. P. Belov, M. Y. Tretyakov, W. Stahl and R. D. Suenram, *J. Mol. Spectrosc.*, 1995, **170**, 478–492.

[119] F. J. Lovas and H. Hartwig, *J. Mol. Spectrosc.*, 1997, **185**, 98–109.

[120] D. Loru, I. Peña and M. E. Sanz, *J. Mol. Spectrosc.*, 2017, **335**, 93–101.

[121] M. S. Snow, B. J. Howard, L. Evangelisti and W. Caminati, *J. Phys. Chem. A*, 2011, **115**, 47–51.

[122] A. K. King and B. J. Howard, *Chem. Phys. Lett*, 2001, **348**, 343–349.

[123] S. K. Stephenson, R. D. Offeman, G. H. Robertson and W. J. Orts, *Chem. Eng. Sci.*, 2007, **62**, 3019–3031.

[124] B. Chen, J. J. Potoff and J. I. Siepmann, *J. Phys. Chem. B*, 2001, **105**, 3093–3104.

[125] K. Ohno, H. Yoshida, H. Watanabe, T. Fujita and H. Matsuura, *J. Phys. Chem.*, 1994, **98**, 6924–6930.

[126] I. A. Finneran, P. B. Carroll, G. J. Mead and G. A. Blake, *Phys. Chem. Chem. Phys.*, 2016, **18**, 22565–22572.

[127] R. L. Rowley, C. M. Tracy and T. A. Pakkanen, *J. Phys. Chem.*, 2007, **127**, 07B605.

[128] A. Vargas-Caamal, F. Ortiz-Chi, D. Moreno, A. Restrepo, G. Merino and J. L. Cabellos, *Theor. Chem. Acc.*, 2015, **134**, 16.

[129] B. Kirchner, C. Spickermann, S. B. C. Lehmann, E. Perlt, J. Langner, M. von Domaros, P. Reuther, F. Uhlig, M. Kohagen and M. Brüssel, *Comput. Phys. Commun.*, 2011, **182**, 1428–1446.

[130] B. Kirchner, F. Weinhold, J. Friedrich, E. Perlt and S. B. C. Lehmann, in *Many-Electron Approaches in Physics, Chemistry and Mathematics*, ed. V. Bach and L. Delle Site, Springer International Publishing, 2014, pp. 77–96.

[131] S. Perkin, B. Kirchner and M. D. Fayer, *J. Chem. Phys.*, 2018, **148**, 193501.

[132] J. Ingenmey, M. von Domaros and B. Kirchner, *J. Chem. Phys.*, 2017, **146**, 154502.

[133] J. Blasius, J. Ingenmey, E. Perlt, M. von Domaros, O. Hollóczki and B. Kirchner, *Angew. Chem.*, 2019, **131**, 3245–3249.

[134] P. Borowski, J. Jaroniec, T. Janowski and K. Woliński, *Mol. Phys.*, 2003, **101**, 1413–1421.

[135] M. Kohns, S. Reiser, M. Horsch and H. Hasse, *J. Chem. Phys.*, 2016, **144**, 084112.

[136] M. Kohns, M. Horsch and H. Hasse, *J. Chem. Phys.*, 2017, **147**, 144108.

[137] G. Wedler, *Lehrbuch der Physikalischen Chemie*, Wiley, 2005.

[138] M. A. Martins, S. P. Pinho and J. A. Coutinho, *J. Solut. Chem.*, 2019, **48**, 962–982.

[139] A. P. Abbott, G. Capper, D. L. Davies, R. K. Rasheed and P. Shikotra, *Inorg. Chem.*, 2005, **44**, 6497–6499.

[140] R. A. Provencal, J. B. Paul, K. Roth, C. Chapo, R. N. Casaes, R. J. Saykally, G. S. Tschumper and H. F. Schaefer III, *J. Chem. Phys.*, 1999, **110**, 4258–4267.

[141] J. Thar and B. Kirchner, *J. Phys. Chem. A*, 2006, **110**, 4229–4237.

[142] K. Wendler, J. Thar, S. Zahn and B. Kirchner, *J. Phys. Chem. A*, 2010, **114**, 9529–9536.

[143] T. Yamaguchi, K. Hidaka and A. K. Soper, *Mol. Phys.*, 1999, **96**, 1159–1168.

[144] M. Brehm and B. Kirchner, *J. Chem. Inf.*, 2011, **51**, 2007–2023.

[145] N. Sieffert, M. Bühl, M.-P. Gaigeot and C. A. Morrison, *J. Chem. Theory Comput.*, 2013, **9**, 106–118.

[146] C. C. Wang, J. Y. Tan and L. H. Liu, *AIP Adv.*, 2017, **7**, 035115.

[147] J. C. W.E. Acree, Jr., in *NIST Chemistry WebBook, NIST Standard Reference Database Number 69*, ed. W. M. Eds. P.J. Linstrom, National Institute of Standards and Technology, 2016, ch. Phase Transition Enthalpy Measurements of Organic and Organometallic Compounds.

[148] J. Polák, S. Murakami, V. T. Lam, H. D. Pflug and G. C. Benson, *Can. J. Chem.*, 1970, **48**, 2457–2465.

[149] B. Kirchner, *Phys. Rep.*, 2007, **1–3**, 1–111.

[150] F. Jensen, *Introduction to computational chemistry*, Wiley, 2017.

[151] O. Redlich and A. T. Kister, *Ind. Eng. Chem. Res.*, 1948, **40**, 345–348.

[152] D. A. Case, R. M. Betz, W. Botello-Smith, D. S. Cerutti, T. E. Cheatham III, T. A. Darden, R. E. Duke, T. J. Giese, H. Gohlke, A. W. Goetz, N. Homeyer, S. Izadi, P. Janowski, J. Kaus, A. Kovalenko, T. S. Lee, S. LeGrand, P. Li, C. Lin, T. Luchko, R. Luo, B. Madej, D. Mermelstein, J. M. Merz, G. Monard, H. Nguyen,

H. T. Nguyen, I. Omelyan, A. Onufriev, D. R. Roe, A. Roitberg, C. Sagui, C. L. Simmerling, J. Swails, R. C. Walker, J. Wang, R. M. Wolf, X. Wu, L. Xiao, D. M. York and P. A. Kollman, *AMBER 2016*, 2016, University of California, San Francisco.

[153] H. Takeuchi, *J. Phys. Chem. A*, 2012, **116**, 10172–10181.

[154] F. Neese, *Wiley Interdiscip. Rev. Comput. Mol. Sci.*, 2012, **2**, 73–78.

[155] J. G. Brandenburg, M. Alessio, B. Civalleri, M. F. Peintinger, T. Bredow and S. Grimme, *J. Phys. Chem. A*, 2013, **117**, 9282–9292.

[156] Y. Marcus, *Solvent Mixtures: Properties and Selective Solvation*, CRC Press, 2002.

[157] A. Kumagai and C. Yokoyama, *Int. J. Thermophys.*, 1998, **19**, 3–13.

[158] W. G. Khan, S. Siddique and M. S. Ansari, *J. Chem. Eng. Data*, 2016, **61**, 1368–1377.

[159] R. Haase and W. Tillmann, *Z. Phys. Chem.*, 1995, **192**, 121–131.

[160] W. M. Haynes, *CRC handbook of chemistry and physics*, CRC press, 2014.

[161] J. A. Nelder and R. Mead, *Comput. J.*, 1965, **7**, 308–313.

[162] K. Yamada, T. Nakano and Y. Okamoto, *J. Polym. Sci., Part A-1: Polym. Chem.*, 2000, **38**, 220–228.

[163] Y. Miura, T. Satoh, A. Narumi, O. Nishizawa, Y. Okamoto and T. Kakuchi, *J. Polym. Sci., Part A-1: Polym. Chem.*, 2006, **44**, 1436–1446.

[164] I. Colomer, A. E. Chamberlain, M. B. Haughey and T. J. Donohoe, *Nat. Rev. Chem.*, 2017, **1**, 1–12.

[165] H. F. Motiwala, C. Fehl, S.-W. Li, E. Hirt, P. Porubsky and J. Aubé, *J. Am. Chem. Soc.*, 2013, **135**, 9000–9009.

[166] O. Hollóczki, R. Macchieraldo, B. Gleede, S. R. Waldvogel and B. Kirchner, *J. Phys. Chem. Lett.*, 2019, **10**, 1192–1197.

[167] K. Neimann and R. Neumann, *Org. Lett.*, 2000, **2**, 2861–2863.

[168] A. Berkessel and M. R. Andreae, *Tetr. Lett.*, 2001, **42**, 2293–2295.

[169] D. F. Evans and M. I. McElroy, *J. Solut. Chem.*, 1975, **4**, 413–430.

[170] Z. Li, Z. Zhang, S. Smolders, X. Li, S. Raiguel, E. Nies, D. E. De Vos and K. Binnemans, *Chemistry*, 2019, **25**, 9197.

[171] M. L. Dietz, *Sep. Sci. Technol.*, 2006, **41**, 2047–2063.

[172] Q. Zhang, K. D. O. Vigier, S. Royer and F. Jerome, *Chem. Soc. Rev.*, 2012, **41**, 7108–7146.

[173] E. L. Smith, A. P. Abbott and K. S. Ryder, *Chem. Rev.*, 2014, **114**, 11060–11082.

[174] A. Malik and H. K. Kashyap, *Phys. Chem. Chem. Phys.*, 2021, **23**, 3915–3924.

[175] A. Malik and H. K. Kashyap, *J. Chem. Phys.*, 2021, **155**, 044502.

[176] D. J. van Osch, D. Parmentier, C. H. Dietz, A. van den Bruinhorst, R. Tuinier and M. C. Kroon, *Chem. Commun.*, 2016, **52**, 11987–11990.

[177] B. D. Ribeiro, C. Florindo, L. C. Iff, M. A. Coelho and I. M. Marrucho, *ACS Sustain. Chem. Eng.*, 2015, **3**, 2469–2477.

[178] W. Deng, L. Yu, X. Li, J. Chen, X. Wang, Z. Deng and Y. Xiao, *Food Chem.*, 2019, **274**, 891–899.

[179] N. V. Belkova, E. Collange, P. Dub, L. M. Epstein, D. A. Lemenovskii, A. Lledós, O. Maresca, F. Maseras, R. Poli, P. O. Revin, E. S. Shubina and E. V. Vorontsov, *Chem. Eur. J.*, 2005, **11**, 873–888.

[180] N. Asprion, H. Hasse and G. Maurer, *Fluid Ph. Equilibria*, 2001, **186**, 1–25.

[181] M. Maiwald, H. Li, T. Schnabel, K. Braun and H. Hasse, *J. Supercrit. Fluids*, 2007, **43**, 267–275.

[182] T. Schnabel, A. Srivastava, J. Vrabec and H. Hasse, *J. Phys. Chem. B*, 2007, **111**, 9871–9878.

[183] T. Schnabel, J. Vrabec and H. Hasse, *Fluid Ph. Equilibria*, 2008, **263**, 144–159.

[184] S. Gehrke and B. Kirchner, *J. Chem. Eng. Data*, 2019, **65**, 1146–1158.

[185] L. Martínez, R. Andrade, E. G. Birgin and J. M. Martínez, *J. Comput. Chem.*, 2009, **30**, 2157–2164.

[186] S. Plimpton, *J. Comput. Chem.*, 1995, **117**, 1–19.

[187] M. Fioroni, K. Burger, A. E. Mark and D. Roccatano, *J. Phys. Chem. B*, 2001, **105**, 10967–10975.

[188] A. Chaumont, E. Engler and R. Schurhammer, *J. Phys. Chem. B*, 2020, **124**, 7239–7250.

[189] J.-P. Ryckaert, G. Ciccotti and H. J. Berendsen, *J. Comput. Phys.*, 1977, **23**, 327–341.

[190] M. Brehm, M. Thomas, S. Gehrke and B. Kirchner, *J. Chem. Phys.*, 2020, **152**, 164105.

[191] J. Kroon and J. A. Kanters, *Nature*, 1974, **248**, 667–669.

[192] M. Kohagen, M. Brehm, J. Thar, W. Zhao, F. Muller-Plathe and B. Kirchner, *J. Phys. Chem. B*, 2011, **115**, 693–702.

[193] A. D. Becke, *Phys. Rev. A*, 1988, **38**, 3098.

[194] S. G. Balasubramani, G. P. Chen, S. Coriani, M. Diedenhofen, M. S. Frank, Y. J. Franzke, F. Furche, R. Grotjahn, M. E. Harding, C. Hättig, A. Hellweg, B. Helmich-Paris, C. Holzer, U. Huniar, M. Kaupp, A. M. Khah, S. K. Khani, T. Müller, F. Mack, B. D. Nguyen, S. M. Parker, E. Perlt, D. Rappoport, K. Reiter, S. Roy, M. Rückert, G. Schmitz, M. Sierka, E. Tapavicza, D. P. Tew, C. Van Wüllen, V. K. Voora, F. Weigend, A. Wodyński and J. M. Yu, *J. Chem. Phys*, 2020, **152**, 184107.

[195] M. Orio, D. A. Pantazis and F. Neese, *Photosynth. Res.*, 2009, **102**, 443–453.

[196] C. W. Murray, G. J. Laming, N. C. Handy and R. D. Amos, *Chem. Phys. Lett.*, 1992, **199**, 551–556.

[197] S. Grimme, S. Ehrlich and L. Goerigk, *J. Comput. Chem.*, 2011, **32**, 1456–1465.

[198] S. Grimme, J. Antony, S. Ehrlich and H. Krieg, *J. Chem. Phys.*, 2010, **132**, 154104.

[199] G. Matisz, W. M. F. Fabian, A.-M. Kelterer and S. Kunsági-Máté, *J. Mol. Struct. THEOCHEM*, 2010, **956**, 103–109.

[200] T. Kosztolányi, I. Bakó and G. Pálinkás, *J. Chem. Phys.*, 2003, **118**, 4546–4555.

[201] S. Bellissima, S. De Panfilis, U. Bafile, A. Cunsolo, M. A. González, E. Guarini and F. Formisano, *Sci. Rep.*, 2016, **6**, 1–10.

[202] M. Haughney, M. Ferrario and I. R. McDonald, *J. Phys. Chem.*, 1987, **91**, 4934–4940.

[203] S. Teh, P.-J. Hsu and J.-L. Kuo, *Phys. Chem. Chem. Phys.*, 2021, 9166–9175.

[204] A. N. Fletcher, *J. Phys. Chem.*, 1971, **75**, 1808–1814.

Acknowledgments

I would like to express my gratitude to my supervisor Prof. Dr. Barbara Kirchner, for her teachings and patience; without her, this thesis would not have been possible.

I also thank Prof. Dr. Thomas Bredow, Dr. Marianne Engeser, and Dr. Gerhild van Echten-Deckert for joining the PhD commission.

I am grateful to the whole Kirchner group, and in particular to Dr. Johannes Ingenmey, Lars Esser, Jan Blasius, and Vahideh Alizadeh for their friendship and support. I would also like to thank the former members Dr. Promit Ray and Roberto Macchieraldo, for all the time spent together in Bonn. Special thanks go to Dr. Werner Reckien for helping with administrative and technical problems.

I wish to express my gratitude to the whole European SOCRATES project; I met wonderful people there and I have grown both academically and as a person thanks to all of them.

Last but not least, I would like to thank my family and friends for their wonderful support, and Linda Goletto, for being the beautiful person she is; doing the PhD was a thrilling but difficult experience, but their presence in my life made it way easier.